Delft University of Technology

MSc Thesis

Tide-induced currents in a phase-resolving wave model

Author:
Floris de Wit

Graduation committee:
Prof. Dr. Ir. A.J.H.M. Reniers
Dr. Ir. M. Zijlema
Ir. J. Bosboom
Dr. Ir. M.D. Klein

Faculty of Civil Engineering and Geosciences
Section Hydraulic Engineering
Department of Environmental Fluid Mechanics

January 2016

Abstract

Alongshore currents are currents parallel to the coastline. In coastal areas they are driven by a combination of wave and tidal forcing. In this study, the validity of the non-hydrostatic, wave-flow model SWASH to predict these currents is investigated. This is done by comparing model predictions with measurement observations. Observations were obtained from the COAST3D data-set at the gently sloping barred beach near Egmond. It contains six weeks of wave and velocity measurements for a wide range of conditions.

An initial study was performed to investigate model settings and parameter sensitivity for correctly capturing wave dynamics. From this study, it can be concluded that two terrain-following layers and 75 grid cells per wave length lead to accurate results for surf zone wave modelling. Although some discrepancies in mean water level set-up were encountered, this is assumed not to affect alongshore current predictions.

The present SWASH model does not allow for the inclusion of alongshore tidal currents. Therefore, this study presents a method to include tidal forcing, which was implemented in the source code. This method enables the user to include the tide by imposing a water level gradient, which is assumed to be time averaged and spatially uniform. These assumptions are reasonable as spatial and temporal model scales are small compared to a tidal wave.

Validation results demonstrate the capability of SWASH to correctly represent wave transformation in a surf zone. Furthermore, modelled velocity predictions are in good agreement with observations for cases with waves from southwest and northward flood tidal currents, which were not disturbed by instabilities. Cases with different forcing were influenced by instabilities due to a bug in the source code. Two cases, which were least influenced by the instabilities, have been analysed in more detail as well. Some discrepancies are observed between model and observations. Further study is required to evaluate whether this is caused by the instabilities, introduced by the bug in the source code, or whether other physical phenomena play a role in the mismatch. Inertia of a tidal wave and bottom friction and processes which could potentially be the cause of the discrepancies.

Preface

This thesis is written as the final step for completion of the Master of Science degree in Hydraulic Engineering at Delft University of Technology. Research for this thesis was partially performed at Royal HaskoningDHV in Rotterdam and for the remainder at the Environmental Fluid Mechanics section at Delft University of Technology.

First of all, I am grateful to the members of my graduation committee: Ad Reniers for being chairman of the committee, his knowledge on alongshore currents and his love for surf zone eddies. Marcel Zijlema for all his support in numerical modelling, the SWASH model and all sorts of programming issues. Judith Bosboom for her expertise on coastal processes and model evaluation. And finally Mark Klein, for his enthusiasm and interest from start to end, and for taking the view from the perspective of an engineering company.

Furthermore, I would like to thank my colleagues in both Rotterdam and Delft for the pleasant time during my graduation period and for all the support provided. A special thanks is expressed to Dirk Rijnsdorp, Pieter Smit and James Salmon of the Environmental Fluid Mechanics section in Delft for sharing their knowledge and providing new ideas when I ran aground.

Contents

Chapter 1

Introduction

In this chapter a problem definition is presented in Section 1.1. Based on this the research question is formulated in Section 1.2, with the corresponding research method in Section 1.3. Finally, the outline of this report is given in Section 1.4

1.1 Problem definition

Modelling currents in the surf zone can on the one hand be useful for assessments on swimmers safety. On the other hand it gives valuable information for beach erosion and nourishment stability. This is of particular importance for a country like the Netherlands, as a considerable amount of money is invested in nourishments to protect the coastline.

Until recently, most model studies to investigate alongshore currents were conducted with phase-averaged models, like DELFT3D and UNIBEST (e.g. Elias et al. (2001); Kleinhout (2000)). These models, however, do not take into account intra-wave action [1]. Therefore, the accuracy to model wave driven currents in the surf zone is limited. Due to developments of phase-resolving models over the past decade, these have become more and more applicable to surf zone studies. SWASH is such a model which is under constant development at Delft University of Technology (Zijlema et al., 2011). Until now, tidal currents have not yet been implemented in such models, whereas they definitely influence surf zone dynamics.

The non-hydrostatic wave-flow model SWASH has extensively been validated for laboratory experiments. However, only few studies have been performed checking the validity

[1] Physical processes within a wave are called intra-wave action. These are not taken into account by most modelled as wave processes are averaged per wave.

of the model in the surf zone with field measurement data. The propagation and transformation of surface gravity waves with SWASH is looked into by Brinkkemper (2013). Rijnsdorp (2015) investigated the infragravity wave dynamics in the surf zone. Both by using data from a field experiment. Until now no studies have been performed to validate the capability of SWASH to model currents inside the surf zone on the basis of field measurement data.

Abundance of flow data is available under a large variety of wave conditions in the COAST3D data-set. At this large-scale field campaign, measurements were performed for six weeks in October and November 1998 near Egmond aan Zee along the Dutch North Sea coastline.

1.2 Research question

Given the problem definition and with knowledge of the performed literature study, the main research question of this Master of Science Thesis will be:

- *What is the validity of the non-hydrostatic model SWASH in predicting alongshore currents in the surfzone?*

This research question is too extensive to answer in one piece. Therefore sub-questions will be answered first, to subsequently be able to answer the main research question:

- *Under what conditions is cross-shore wave propagation and transformation modelled correctly?*
- *To what extent is SWASH capable of modelling alongshore currents and its distribution over the surf zone?*
  - *wave induced currents*
  - *tide induced currents*
  - *combined wave and tide induced currents*

As stated above the alongshore current will first be considered for the different forcing types separately. Finally, all forcing terms will be combined.

1.3 Research method

To answer the above mentioned research questions, a research method has been developed. Directly setting up a complex 3D model is unconventional, because when errors or inaccuracies occur it is very hard or even impossible to find the mistakes made. It is important to initially understand the model and behaviour of parameters before making it more complex. Therefore the research is separated in several studies.

- **Wave study:** Although the research concerns currents, waves are an important driving force for currents. Therefore, firstly the propagation and transformation of waves into shallow water will be investigated with a one dimensional model. Model settings and physical parameters will be varied to get insight in the model behaviour and to make well-founded choices for the following current studies.
- **Alongshore current study:** When the transformation of waves is modelled correctly, the domain will be extended in alongshore direction to simulate alongshore currents. Firstly, attention will be given to model settings and sensitivity of all parameters. Then the correct implementation of all driving forces in the model will investigated.
- **Calibration and validation:** Some parameters will be calibrated by using COAST3D data. Finally, the model will be validated with COAST3D data for different wave and tidal climates.

1.4 Outline

Within this first chapter the problem definition, research question and research method were elaborated on. In Chapter 2 background information will be given which is useful to read prior to the actual modelling.

Chapter 3 deals with correctly modelling wave propagation and transformation with SWASH. In Chapters 4 and 5 the implementation, model settings and parameter sensitivity of wave and tide induced currents are described. COAST3D cases are selected in chapter 6 which are used for calibration and validation of the SWASH model in Chapter 7.

In Chapter 8 results of all model studies will be discussed, including shortcomings and assumptions made. Finally, conclusions will be drawn and recommendations are given in Chapter 9.

To improve readability, abbreviations and symbols will only be explained the first time they are mentioned in text. For an overview of all abbreviations and symbols is referred to pages 85 and 87, respectively.

Chapter 2

Background information

Information on the COAST3D data set is given in Section 2.1 and Section 2.2 describes the SWASH model, which will be used. Finally, physical background, including formulae, will be given on wave transformation, tide, alongshore currents and current instabilities in Section 2.3.

2.1 COAST3D

In October and November 1998 a consortium of 11 partners performed field measurements as part of the COAST3D project at Egmond aan Zee, which is located along the Dutch North Sea coast. Together these parties collected data of waves, currents, sediment transport and morphodynamics. One of the main purposes was validation of existing hydrodynamic and morphodynamic models (Soulsby, 1998).

The Egmond coast is characterised by a double barred system with a gently sloped, sandy beach. Waves are measured by a directional wave buoy, located 5km offshore in 16m water depth (Rijnsdorp, 2015). During the six week experiment a wide range of conditions occurred. The significant wave height varied from 0.2m to 5.2m with a corresponding peak period ranging from 2s to 11s. The tidal range varied between 1.4m and 2.1m for neap and spring tide respectively (van Rijn et al., 2002).

Until the end of October bathymetric gradients in alongshore direction were small, so this bathymetry can be assumed to be alongshore uniform. During storm conditions on 29 October, however, a rip channel developed leading to non uniformities (Ruessink et al., 2001).

Data was collected at several locations by different parties. The most interesting locations are on the main transect in the middle of the $500 \times 500m$ area. Current data

is available at twelve locations distributed over the near shore, including four close to each other near the inner bar. See Figure 2.1. For a more extensive description of the site and measurement locations, is referred to Appendix A. This appendix also contains information on the accuracy of measurement devices.

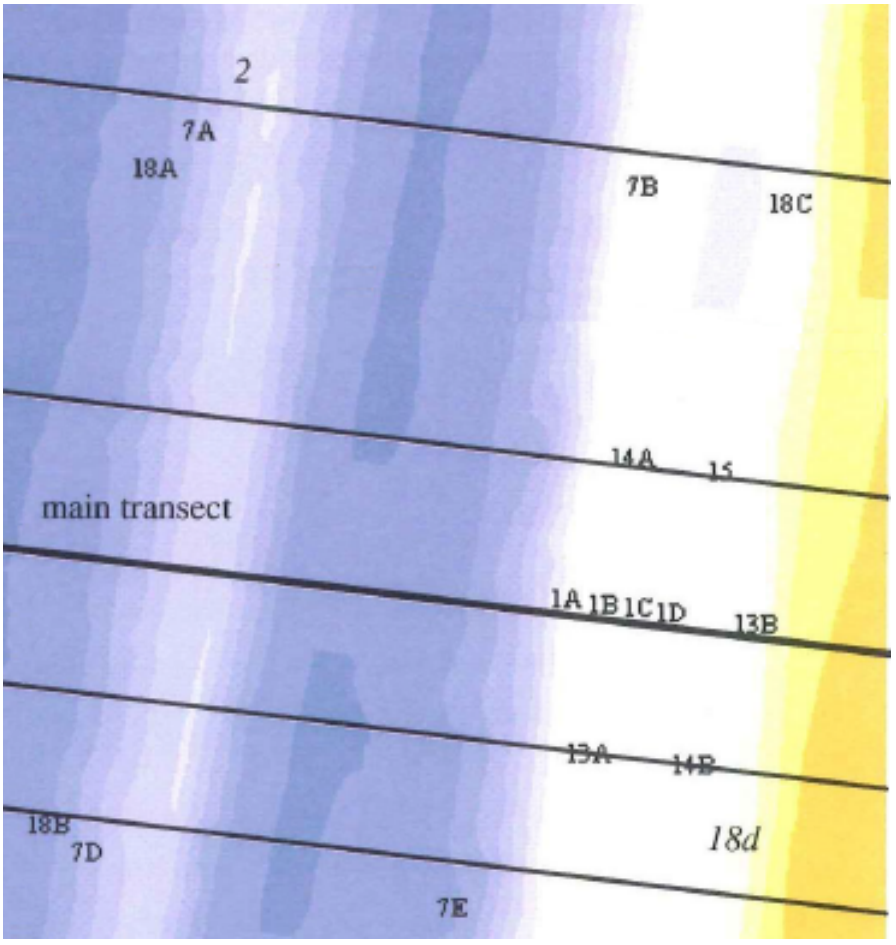

FIGURE 2.1: COAST3D measurement locations (van Rijn et al., 2002)

2.2 SWASH model

Developments over the last decade led to the open-source code SWASH, which is an acronym for Simulating WAves till SHore. It is a non-hydrostatic wave-flow numerical model. SWASH provides an efficient and robust model that allows a wide range of time and space scales of surface waves and shallow water flows in complex environments to be applied (Zijlema et al., 2011).

SWASH calculates the Reynolds-averaged Navier-Stokes (RANS) equations for an incompressible fluid with a free surface. For readability purposes only the two-dimensional

formulae are presented. Extension to a three-dimensional reference frame means including the y-direction and thus v-terms. It is straightforward and the formulae have the same form but slightly extended. The governing equations for a vertical two-dimensional framework bounded by the free surface $z = \zeta(x,t)$ and the bottom $z = -d(x)$ are:

$$\frac{\partial u}{\partial x} + \frac{\partial w}{\partial z} = 0 \tag{2.1}$$

$$\frac{\partial u}{\partial t} + \frac{\partial uu}{\partial x} + \frac{\partial wu}{\partial z} = \frac{1}{\rho}\frac{\partial (p_h + p_{nh})}{\partial x} + \frac{\partial}{\partial x}\left(\nu^h \frac{\partial u}{\partial x}\right) + \frac{\partial}{\partial z}\left(\nu^v \frac{\partial u}{\partial z}\right) \tag{2.2}$$

$$\frac{\partial w}{\partial t} + \frac{\partial uw}{\partial x} + \frac{\partial ww}{\partial z} = \frac{1}{\rho}\frac{\partial (p_h + p_{nh})}{\partial z} + \frac{\partial}{\partial x}\left(\nu^h \frac{\partial w}{\partial x}\right) + \frac{\partial}{\partial z}\left(\nu^v \frac{\partial w}{\partial z}\right) - g \tag{2.3}$$

These equations are solved in time t and along directions x and z. The horizontal and vertical velocities are represented by $u(x,z,t)$ and $w(x,z,t)$. The water pressure is separated into a hydrostatic part p_h and a non-hydrostatic part p_{nh}. ν_h and ν_v are the horizontal and vertical eddy viscosity and g is the gravitational acceleration. The free-surface is expressed by:

$$\frac{\partial \zeta}{\partial t} + \frac{\partial}{\partial x}\int_{-d}^{\zeta} u dz = 0 \tag{2.4}$$

For a more comprehensive description of the model see Appendix B.

To create a SWASH input file, firstly a computational and a bathymetry grid have to be generated. Then initial and boundary conditions have to be defined. Usually the offshore boundary condition of coastal models includes a wave maker to send waves into the domain. By adding commands several physical parameters can be defined, like friction, wave breaking and viscosity parameters. The numerical methods are determined afterwards. Several schemes can be chosen for the approximation of non-hydrostatic pressure, space discretisation and time integration. The points in space and time for output are defined including a request for the required output. Finally the compute command starts the simulation after begin time, time step and end time are given.

2.3 Coastal dynamics

Waves can be described to be vertical disturbances of the mean water level. Waves can be ordered by their period and wave length. In coastal waters the periods of interest range from a few seconds for wind waves to approximately one day for tides, corresponding wave lengths vary between a couple of metres to thousands of kilometres (Holthuijsen, 2007). In Subsection 2.3.1 the generation of wind waves and transformation when propagating into shallow waters will be described. Subsection 2.3.2 will describe the tide,

which is encountered in the area of interest. Generation of the tide will only be touched upon briefly because it is outside the scope of this thesis. Subsection 2.3.3 will elaborate on alongshore currents and its forcing terms. Finally, Subsection 2.3.4 will discuss instabilities and eddies which occur in the surf zone when currents are present.

2.3.1 Wind waves

Waves generated in storm fronts are called wind waves or storm waves and typically have a period ranging 2-20s. A distinction can be made between sea waves and swell waves by the distance the waves have travelled before reaching the coast. Sea waves are generated in storms close by and are characterised by an irregular, energetic climate with short wave periods. Swell is generated in storms far away (thousands of kilometres) and has travelled over long distances. Due to frequency and direction dispersion it is generally more regular, less energetic and has a longer wave period. A combination of sea and swell waves is possible, which can be observed along the Holland coast.

Waves propagating from deep into shallower waters will pass several regions before reaching the beach, namely the shoaling zone, breaker or surf zone and run-up or swash zone (see Figure 2.2).

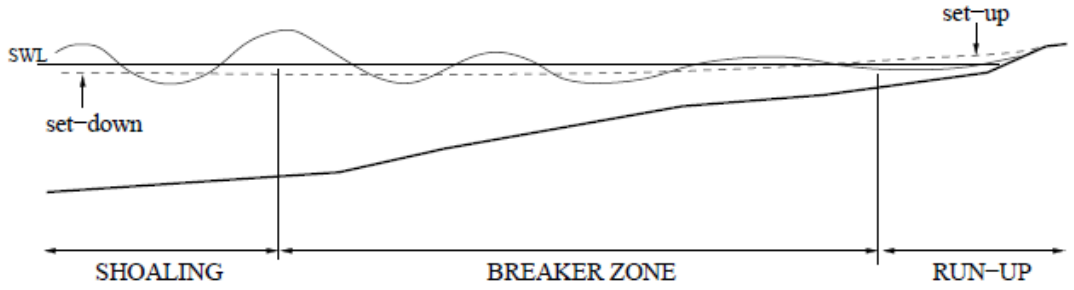

FIGURE 2.2: Nearshore zones (Stelling and Zijlema, 2010)

From the moment that water depth is approximately half the wave length, waves start to be affected by the bottom and will subsequently transform. In this shoaling zone waves will slow down and consequently become shorter. This results in a concentration of wave energy and thus an increase in wave height, which is called shoaling. Differences in water depth and wave speed also occur along a wave crest. Therefore the crest has a higher velocity at the deeper water depth, resulting in waves turning towards shore-normal. Consequently wave energy is accumulated or spread, leading to changes in wave height. This phenomena is called refraction. Due to a combination of shoaling and refraction, waves get higher, shorter and thus steeper. When the wave front becomes too steep waves start breaking, resulting in energy loss. The energy balance for a wave field is

described by the following formula:

$$\frac{\partial E}{\partial t} + \frac{\partial}{\partial x}(Ec_g cos\theta) + \frac{\partial}{\partial y}(Ec_g sin\theta) = S - D \tag{2.5}$$

in which S and D describe source and dissipation terms, c_g is the group velocity, θ is the angle of incidence and E is the wave energy given by:

$$E = \frac{1}{8}\rho g H^2 \tag{2.6}$$

When waves get into shallower water they get more nonlinear influences. The first nonlinear contributions can be subscribed to the difference interaction between wave components (bound sub harmonics or infragravity waves) and the sum interactions of the components (bound super harmonics) which are observed as skewness and asymmetry in waves. Together with the linear wave components these sub and super harmonics are described by the second order Stokes wave theory (Herbers and Burton, 1997).

Equation 2.7 presents the cross-shore momentum balance. It is obtained from Svendsen (1984) and is based on the 1D, depth integrated, time averaged, cross-shore momentum balance (Longuet-Higgins and Stewart, 1964). These simplifications, including the use of radiation stress, are not made in SWASH, but suit the purpose of describing the physical processes well.

$$\underbrace{\frac{\partial S_{xx}}{\partial x}}_{\text{wave forcing}} = - \underbrace{\rho g h \frac{\partial \zeta}{\partial x}}_{\text{water pressure}} - \underbrace{\tau_b}_{\text{bottom shear stress}} \tag{2.7}$$

S_{xx} = radiation stress of x-momentum in x-direction

$\frac{d\zeta}{dx}$ = cross-shore water level gradient

τ_b = bottom shear stress

Equation 2.7 describes the balance between wave forcing which is counteracted by a water pressure gradient and bottom shear stress. A limitation of this formula is that the water pressure term is uniform over depth, whereas wave forcing and bottom shear stress are definitely not. Currents perpendicular to the coastline are called cross-shore currents. As above equations are depth averaged, the vertical profile of the cross-shore current can not be modelled with above equations. Above wave trough level a net onshore mass flux is observed due to wave forcing. Due to continuity this flux has to be countered by a mass flux below wave trough level. This flow is the so called undertow. The result is a circulation inside the surf zone.

2.3.2 Tide

Tide is the periodic rising and falling of sea levels induced by the gravitational pull of sun and moon combined with rotation of the earth. The difference between high tide and low tide is called the tidal range and depends on the volume of water adjacent to the coast, and the geography and bathymetry of the basin the water is in. Typically the tidal period is approximately 12 hours (semi-diurnal tide) or 24 hours (diurnal tide). The vertical rise and fall of water level can induce horizontal velocities, which are called tidal currents.

Since the tidal movement is deflected by Coriolis it tends to circle around a node which is called an amphidromic point. As the Coriolis deflection is to the right in the Northern hemisphere counterclockwise rotating systems appear in the North Sea basin. Figure 2.3 shows that an amphidromic point is located approximately 50 kilometres from Egmond. Due to this location relatively strong alongshore velocities are driven by the tide. Near Egmond aan Zee a semi-diurnal tide can be observed with a tidal range varying from 1.4m and 2.1m, corresponding tidal currents are up to 1m/s.

When neglecting terms which are irrelevant for a long tidal wave propagating along a coast the alongshore momentum balance reduces to equation 2.8. It can be seen that forcing, the alongshore water level gradient, is balanced by inertia and friction. In deep water friction can be neglected, whereas in shallow water inertia can be neglected (Bosboom and Stive, 2012).

$$\underbrace{g\frac{\partial \zeta}{\partial y}}_{\substack{\text{alongshore water} \\ \text{level gradient}}} = \underbrace{-\frac{\partial v}{\partial t}}_{\text{inertia}} \quad \underbrace{-\frac{c_f v|v|}{h}}_{\text{friction}} \tag{2.8}$$

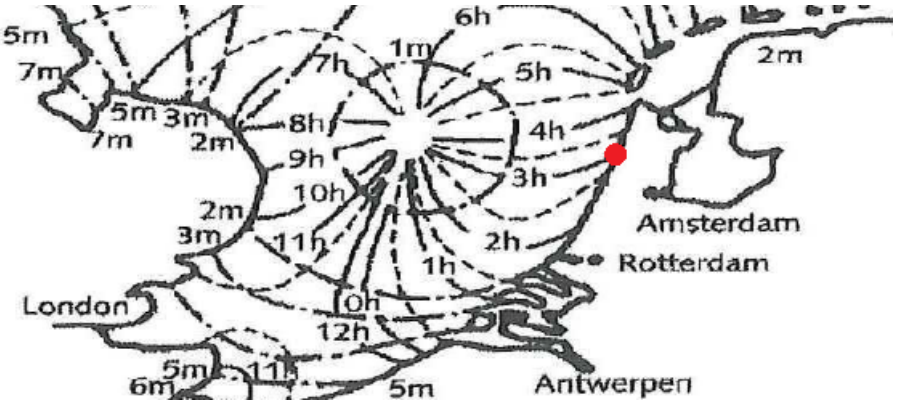

FIGURE 2.3: Amphidromic system in the North Sea (Bosboom and Stive, 2012), red dot indicates Egmond aan Zee

2.3.3 Alongshore currents

Currents which are directed parallel to the coastline are so-called alongshore currents. They are forced by waves, wind, tide or combinations of all three, balanced by bottom friction and spread over the surf zone by lateral mixing terms. Similar as with cross-shore currents the occurrence can be described by considering the 1D, depth integrated, time averaged, momentum balance. However, this time in alongshore direction. According to Ruessink et al. (2001) the momentum balance reads:

$$\underbrace{-\frac{1}{\rho}\frac{dS_{yx}}{dx}}_{\text{wave forcing}} + \underbrace{\frac{\tau_y^w}{\rho}}_{\text{wind forcing}} - \underbrace{gh\frac{d\zeta}{dy}}_{\text{tidal forcing}} = \underbrace{c_f\langle|\overrightarrow{u}|v\rangle}_{\text{bottom stress}} - \underbrace{\frac{d}{dx}\left(\nu\frac{d\overline{v}}{dx}\right)}_{\text{lateral mixing}} \tag{2.9}$$

S_{yx} = radiation stress of y-momentum in x-direction

τ_y^w = alongshore wind stress

$\frac{d\zeta}{dy}$ = alongshore water level gradient

c_f = friction coefficient

ν = eddy viscosity

Under certain assumptions, the cross-shore gradient of S_{yx} can be written just in terms of wave breaking roller dissipation D_r, wave celerity c and angle of wave incidence θ (Deigaard (1993); Reniers and Battjes (1997)).

Ruessink et al. (2001) investigated the COAST3D data set. The 1D approach proved to be good as long as the alongshore bathymetry was approximately uniform. From this study it followed that the roller energy and the eddy viscosity are important parameters for distributing the alongshore currents correctly in cross-shore direction (so the surf zone).

2.3.4 Surf zone vorticity

In absence of turbulence it is commonly assumed that the fluid motions under surface gravity waves are irrotational. Nevertheless, there is clear evidence of rotational motions inside the surf zone. These vorticity motions can be a result of shear instabilities, which result from shear due to gradients in alongshore velocity over the cross-shore direction (Bowen and Holman, 1989). Shear instabilities can be seen as periodic disturbances of the alongshore current.

Besides, Peregrine (1998) proposed another generating mechanism. Vorticity can be a result of short crested wave breaking, which results in vorticity around the tips of the wave crest (also possible for long-crested waves over a variable bathymetry). This can also be a result of variability in wave breaking due to temporal and spatial variability in wave groups (Reniers et al. (2004); Spydell et al. (2007)).

According to Long and Özkan-Haller (2009) the vorticity production due to shear instabilities and wave groups is of the same order of magnitude. All these vorticity motions contribute to mixing and dispersion, thus affecting the alongshore current distribution (Bühler and Jacobson, 2001).

Vorticity of a velocity field (u, v), can be calculated with Equation 2.10.

$$\Omega = \frac{dv}{dx} - \frac{du}{dy} \tag{2.10}$$

Chapter 3

Wave transformation

As formulae in Chapter 2 showed, currents in the nearshore are for a significant part induced by wave transformation. Therefore proper representation of waves is essential for subsequently being able to correctly model currents.

This chapter describes considerations regarding the model settings. The choices made were mostly concerned with making compromises between accuracy and computational time. On the one hand more layers, a finer grid resolution and longer simulation time result in more accurate results. The computational time, on the other hand, will increases with all options above. Keeping in mind that this model will be extended in alongshore direction later on, means that limiting computation time is an important aspect.

Section 3.1 will present the model approach. Hereafter, in Section 3.2 the general set-up for all simulations will be described. Section 3.3 discusses results and findings and finally conclusions on this research are drawn in Section 3.4

3.1 Model approach

A 1D [1]/2DV [2] model will be used to verify under which settings and conditions waves are modelled correctly. The direction of the computational and bottom grid is perpendicular to the coastline. At the seaward boundary, waves will be generated by a numerical wave maker. The waves will propagate towards the coast and for varying input it is investigated to what extent the transformation of waves into shallower water is modelled correctly. Runs will be performed using three wave climates, described in Table 3.1.

[1] 1D model: model with only one horizontal direction and depth averaged computations.

[2] 2DV model: two dimensional vertical model, so with just one horizontal direction and multiple layers.

Climate	Significant wave height [m]	Wave peak period [s]
Low wave climate	1.0	6.0
Medium wave climate	2.0	7.0
High wave climate	3.0	8.0

TABLE 3.1: Wave climates, imposed at the numerical wavemaker boundary according to a JONSWAP spectrum

Comparing unidirectional SWASH results with field measurements is difficult. On the one hand there is a lack of COAST3D data available with waves perpendicular to the coast. On the other hand alongshore processes like tide and wave driven currents and refraction will not be taken into account by the model, although they definitely influence wave transformation. Therefore it is decided to not compare wave model results with field measurement data, but instead with other simulations. Simulations will be performed with varying simulation time, number of layers, grid size, physical and numerical parameters. This to get insight in the performance and afterwards to determine settings for the subsequent current models.

3.2 Model set-up

The bottom profile of the main transect at 24 October of COAST3D experiment is used as bathymetry for the simulations. This is done to get a feeling of wave transformation over the double barred system. Waves, defined in Table 3.1, are introduced at the western boundary and propagate over the bathymetry through the model domain as can be seen in Figure 3.1. Numerical settings are discussed in Subsection 3.2.1. A description of the way the required simulation time is determined can be found in Subsection 3.2.2. The wave maker and boundary conditions are described in Subsection 3.2.3.

3.2.1 Numerical settings

Numerical settings used slightly differ from default SWASH settings and are adopted from Rijnsdorp (2015). Horizontal advective terms are considered to be strictly momentum conservative. Discretisations of the advective terms in the momentum equations are presented in Table 3.2. The use of the MUSCL limiter for the horizontal advective terms prevents generation of wiggles in case of steep gradients (Hirsch, 1988).

As recommended in the SWASH Manual, the vertical pressure gradient (so the non-hydrostatic pressure) is disretised by a Keller-box scheme. This results in accurate numerical dispersion when a few layers are used. The sensitivity of this setting was considered by also performing simulations with the alternative, standard discretisation.

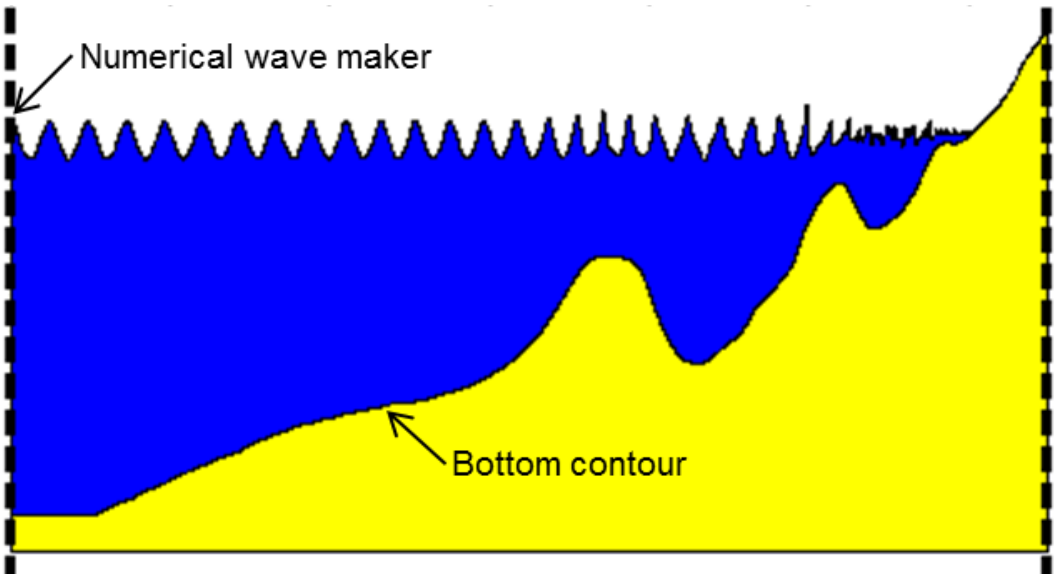

FIGURE 3.1: Schematisation of model set-up (horizontal and vertical scale are not similar)

Term	**Default SWASH**	**Adapted**
Horizontal advection of u/v-momentum	BDF	MUSCL
Vertical advection of u/v-momentum	FIRST	MUSCL
Horizontal advection of w-momentum	BDF	BDF
Vertical advection of w-momentum	FIRST	FIRST
Water level in velocity points	MUSCL	MUSCL

TABLE 3.2: Discretisation of advective terms. BDF: 2^{nd} order backward differences scheme; 1^{st} order upwind scheme; MUSCL: MUSCL limiter.

This did not result in a significant difference in outcome. Time integration is chosen to be explicit. This requires the use of a minimum and maximum Courant number. When one of these values is exceeded, the time step will be doubled or halved, respectively. This is done to prevent unnecessary high computational effort on the one hand and instabilities on the other hand. These values were set to 0.2 and 0.6.

3.2.2 Spin-up and simulation time

Total simulation time of a run is proportional to the computational effort of the computation. Simulation time can be divided in spin-up time and output time.

Due to lack of initial data, water levels and velocities at $t = 0$ in the domain are conditioned to be zero. Spin-up time is time necessary for waves to propagate through the entire domain and thus to obtain realistic water level and velocity values at all grid cells. The shoreward boundary will be reached by the waves at last, thus this location determines the required spin-up time before reliable output can be generated. Because

the beach near Egmond is characterised to be dissipative, it is assumed that it is not necessary to increase spin-up time to take reflected waves into account. The spin-up time is visualised near the shoreward boundary in Figure 3.2. From this figure it is concluded that a spin-up time of 10 minutes is sufficient.

Output time is the period during which output is generated. Output should be reliable and thus not disturbed by the above mentioned spin-up effects. Furthermore, output time should be long enough to produce an accurate spectrum with Fourier analysis. This depends on the physical processes to be considered. The scope of this particular study is short wave propagation, which requires approximately 300-500 waves to have travelled through the domain. With peak periods ranging 6 to 8s this leads to an output time of 50 minutes. Combined with spin-up, total simulation time will be 60 minutes.

The cycle time is the cyclic period of the time series synthesised by the numerical wave maker. It should be noted that cycle time should equal the output time. SWASH namely ensures that the imposed wave characteristics are correctly represented during one cycle. This is not necessarily the case when only part of a cycle is used to calculate wave characteristics. This is visualised in Figure 3.3 with a cycle time of 20 min. What can be observed is that the imposed wave height of 1m is only well represented when the output time is a multiple of 20 minutes.

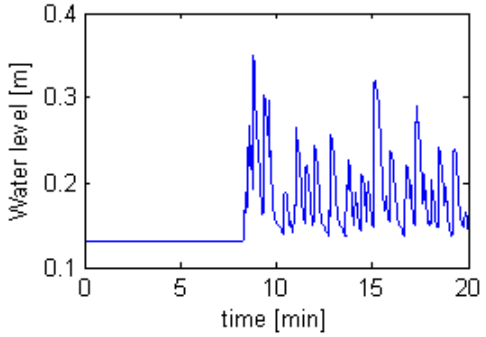

FIGURE 3.2: Indication of spin-up time

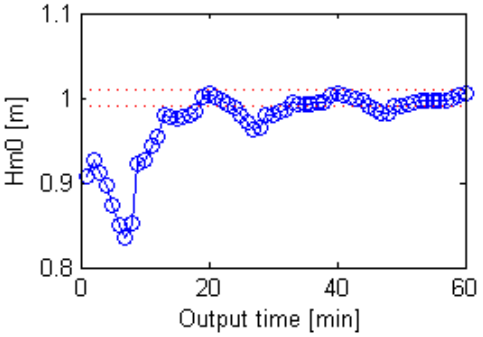

FIGURE 3.3: Wave height as a function of output time

3.2.3 Boundary conditions

At the shoreward boundary waves are created by means of a numerical wave maker. The requested JONSWAP spectrum is created by prescribing horizontal velocity components at the boundary according to weakly nonlinear wave theory (Rijnsdorp et al., 2014). A more extensive description of the wavemaker can be found in Appendix B.1.1. (Weakly) linear wave theory requires depth to be constant along the boundary and nonlinearity of the wave field should be small. Constant depth is taken care of by including a region

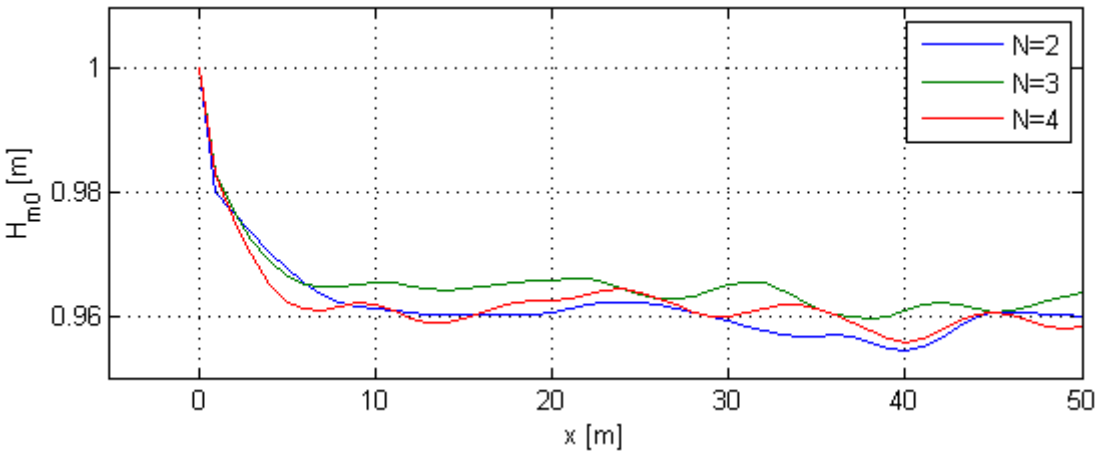

FIGURE 3.4: Error close to the boundary for $\Delta x = 0.5m$ and different number of layers

of constant depth at the wavemaker boundary side. Nonlinearity of incoming waves is quantified by the dimensionless Ursell number $N_{Ursell} = \frac{HL^2}{d^3}$. According to Holthuijsen (2007) the weakly nonlinear wave theory is applicable when $N_{Ursell} < 10$.

To be within the above mentioned applicability ranges of the Ursell number, a boundary depth of 10m is sufficient for low and medium wave climate. Because the higher wave climate results in too high nonlinearity, a depth of 10m is insufficient for the high wave climate. Therefore, the depth is increased to 15m. Horizontal distance from the wavemaker to the coast is determined by the depth at the boundary. The distance from the coastline to a depth of 10 and 15m is approximately 1100 and 1900m, respectively. With addition of a horizontal region near the wave maker and sufficient beach run-up length this leads to a domain length of 1300m for the low and medium wave climates and 2100m for the high wave climate.

Although the boundary wave height can be simulated really well by SWASH, a sudden drop in wave height occurs in vicinity of the boundary. Waves are generated by the wave maker by imposing horizontal velocities for every layer according to linear wave theory. The drop at the boundary probably has to do with the fact that waves are not according to linear wave theory and that the assumed vertical orbital velocity profile is not entirely correct. Consequently, within one wave length from the boundary, wave height decreases up to 5%, while the water depth is constant (see Figure 3.4). This error seemed to be insensitive to changes in grid size and number of layers. Dobrochinski (2014) encountered the same problem and his practical solution will be applied here as well. The drop has to be quantified after which a certain additional wave height should be applied in following runs to account for the sudden drop.

3.3 Model results

This section describes findings from model simulations within this research. First the number of layers and grid size is investigated in Subsection 3.3.1. A note on the proper representation of skewness and asymmetry of waves by the model is given in Subsection 3.3.2. Then the sensitivity of friction and wave breaking parameters is discussed. Finally, differences in set-up which were observed during the simulations are elaborated on in Subsection 3.3.5.

3.3.1 Number of layers and gridsize

To determine the required number of layers N and grid size Δx, to model wave transformation correctly, 24 runs were performed per wave climate (1, 2, 3, 4, 5 and 10 layers are considered for a grid size of 1m, 0.5m, 0.25m and 0.125m).

To determine the number of layers, comparisons were made between simulations with different number of layers and equal grid size. Spectral wave height and mean water level results, are compared to results from an accurate reference simulations with 10 layers and the same horizontal grid size. In Appendix D.2, it is shown that differences between a simulation with 10 and 20 layers are negligible. Therefore, it is assumed that using 10 layers for the reference simulation is enough. Differences were observed in wave set-up between model results with low and high vertical resolution (can be observed in the upper panel of Figure 3.5). These variations will be elaborated on in Subsection 3.3.5. Hence the comparison is limited to the pre-breaking region (shoaling zone). Resulting graphs and error metrics are presented in Appendix D.6. As an example, Figure 3.5 shows results for simulations with low wave climate and $\Delta x = 0.5m$.

As Figure 3.5 shows, depth averaged simulations ($N = 1$) show considerable deviation from all other runs. This is caused by the cut-off of evanescent wave components by SWASH (see Appendix B.1.3). To avoid this there are three options: reducing depth at the boundary, increasing wave period or using more layers. As first two options are unrealistic, more than one layer should be considered.

The purpose of this thesis is to investigate the accuracy of SWASH to predict currents. Besides, performing the simulations should be feasible for a company like Royal HaskoningDHV, therefore computational time is a limiting factor. Using more than two layers in 3D-mode complicates matrices to be solved by the model significantly and as a result computational time will increase more than linearly. Furthermore SWASH is successfully validated with 2 layers for predicting wave transformation (Zijlema et al., 2011),

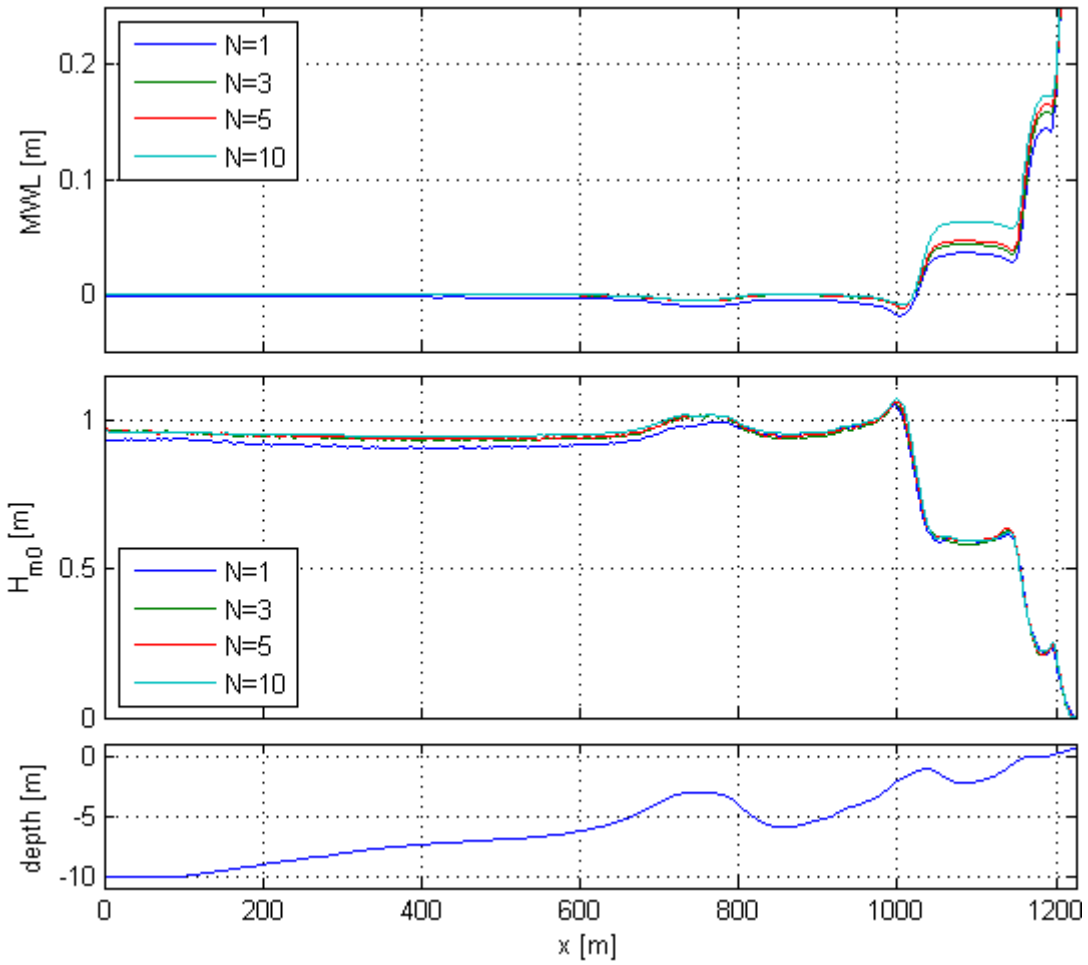

FIGURE 3.5: Mean water level, spectral wave height and bottom profile for comparison simulations for 1, 3, 5 and 10 layers.

breaking, set-up (Smit et al., 2014) and infragravity waves (Rijnsdorp, 2015). Additionally no significant differences were observed in the shoaling zone between simulations with 2, 3, 4 or 5 layers. So it is chosen to use two layers in the following simulations.

Grid size Δx is an important parameter as computational time in 3D simulations is inversely proportional to $(\Delta x)^3$. This is caused by the fact that both Δy and Δt are proportional to Δx. The dependency of Δt is due to the explicit time integration which is applied. The time step will be adjusted automatically by the model when the upper or lower Courant limit is reached. Because it was concluded above that using two layers is sufficient, only two layers will be considered to determine the grid size. So the required grid size is investigated by making a comparison between runs with varying grid size and 2 layers. As grid size is a sensitive parameter, determining computational time of future runs, additional simulations were performed with $\Delta x = 0.65m$ and $\Delta x = 0.80m$ with two layers. For all wave climates it is investigated how many grid cells per wave length lead to accurate results. Results and graphs are shown in Appendix D.8.

Instabilities were observed for a few runs with extremely fine grid size of 0.125m. However, successful simulations with 0.125m show negligible differences ($E_{RMS} = O(0.1mm)$) with simulations with 0.25m. Therefore it is assumed that considering 0.25m as the smallest grid size is valid. For validity of this assumption, see Appendix D.4.

From results, presented in Appendix D.8, it was observed that to obtain accurate wave height and water level predictions, a different grid size is required per wave climate. Final results can be found in Table 3.3. Waves with a longer period have a longer wave length. For longer waves a larger grid size suffices to get the same amount of grid cells per wave length. For all three wave climates approximately 75 grid cells per wave length are required. This is in accordance with the SWASH User Manual.

Wave climate	H_s [m]	T_p [s]	L [m]	Δx [m]	$L/\Delta x$ [-]
Low	1	6	50	0.65	77
Medium	2	7	60	0.80	75
High	3	8	80	1.0	80

TABLE 3.3: Grid size per wave climate

3.3.2 Skewness and asymmetry

Dimensionless skewness and asymmetry (Equations D.1 and D.2) are compared for several runs to verify if they are represented well with 2 layers and the above determined grid size.

Waves in deep water can be assumed to be linear waves. When these waves shoal towards the coast they get more nonlinear influences, which change the wave shape. The crest becomes narrow and peaked with a corresponding long and flat trough, this is called skewness. Besides the wave crest pitches forward as the wave crest propagates faster than wave trough. This asymmetry relative to the vertical axis is simply called asymmetry. Skewness and asymmetry are important parameters influencing wave breaking and currents, amongst other things. Therefore proper representation is essential.

Differences between simulations with varying model settings are small. Therefore, it is assumed that these settings suffice to correctly model skewness and asymmetry. Comparison graphs can be found in Appendix D.8.

3.3.3 Friction

The default setting in SWASH for bed friction is using the Manning formulation, which is based on depth averaged velocity. The Manning friction coefficient is derived from open

channel flow, similar as the Chézy coefficient, based on a more or less constant velocity in one direction. In a surf zone, velocity is far from constant and changes direction every couple of seconds. Therefore Manning is not very applicable to surf zone models. Another problem is that a combination of Stokes drift and undertow might lead to a near zero depth averaged velocity, while in reality an offshore directed current is present near the bed. As bottom friction is based on this depth averaged velocity, friction is underestimated.

As an alternative the LOGLAW command is used for friction. This means that the logarithmic wall law is applied, which depends on Nikuradse roughness height and local velocity, by assuming a logarithmic velocity profile over the vertical. For sensitivity to the roughness height see Appendix D.11. When the LOGLAW command is used, SWASH requires the use of the $k - \epsilon$ model for the vertical turbulent mixing. This enables spreading to above lying layers of diffusion and turbulence by bed friction.

Before inclusion of logarithmic wall law friction and turbulent mixing, instabilities were encountered at several runs. These instabilities were probably caused by a lack of diffusion between the layers. In that case the layers act individually and as a result large gradients occur at the layer interfaces. So using the logarithmic wall law brings the model closer to reality and additionally provides more stability. Other measures to overcome this problem are adding or increasing background viscosity at the layer interfaces or using a different, more dissipative numerical scheme for the advective terms. The last two options are more ad hoc solutions to fix the model than representing reality.

3.3.4 Wave breaking

When using few layers (e.g. 2 or 3), particle velocities near surface are underestimated, postponing waves from getting more asymmetrical and consequently delaying wave breaking (Smit et al., 2013). The built-in BREAK command can be used to control the onset and offset of wave breaking. The underlying idea is that when steepness exceeds value α the non-hydrostatic pressure contribution is set to be zero until steepness reduces below β. As pressure at the wave front is made hydrostatic this measure is called the Hydrostatic Front Approximation (HFA). A more detailed description of implementation in the SWASH model can be found in Appendix B.1.3. For these idealised simulations default α and β parameters performed pretty well. For sensitivity of the breaking parameters is referred to Appendix D.13. When differences appear between observations and simulations during calibration, the onset and offset of wave breaking should be controlled by these two parameters.

3.3.5 Set-up differences when waves are breaking

As described before, differences were observed between high (10 and 20 layers) and low vertical resolution (2 to 5 layers) models. With some wave breaking parameter calibration it is possible to match wave heights pretty well for runs with few and many layers. In mean water level predictions, on the other hand, clear differences were observed. Especially, behind the inner bar, when waves have just broken, a considerable difference in set-up is observed. The mean water level prediction for a 2 and 20 layer SWASH model is presented in Figure 3.6.

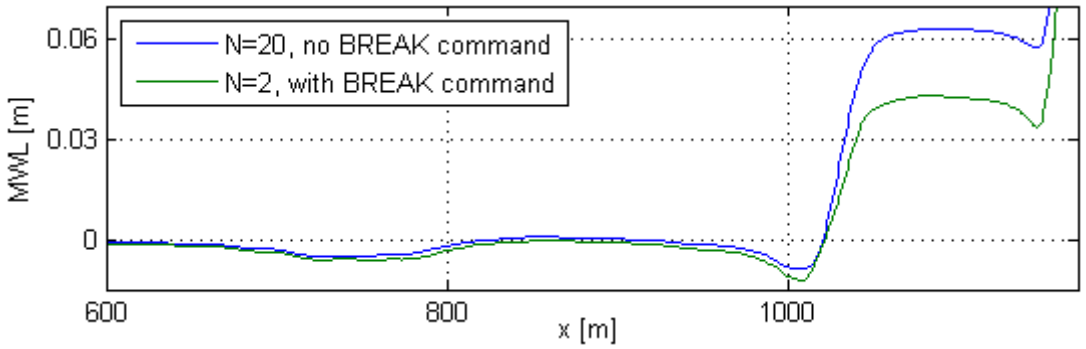

FIGURE 3.6: Mean water level prediction with 2 and 20 layers

It should be noted that when changing the number of layers, a comparison between both simulations is like comparing apples and oranges. A model with 20 layers is capable of producing a reasonable velocity structure over the vertical, whereas it is highly questionable whether a 2 layer model can do so. Furthermore, a low vertical resolution model needs the BREAK command to initiate and terminate wave breaking, which is not necessary when enough layers are applied.

Numerous tests were performed, including variation in friction, breaking parameters and numerical settings. Eventually a clear correlation was found between the time averaged non-hydrostatic pressure integrated over the surf zone and the set-up, shown in Figure 3.9. This led to the following explanation of the under predicted set-up for a low resolution model.

1. Different amount of layers, grid size and wave characteristics lead to a different local steepness calculated by SWASH. A larger grid size results in a steepness which is calculated over a longer distance. So peaks in steepness will be flattened out when grid size is to coarse, this is illustrated in Figure D.11. When using more layers, the dispersion relationship is solved more accurately. This means that more higher frequent components are taken into account, which influence the steepness. Additionally the higher waves lead to higher steepness.

2. The HFA is purely steepness induced. So when it is applied depends on above-mentioned model parameters. Proof for differences in steepness is given by Figure 3.7 which shows how often in time the Hydrostatic Front Approximation by the BREAK command is applied.

3. The non-hydrostatic pressure component is temporarily set to zero by the BREAK command when steepness is above a certain threshold value. As the HFA is only applied below wave crest level, only onshore directed impulse contributions are removed. See Figure 3.8.

4. Time averaged this leads to a resulting offshore directed force at locations where waves break. This resultant force leads to an under prediction of set-up.

As can be seen in Figure 3.9, set-up converges more quickly to the 10 and 20 layer set-up values for a coarse grid size (left panel) than a fine grid size (right panel). This can again be explained by the fact that peaks in steepness are flattened out with a coarse grid size and therefore the HFA is less frequently applied, reducing the resultant offshore directed force. However, wave breaking is less well represented.

Additionally, differences can be observed in calculated maximum set-up (for 20 layers) between coarse and fine grid size. Differences are minor between $\Delta x = 0.25m$ and $\Delta x = 0.5m$, whereas $\Delta x = 1m$ deviates significantly. The main difference with $\Delta x = 1m$ can be attributed to a significantly larger drop at the boundary wave maker (see Figure D.12). This clear difference in wave height prediction undoubtedly influences the set-up, making it hard to make a good comparison. Minor differences can be explained by (a combination of) the following phenomena:

- It was clearly shown that the breaking parameters should be grid size dependent due to the steepness. Until now they were chosen independent of the grid size, so differences occurred in wave height and thus set-up prediction.

- Steepness, namely ka, is a term in the non-linear dispersion relationship, described by: $\omega^2 = gk(1+(ka)^2)$. Therefore, it is quite plausible that differences in steepness lead to differences is non-linear contributions. These might affect wave transformation and set-up.

The main topic of this thesis is on alongshore currents. Therefore, the effect of the differences in non-hydrostatic pressure and set-up on the alongshore forcing are investigated. As can be seen in the radiation stress formulations of Holthuijsen (2007) (Equations C.1 until C.6), the dynamic pressure is present in S_{xx} and S_{yy}. That is the reason why it clearly influences set-up. It is assumed, however, that forcing in alongshore direction is not considerably influenced when the bathymetry is approximately alongshore uniform.

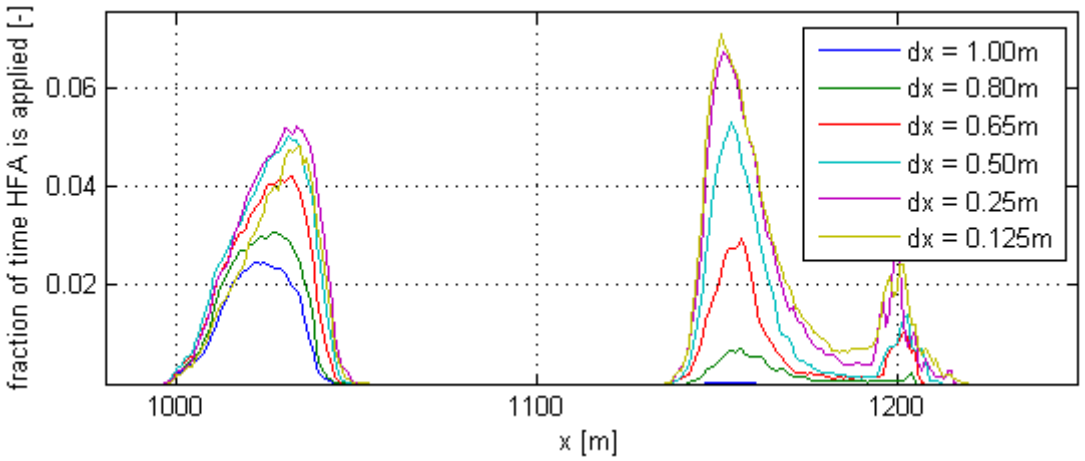

FIGURE 3.7: Percentage of time HFA is applied for simulations with 2 layers and varying grid size

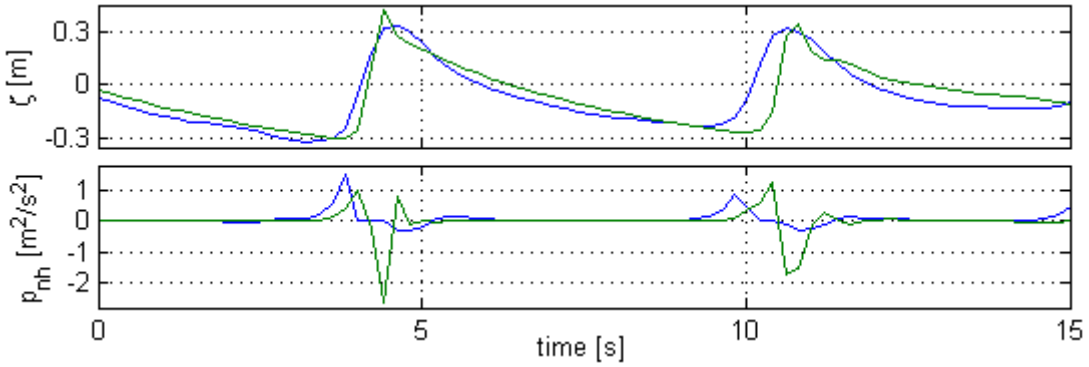

FIGURE 3.8: Cut-off of onshore directed impulse due to HFA approximation under breaking waves (Blue line = 2 layer model and green line = 20 layer model)

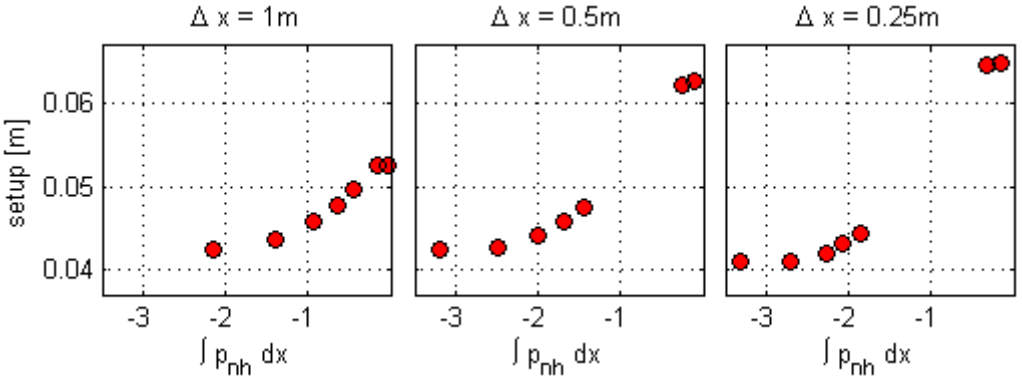

FIGURE 3.9: The correlation between set-up and the non-hydrostatic pressure integrated over the surf zone for a grid size of 1m, 0.5m and 0.25m. From left to right the dots represent: 2, 3, 4, 5, 6, 10 and 20 layers.

3.4 Conclusions

The goal of this chapter was to get insight in model behaviour and to determine which model settings are necessary to simulate wave propagation correctly. Main findings are summarised below:

- Simulation time is the sum of spin-up time and output time. Spin-up time is the time necessary for water levels and velocities to develop through the entire domain before output can be generated. This time depends on the domain length, group speed and thus depth. For the considered cases a simulation time of 60 minutes is sufficient. This time is split into 10 minutes of spin-up time and 50 minutes to generate sufficient output.
- To satisfy requirements of the weakly nonlinear wavemaker, nonlinearity should not be too high at the boundary. This can for instance be determined with the Ursell number, which should be below 10 for weakly nonlinear wave theory. The offshore boundary depth will be at 10m for the low and medium wave climate and 15m for higher wave climates. This results in a horizontal model length of 1300m and 2100m respectively.
- To counteract the sudden drop in wave height in vicinity of the offshore boundary a initial over-height should be added to the inputted wave height.
- The minimal depth at the offshore boundary requires a minimum of two layers to be applied in surf zone simulations to prevent energy cut-off due to evanescent modes and to accurately solve the dispersion relationship. So two layers will be used because this is sufficient to properly model wave propagation. Besides, using more layers would result in too long computational time.
- For all wave climates, approximately 75 grid cells per peak wave length proved to be sufficient to accurately model wave transformation.
- Friction will be according to logarithmic wall law based on local velocities. Furthermore vertical eddy viscosity will be calculated using the k-ϵ model. These settings are more realistic than default SWASH settings and additionally provide more stability.
- The moment that waves start and stop breaking can be calibrated with wave breaking parameters α and β. Results in very shallow water (<1m) can be calibrated with the friction parameters, outside this area friction has negligible influence.
- The steepness calculated by SWASH depends on the used grid size. Therefore breaking parameters α and β do not only depend on the number of layers, but

also on the grid size. These parameters should be calibrated for the number of layers and grid size which are used.

- The locally applied Hydrostatic Front Approximation below wave crests results in a cut-off of onshore directed impulse. This eventually results in under predicting the set-up. This under prediction depends on how frequently the HFA is applied, thus on number of layers, grid size, wave climate and the breaking parameters.

Chapter 4

Wave induced alongshore current

This chapter focuses on model settings and parameters to properly model the alongshore current forced by waves. Furthermore, sensitivity to certain physical parameters will be investigated in this chapter. The same will be done in Chapter 5, but then for tidal forcing. Subsequently, settings derived from these two chapters will be used for calibration and validation simulations in Chapter 7.

In Section 4.1 the model approach for the above mentioned research is described, hereafter Section 4.2 shows the general model set-up for all simulations. Section 4.3 will present the modelling results and finally main conclusions are summarised at the end of this chapter.

4.1 Model approach

To investigate alongshore currents, a 3D model is applied. This means that more physical processes are taken into account and more model parameters have to be considered with respect to previous modelling. To only check on the influence of wave induced currents, no other forcing terms will be applied. An alongshore uniform bathymetry is used to preclude effects due to alongshore non uniformities. Most effects are investigated under constant wave conditions ($H_{m0} = 1m$, $T_p = 6s$, $\theta = 20°$ and $\sigma_\theta = 20°$). However to check on the sensitivity of wave input also variation in wave conditions is considered. These variations can be found in Table 4.1.

Significant wave height and peak period	1m and 6s, 2m and 7s
Direction	10°, 20°, 30°
Directional spreading	0°, 10°, 20°, 30°, 40°

Table 4.1: Variation in wave climates

In Chapter 3 the required model settings and performance were investigated for wave propagation and transformation with only one horizontal dimension. These results are used in following 3D models. Besides, there are 3D model settings (e.g. alongshore domain length, grid size) which should be considered as well before calibration and validation simulations can be performed. This is the first study which is conducted in this chapter. Afterwards sensitivity of friction and mixing parameters will be investigated.

4.2 Model set-up

To obtain an alongshore uniform bathymetry, the main transect, which was used in the 1D simulations, is extended in alongshore direction. Changes in numerical settings and elaboration on spin-up and simulation time can be found in Subsections 4.2.1 and 4.2.2. The numerical wavemaker is again located at the west boundary and the lateral boundaries are so called cyclic boundaries. These are described in more detail in Subsection 4.2.3.

4.2.1 Numerical settings

Similar numerical settings are used as described in Subsection 3.2.1. The only difference is that the Smagorinsky subgrid model is added for horizontal mixing (Smagorinsky, 1963). This adds horizontal exchange of momentum to the large scale flow motions and is a function of gradients in the velocity field (Smit et al., 2010). The influence in regions with non breaking wave propagation is negligible. However, more exchange of momentum is added where waves are breaking. This is beneficial to compensate for the lack of turbulence due to wave breaking, which is not included in the present SWASH model.

4.2.2 Spin-up and simulation time

Water level and orbital velocity signals only need a few waves to develop into realistic values, hereafter output can be generated. Time averaged currents like the wave driven alongshore current need a longer period to develop into a sort of steady state. From test simulations it was concluded that a spin-up time of 20 minutes suffices.

As already mentioned above, time averaged currents have larger time scales than short waves. Therefore the output time should be increased as well. The alongshore current varies on the time scale of shear instabilities, which have time scales of a couple of minutes . Preferably one would want to include at least one hundred times the considered

physical phenomenon to obtain good time averaged results. As it would require a lot of computational effort this is not feasible. To keep computational effort within reasonable limits it is decided to use an output time of 60 minutes. It should be noted that due to this limitation, model results can give slightly different results when comparing locations in the model domain, as results are not fully developed in time.

4.2.3 Boundary conditions

Irregular waves will be imposed at the western boundary, according to a JONSWAP spectrum created with bulk parameters (see Table 4.1). A cyclic boundary condition is applied for the northern and southern boundaries to allow for alongshore currents to occur without using an exceptional long domain. To satisfy continuity, water level and velocity signals will be copied from one boundary to the other and thus be similar at both boundaries. In this way a northerly directed current will be introduced at the southern boundary again when leaving the domain in the north, and vice versa. An additional advantage is that the short wave signal leaving the northern boundary will also be copied to the south. This means that the southern boundary also behaves like a wavemaker, which reduces the required alongshore model length.

4.3 Model results

During this study model simulations were performed to get insight in performance of the model under varying settings and parameters. In Subsection 4.3.1, the required alongshore domain length is determined, which depends on a number of factors. Secondly, required grid size is investigated in Subsection 4.3.2. Finally, Subsections 4.3.3 and 4.3.4 elaborate on the sensitivity of wave direction, spreading, bottom friction and mixing.

4.3.1 Alongshore domain length

Computational time is proportional to the alongshore domain length, which is thus an important parameter. On the one hand, it should be long enough to properly represent wave propagation and for an alongshore current to develop. On the other hand, as Equation 2.9 shows, the alongshore current is mainly driven by gradients in cross-shore direction, certainly with an alongshore uniform bathymetry. So it is questionable whether a long domain is needed. That is investigated in this subsection according to four possible determining factors.

Runs were performed with alongshore domain lengths varying between 100 and 1000m. For an extra reference, model results are visualised in Figures E.1 until E.3.

1. **Alongshore refraction pattern length**:
   The direction of obliquely incident waves changes towards shore normal when approaching the coast. This phenomenon is called refraction. So wave crests turn towards the coast. According to Holthuijsen (2007), along a wave ray $sin(\theta)/c$ is constant, which is a form of Snel's Law. For the used bathymetry the refraction pattern (see Figure 4.1) is calculated for several angles of incidence. Figure E.3 shows that the order of magnitude of the alongshore current is similar for a domain length of 200m and 500m with $\theta = 30°$, although the alongshore length of the refraction pattern is longer. This is caused by the fact that waves leaving the northern boundary are imposed at the southern boundary, which operates as a proper wavemaker. Therefore it can be concluded that the alongshore refraction pattern length does not determine the required alongshore domain length.

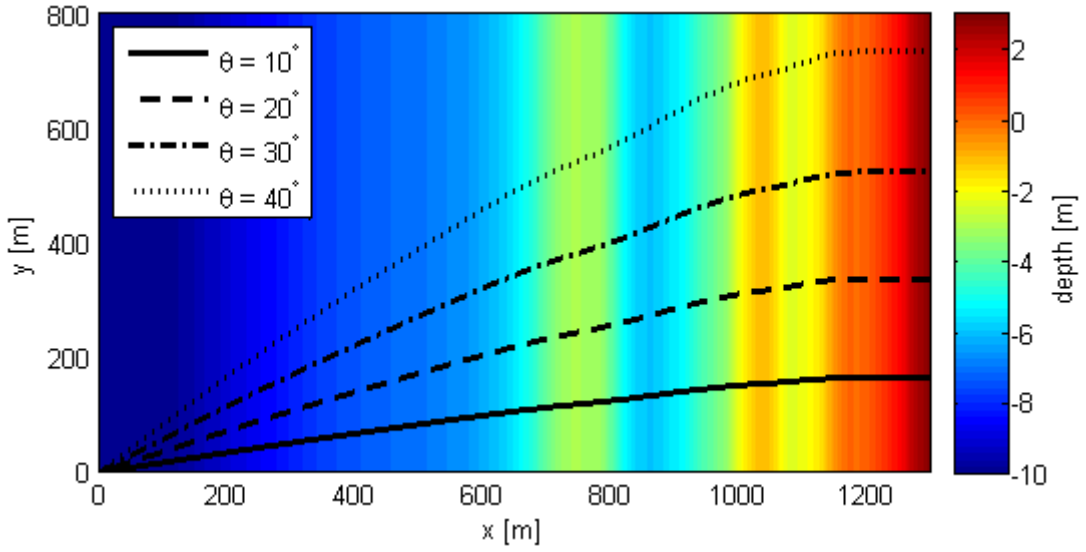

FIGURE 4.1: Refraction pattern based on the alongshore uniform bathymetry for varying direction according to Snel's Law

2. **Possible number of directions**:
   The direction of imposed waves is randomly drawn by the numerical wavemaker according to a probability density function. This probability density function depends on the mean wave direction and directional spreading (Rijnsdorp, 2015). As mentioned before, cyclic boundary conditions require water levels to be equal at the northern and southern boundary for continuity reasons. This can only be ensured when the alongshore domain length is an integer multiple of the alongshore wave length. SWASH changes the incoming direction in such a way that the alongshore wave number, k_y is equal to the closest integer multiple of $2\pi/L_{y,domain}$

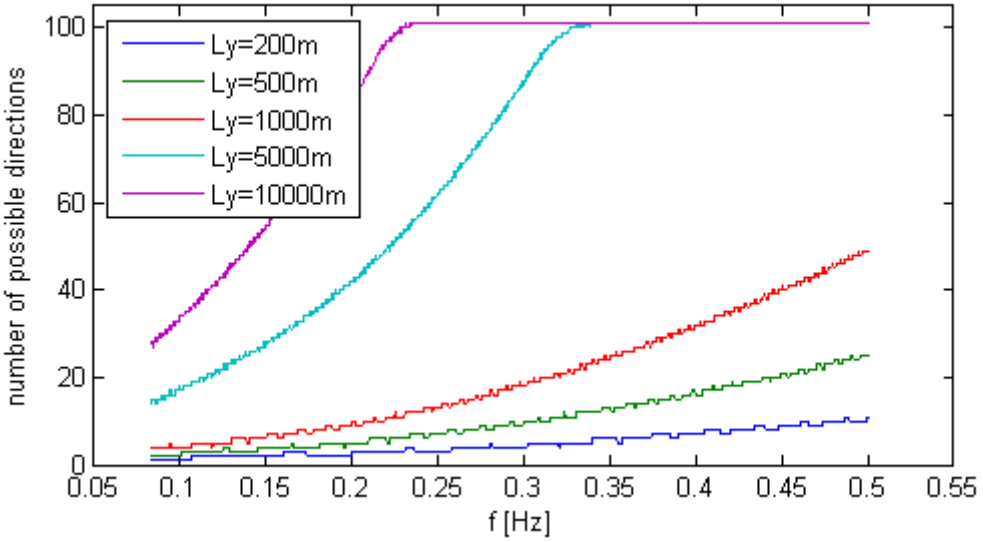

FIGURE 4.2: Number of possible directions for an introduced wave signal with $T_p = 6s$, $\theta = 30°$, $dd = 20°$ and varying alongshore domain length

(Van Dongeren et al., 2003). Although this does not change the overall wave direction considerably, some wave components are significantly affected. Long wave components, certainly under a small angle of incidence have a long alongshore wave length. When this length is larger or in the order of the alongshore domain length, all directions will be adjusted to one or a few directions. So a small alongshore domain length limits the possible number of directions for incoming waves.

To quantify this, the mismatch between imposed and modelled direction is determined. Besides the number of directions possible in SWASH per frequency for a given alongshore domain length is calculated. This is done for a wave with peak period $6s$, mean direction of 30° and directional spreading of 20°. For this study the direction is uniformly distributed in 100 values between 10 and 30° and frequencies between $f_p/2$ and $3f_p$. For all combinations of directions and frequencies the by SWASH adjusted direction is calculated. The error seems to be bigger for a shorter alongshore domain length, but also for smaller angle of incidence, mean direction and frequency, as can be concluded from Tables E.1 and E.2. Figure 4.2 shows the number of possible directions (out of 100) in SWASH per frequency for different alongshore domain lengths. It can be seen that with a limited alongshore domain length the low frequent terms, so longest wave components, all tend to have a rather limited amount of similar directions.

3. **Vorticity**:

   As explained before all sorts of instabilities occur which spread the alongshore currents trough the surf zone. To allow for these instabilities to develop and to influence the currents the model should be long enough, both in a temporal and

spatial sense. To analyse instabilities vorticity should be considered. Vorticity of a velocity field can be calculated with Equation 2.10. Figure 4.3 shows the vorticity in the surf zone at a certain moment. The eddies spread the currents through the surf zone. A simulation with regular waves and without directional spreading showed that SWASH is also capable of modelling shear instabilities as can be seen in Figure 4.4. Maximum length scales of the observed vortices were approximately 100m. This is considerably shorter than the alongshore domain lengths considered, so it is not a limiting factor.

4. **Alongshore non-uniformities**:
   It is important to also keep in mind that alongshore non-uniformities play a roll. Until now an alongshore uniform bathymetry is used. For the comparison with COAST3D data it is important that the currents pass by the actual bathymetry before reaching the measuring devices. So a certain alongshore distance with actual bathymetry should be present between the lateral boundary and the measuring devices. This length is assumed to be in the order of a few hundred metres.

Eventually, the possible number of directions is decisive for the alongshore domain length. To allow for some directional spreading (a few directions possible even for the low frequent components) it is decided to use an alongshore domain length of 1000m. The refraction pattern did not seem to influence model results and requirements from vorticity and bathymetry point of view were considerably smaller.

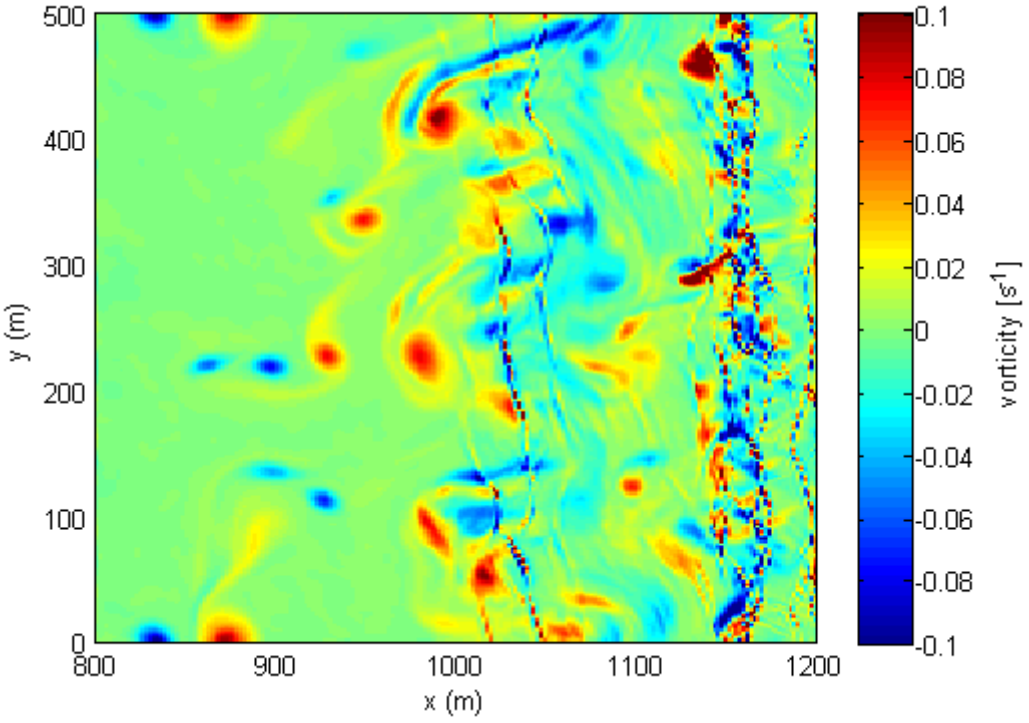

FIGURE 4.3: Vorticity in the surf zone with irregular waves and directional spreading

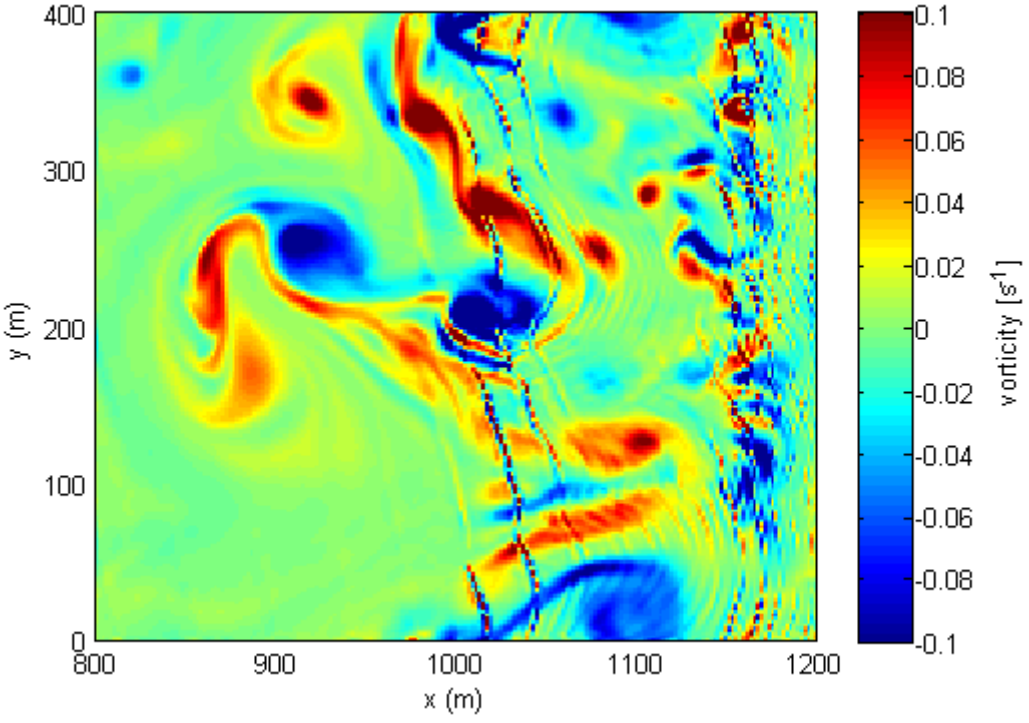

FIGURE 4.4: Vorticity in the surf zone with regular waves and without directional spreading

4.3.2 Grid size

In Subsection 3.3.1 the appropriate grid size was determined for simulations with one horizontal dimension. It was concluded that approximately 75 cells per peak wave length led to good results. For simulations with two horizontal dimensions, waves should be represented by a sufficient amount of grid cells both in cross-shore and alongshore direction. This depends on the cross-shore and alongshore wave length, described by: $L_x = L/cos(\theta)$ and $L_y = L/sin(\theta)$. So the number of grid cells per alongshore wave length should approximately be similar to the number in cross-shore direction. This is the case when the following criterion is satisfied: $\Delta x/\Delta y = tan(\theta)$.

To verify this theory and check on the sensitivity of the alongshore grid size, simulations are performed with $\Delta x = 1m$ and Δy varying from 1m until 4m. Wave height predictions in Figure E.4 show convergence for $\Delta y = 1.5m$ and smaller which is in agreement with the above mentioned criterion.

4.3.3 Wave direction and directional spreading

The wave direction influences the magnitude of the alongshore current. It follows from the radiation stress formulation, in equation C.9, that the wave forcing dS_{yx}/dx is proportional to $sin(\theta)$. The distribution of the alongshore current over the surf zone for waves incident under an angle of 10, 20 and 30° is shown in Figure 4.5. The influence of directional spreading on the alongshore current is less clear on the alongshore current, but does influence the instabilities. It is visualised in Figure E.5.

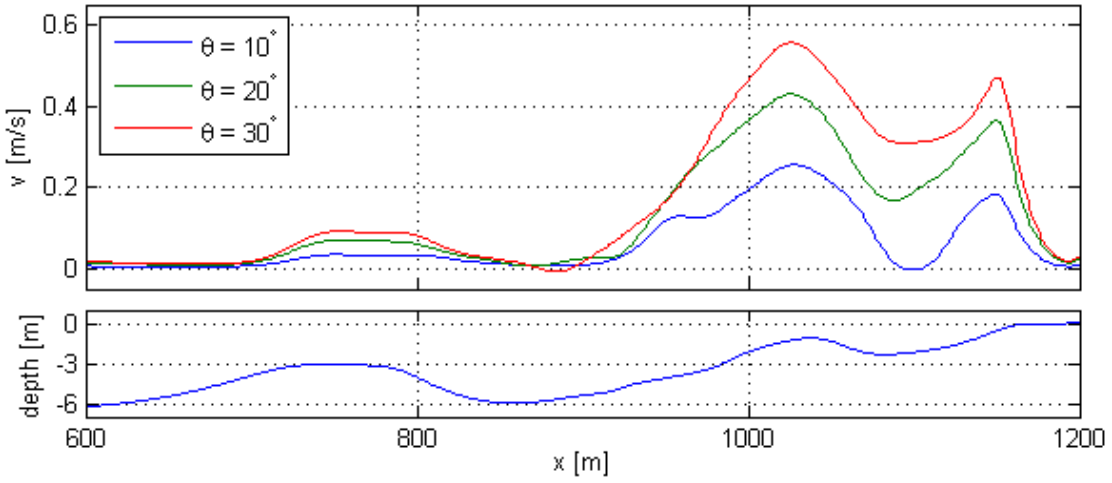

FIGURE 4.5: Alongshore current for different wave angles

4.3.4 Sensitivity to friction and mixing parameters

The only counteracting force in the alongshore momentum balance is bottom friction. Therefore this will be an important calibration parameter for the magnitude of the alongshore current. The logarithmic wall law friction formulation is used which depends on the Nikuradse roughness height. Sensitivity is investigated by varying the roughness height. As an initial value was chosen for 2.5 times the grain diameter. As $D = 300\mu m$, this results in a roughness height $k_r = 750\mu m$. Whereas it was shown in Subsection 3.3.3 that in the cross-shore the influence of friction was only visible in very shallow water, this is different in a 3D sense. The upper panel of Figure 4.6 shows the time averaged alongshore current distributed over the surf zone for a varying roughness height. What can be seen is that increasing the roughness height results in a decrease of velocities for the entire domain.

As described in Subsection 4.2.1 horizontal mixing is added with the Smagorinsky subgrid model. According to the SWASH manual the default value for the Smagorinsky constant is 0.2 and according to Smit et al. (2010) this value should vary between 0.1 and 0.3. To check on the sensitivity of this mixing parameter simulations were performed with values of 0.1, 0.2 and 0.3. The result of this parameter on the alongshore current can be seen in the middle panel of Figure 4.6. Whereas friction resulted in a increase or decrease of velocity in the entire domain, mixing does not. Increasing mixing means a reduction of peak velocities which are spreaded to the troughs.

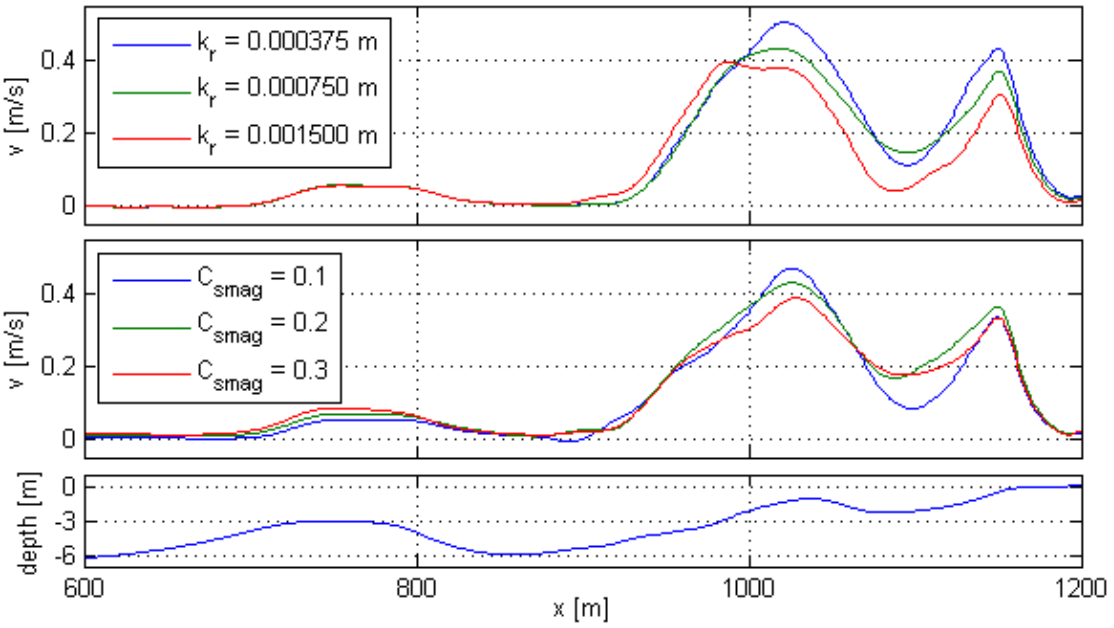

FIGURE 4.6: Sensitivity of the roughness height and mixing parameter on the alongshore current

4.4 Conclusions

- The required alongshore domain length does not depend on the alongshore length of the refraction pattern. The cyclic boundary functions as a wavemaker. Therefore refraction is correctly represented although passing through the lateral boundaries.
- Length scales of alongshore non-uniformities in bathymetry and surf zone vortices are maximum O(100m), so do not determine the alongshore domain length.
- Eventually, the number of possible directions for incoming wave components determines the alongshore domain length. This number is a function of the alongshore domain length and is limited when a small domain is used.
- It is decided to use an alongshore domain length of 1000m. In this way even the low frequent wave components have some directional spreading.
- To properly model wave transformation enough grid points per cross-shore and alongshore wave length should be used. 75 points per peak wave length should be enough. Using a similar amount of cells in x and y direction leads to the relationship $\Delta x/\Delta y = tan(\theta)$.
- Wave direction and friction influence the magnitude of velocities over the entire domain. Mixing results in spreading of velocities from the peaks to the trough.

Chapter 5

Tide induced alongshore current

In Subsection 2.3.2 it was described that an amphidromic tidal system is present in the North Sea. This induces alongshore tidal currents which are of the same order of magnitude as wave driven alongshore currents. Until now no function was implemented in SWASH to include these tidal currents. This chapter will describe the method to make it possible to include these currents.

The implementation of the tide in the SWASH source code is discussed in Section 5.1. Model experiments are defined in Section 5.2. Results are described in the next section. Finally, conclusions of this chapter can be found in Section 5.4.

5.1 Implementation

Including the tide in a wave-phase resolving model like SWASH is complex as temporal and spatial scales of tidal waves and short wind waves differ substantially. Until now, such a model application was never practised in such detailed modelling. This is probably because strong alongshore tidal velocities only occur in rare amphidromic systems like the North Sea.

To include the alongshore horizontal tide, several options were considered. Firstly, an initial flow field was introduced. As there was no driving force velocity damped out in time. Then it was considered to add a velocity as a lateral boundary condition at the south. As this velocity would for a significant part flow out of the domain in the north, it would be added again in the south. This would eventually lead to an accumulation and thus a too high velocity.

According to Ruessink et al. (2001), the tide can be modelled by including a time averaged alongshore water level gradient in the y-momentum balance as a driving force

(See Equation 2.9). However, an alongshore water level gradient causes a water level difference between the northern and southern boundary. This is in conflict with continuity for the cyclic boundary condition, which was found to be needed in the previous chapter.

Eventually a new term was introduced in the alongshore momentum balance. It provides a similar pressure gradient as would result from a water level gradient, but without the actual water level gradient. The pressure term in the alongshore momentum balance in the standard SWASH version is described by:

$$\frac{1}{\rho}\frac{\partial(p_h + p_{nh})}{dy} \tag{5.1}$$

This has been extended to:

$$\frac{1}{\rho}\frac{\partial(p_h + p_{nh})}{dy} + \frac{1}{\rho}\overline{\frac{\partial p_{tide}}{dy}} \tag{5.2}$$

The extra term adds the pressure gradient induced by the time averaged alongshore water level gradient (due to tide) to the momentum balance. This pressure gradient results in a velocity similar to that which would have been induced by an actual alongshore water level gradient. Because the time over which output is generated is small compared to the tidal period it is assumed that taking the alongshore water level gradient due to the tide constant over the simulation period is reasonable.

This option can be switched on in SWASH by defining the time averaged alongshore water level gradient in the input file. A time averaged water level gradient is imposed, whereas it will not actually be present in the model. Therefore, it is from now on referred to as the pseudo alongshore water level gradient. For the implementation in the SWASH source code is referred to Appendix F.

5.2 Model approach

To verify whether the above mentioned pseudo alongshore water level gradient leads to satisfactory and reliable results, a number of test experiments are performed. All experiments are performed with 2 layers. However, changing this does not influence results because forcing is identically implemented for every layer as tidal currents are assumed to be vertically uniform.

1. The effect of this forcing term is considered in a closed basin of $100x100m$ without any other forcing terms.

2. The velocity as a result of the forcing is considered in an open channel with constant depth and friction according to Chézy. This will be done with and without additional wave forcing.

3. For a number of realistic gradients, obtained from COAST3D measurements, the effect on the velocity field over the actual Egmond bathymetry will be investigated. Besides, spin up time and initial values will be determined.

5.3 Model results

5.3.1 Closed basin

The behaviour of the pseudo water level gradient is investigated in a closed basin without other forcing terms. It is expected that eventually the water level gradient in the basin will match the inputted pseudo gradient of 10^{-5}. As can be observed in Figure 5.1, for all simulations the mean gradient is predicted correctly by the model. The time for the water level to converge to a steady state depends on the dissipation due to friction and the initial water level gradient. In absence of dissipation, which is the case for a water depth of 5m the water level will oscillate around the equilibrium value without convergence (yellow line). When the water depth is reduced, the water movement starts feeling the bottom, resulting in dissipation. This leads to faster convergence towards the equilibrium (light and dark blue lines). When an initial gradient is introduced at $t = 0$, the water level remains steady at this equilibrium value. So it can be concluded that the mean water level is exactly predicted as expected by the pseudo gradient. The convergence rate increases with increasing dissipation. As much more dissipating mechanisms are present in a coastal area than in this idealised basin, this will probably not be a problem.

5.3.2 Open channel flow

To verify whether the pressure gradient leads to the expected flow velocities, an open channel is considered with a Chézy friction formulation. Again the only forcing is the pseudo water level gradient in longitudinal direction, which will be balanced by the friction. To simulate an infinitely long channel, a cyclic boundary condition will be applied for the open boundaries.

Figure 5.2 shows the evolution of the velocity in the channel as a function of time. What can be observed is that velocity and Chézy equilibrium velocity, calculated by $v = C\sqrt{hi}$, match quite well. Initially instabilities occurred, they can be subscribed to

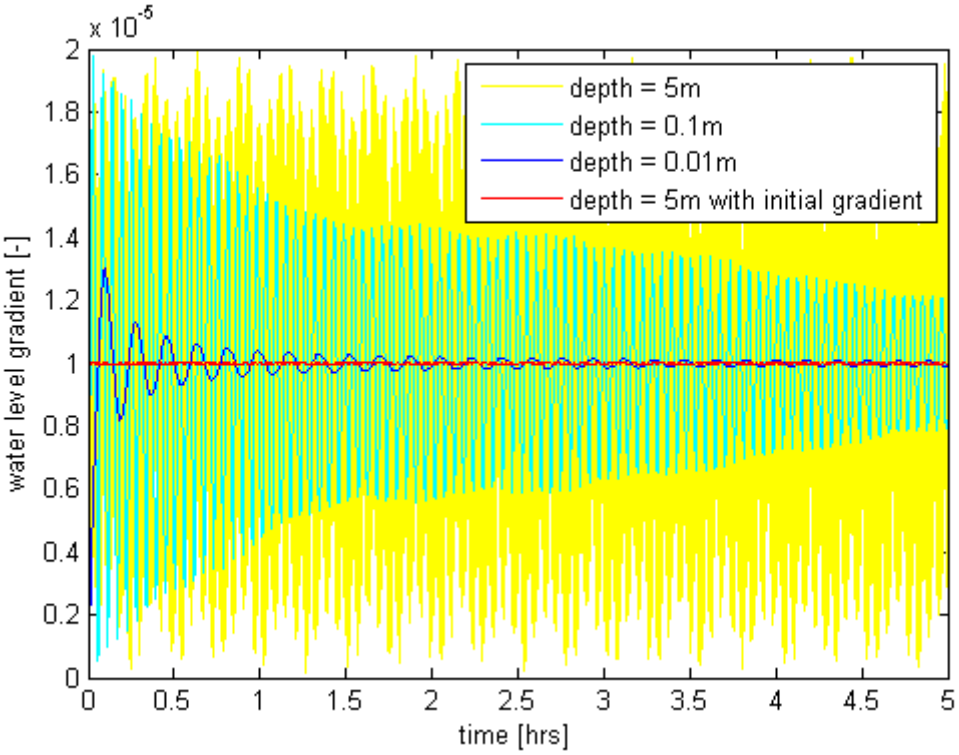

FIGURE 5.1: Water level in the main transect of a closed basin with only the pseudo water level gradient forcing

the lack of dissipation for minor disturbances in water level which can freely propagate through the cyclic boundaries and grow (see Figure G.2). By adding monochromatic waves perpendicular to the current as a dissipating mechanism this problem was resolved as can be seen in more detail in Figure G.2.

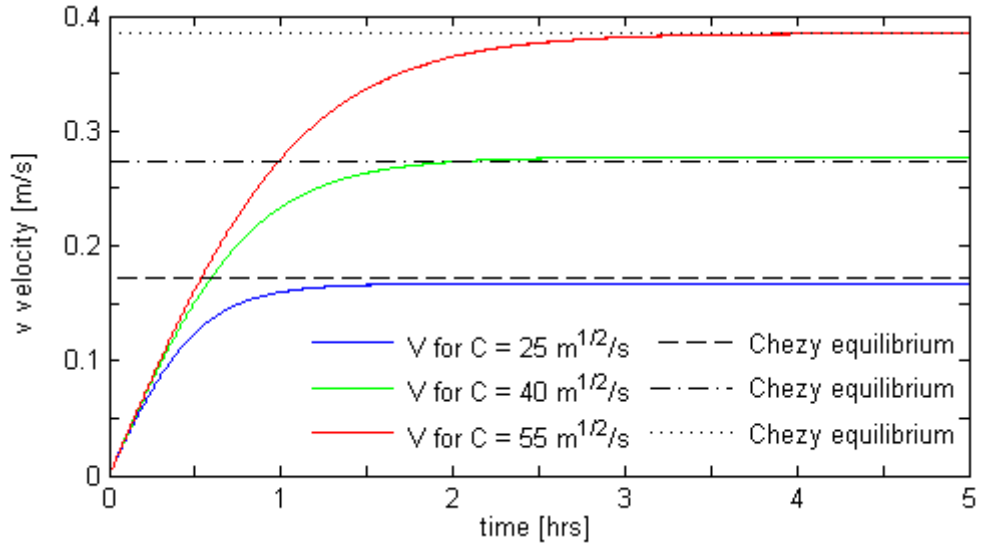

FIGURE 5.2: Flow velocity through an open channel as a result of the pseudo water level gradient for different Chézy values and their corresponding equilibrium velocity

5.3.3 Egmond bathymetry

Previous experiments showed the capability of the pseudo gradient to add a pressure gradient to the alongshore momentum balance which results in an alongshore current. In this study the influence of the parameter will be investigated with the alongshore uniform bathymetry. The maximum occurring time-averaged alongshore water level gradient due to the tide is $2 * 10^{-5}$ (Ruessink et al., 2001). For this case the response of the system to forcings between $5 * 10^{-6}$ and $2 * 10^{-5}$ will be studied.

For all cases, the equilibrium flow after five hours is visualised in Figure 5.3. What can be seen is that the equilibrium flow is depth dependent and will be lower for lower water depth due to bottom friction influences. In Appendix G the equilibrium velocities for varying alongshore gradients are plotted as a function of the local water depth in Figure G.4.

From simulations it was concluded that it took almost 5 hours for the tidal velocity to build up to equilibrium velocity. This is a multitude of the spin-up time considered for waves and wave driven currents. The solution provided for this problem is using an initial velocity field. This initial velocity field is estimated with Equation 5.3 and 5.4, which are retrieved from the Unibest model from (Bosboom et al., 2000). They are based on local water depth and roughness height which is used in the model.

$$\overline{v_{tide}} = C\sqrt{h\frac{dh}{dy}} \tag{5.3}$$

$$C = 18log(\frac{12h}{k_r}) \tag{5.4}$$

Results with an initial velocity field led to a considerable spin-up time reduction to approximately 20 minutes. This is similar as was found for wave driven currents. In Figure G.4, it is shown that this estimation is accurate to predict the equilibrium velocity.

5.4 Conclusions

Key findings of this chapter are listed below.

- To allow for tidal alongshore currents to flow through a coastal domain a new method is developed. The pseudo alongshore water level gradient is introduced and implemented in the SWASH source code. It adds a pressure gradient similar in size as would normally result from the water level gradient. This pressure gradient eventually leads to tidal velocities through the domain.

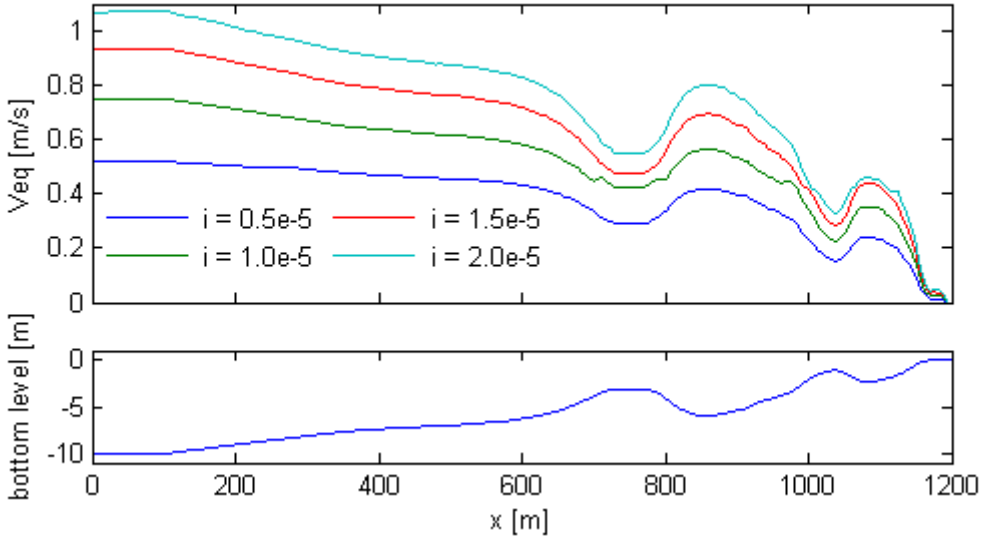

FIGURE 5.3: Equilibrium alongshore flow induced by varying pseudo water level gradient

- Experimental tests showed that this method is accurately capable of adding the correct pressure gradient and subsequent currents.
- To ensure stability, other forcing terms might be required for dissipation. Otherwise initial, small, water level disturbances might blow up the simulation.
- Spin-up times are in the order of hours, which is undesirably long. This time can be reduced by using an initial flow field based on an estimated tidal velocity to start the simulation.

Chapter 6

COAST3D case selection

This chapter describes the process of selecting COAST3D cases for calibration and validation. Requirements for the cases are described in Section 6.1. The method to obtain wave and tide input from the COAST3D data set is discussed in Sections 6.2 and 6.3. Subsequently, the cases which will be used are presented in Section 6.4. Finally, concluding remarks are given in Section 6.5.

6.1 Requirements

At first sight, it seemed easy to find useful cases for calibration and validation. During the process, however, it became clear that more requirements than expected were involved. These requirements are listed below.

- Firstly, alongshore non uniformities in bathymetry should be avoided as much as possible. This is to limit the alongshore domain length. Besides, this is necessary to make the assumption of Subsection 3.3.5 valid, that wave driven alongshore currents are mainly driven by $dSyx/dx$ compared to $dSyy/dy$. During the storm at the end of October a rip-channel developed, which would be present for the remainder of the measurement campaign. Therefore only cases before this storm will be considered.
- It is important that comparisons can be made between the model and measurements. This requires (most) measurement equipment to be working during the case. This was not so straightforward as was hoped initially.
- Current meters were mostly located around the inner bar. Wave conditions should be such that most wave breaking action is in this region. So the wave height should not be too high. Otherwise, waves have already broken above the outer bar.

- Wave climates with relatively long wave periods are preferred as this leads to longer waves. Consequently a coarser grid resolution can be applied.
- Waves should be incident under an angle. Otherwise there is no wave induced alongshore current.
- Cases should be chosen such that waves incident from both northwest and southwest are considered.
- For calibration runs it is chosen to consider one case without (limited) tidal currents and one with a tidal current.
- The model will be validated for various tidal conditions. Therefore, a distinction is made between cases with flood tidal velocities and ebb tidal velocities.

6.2 Wave input

Information on wave characteristics is needed at the offshore boundary as input for the model. Wave data is available at two locations in the vicinity of the COAST3D measurement area, shown in Figure 6.1. Waves were measured 5 kilometres offshore at a water depth of 16m with a DIWAR buoy[1]. Unfortunately, at that time the importance of raw wave data was not recognised and only hourly averaged wave characteristics were stored (H_{m0}, T_p, θ). A shortcoming of the available data is the lack of directional spreading data and spectral shape. Apart from the local wave buoy, wave data can also be obtained from the permanent Rijkswaterstaat measuring station, IJmuiden Buoy. This is located approximately 35km offshore and 10km to the south. At this location 2D spectra (so distribution in frequency and direction) are available every 3 hours.

The spectral model SWAN is used to propagate waves from the IJmuiden buoy to the COAST3D area. Default settings were used for the SWAN simulations, including wind growth, whitecapping, depth-induced breaking, quadruplet and triad wave-wave interactions (Booij et al., 1999). The accuracy of this model was verified by comparing SWAN model data with the bulk measurement parameters of the DIWAR buoy (location 8) and buoys at location 7a and 7b (See Figure 2.1).

Results demonstrated that the SWAN model is well capable of predicting the order of magnitude of the wave characteristics. However, as can be seen in Figure 6.2, results range between plus and minus 20% accuracy for wave height and period and 20 degrees for wave direction. Also larger errors occurred, but they were all concerned with offshore or very low wind conditions, at which SWAN's accuracy is questionable. These

[1]DIWAR buoy = DIrectional WAve Rider buoy

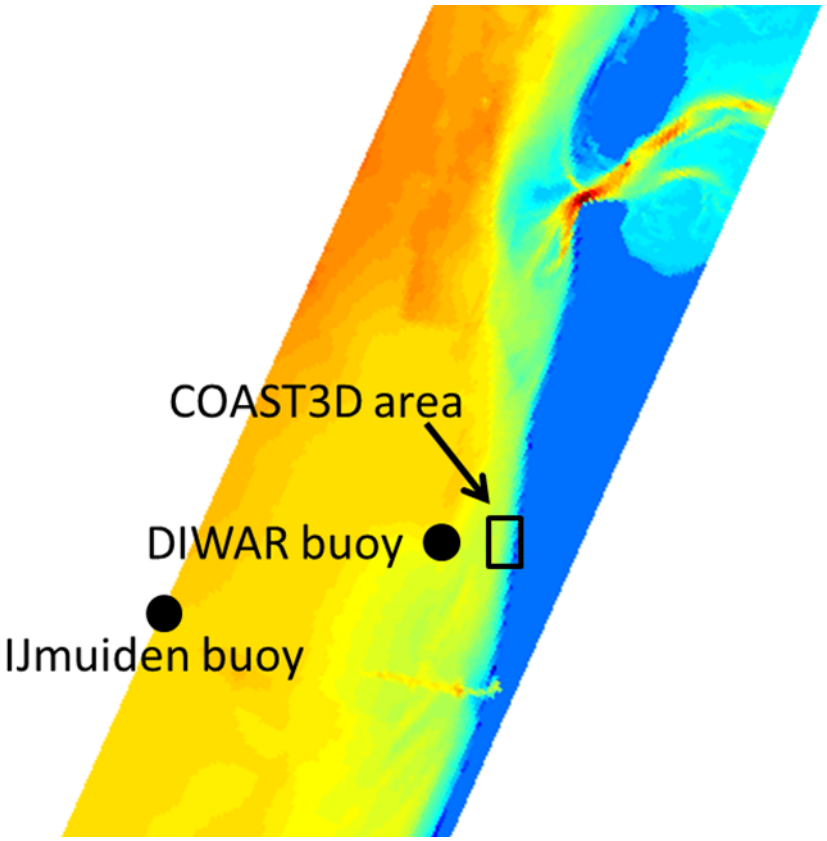

FIGURE 6.1: Locations of wave data availability in North Sea domain

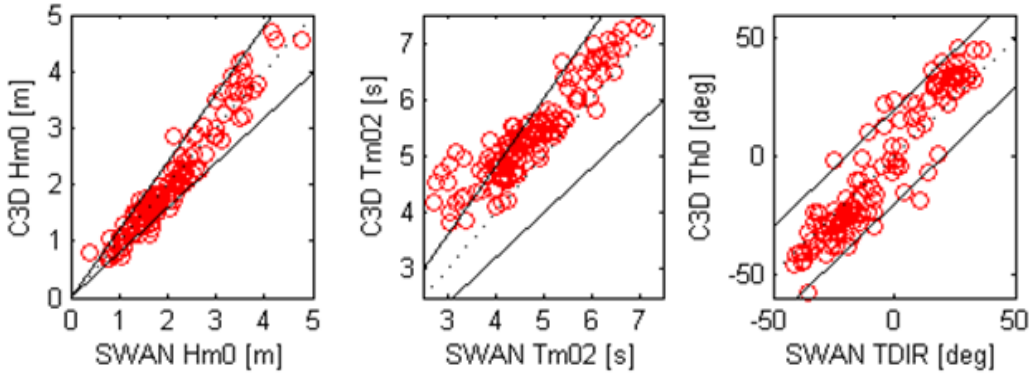

FIGURE 6.2: Comparison between COAST3D measurements and SWAN model results for from left to right: Wave height, period and direction at location DIWAR buoy. The black lines represent 20% deviation for wave height and period and 20 degrees deviation for wave direction.

conditions were filtered out for Figure 6.2 but can be observed in Appendix H, where a description of this SWAN model and further elaboration on its accuracy can be found.

Eventually, it is decided that bulk parameters from the DIWAR buoy with addition of directional spreading from the SWAN North Sea model will be used to generate wave input conditions for the offshore SWASH boundary location. In this way, it is prevented that errors up to 20% are initially made at the boundary. A small local

SWAN model has been used to transform waves from the DIWAR buoy to the offshore boundary location of the SWASH model. This method means that a spectral shape should be assumed at this location. The COAST3D cases under consideration showed a JONSWAP alike spectral shape at the most offshore located pressure sensor (location 7a) of the COAST3D data set. Therefore, this shape is also assumed as input for the local SWAN model. Output spectra were generated at 20 locations on the 10m depth contour near the COAST3D area. An average of these spectra will be used as input for the SWASH model. To prevent confusion about all models used to obtain wave input, the method is schematised in Figure 6.3.

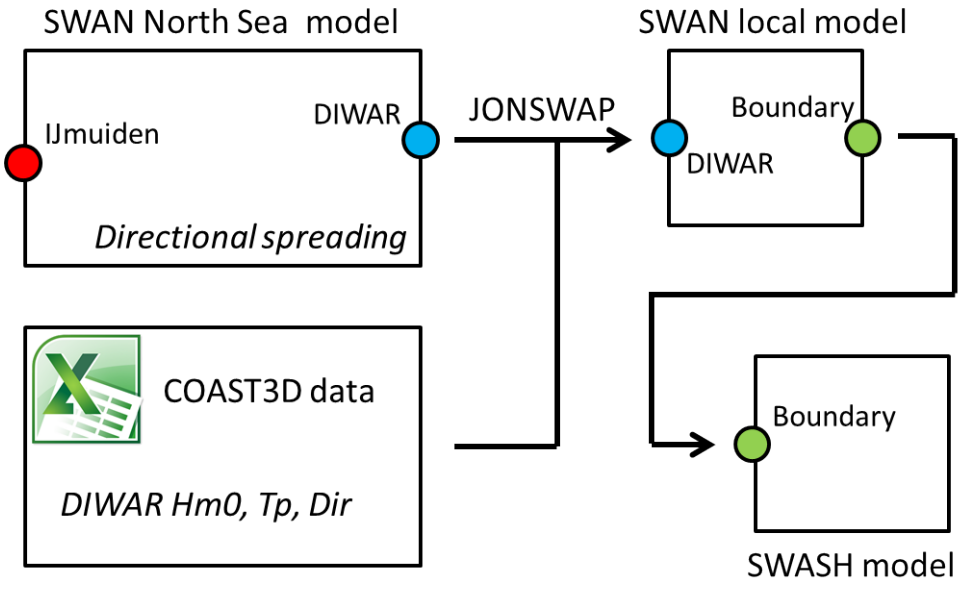

FIGURE 6.3: Wave model schematisation from IJmuiden buoy to SWASH offshore boundary

6.3 Tide input

This section describes in which way tidal input for the SWASH model is obtained from the COAST3D data set. The tide influences the hydrodynamics near Egmond in two ways:

- Water level variation
- Alongshore currents

The first influence is easily included by taking the time averaged water level at the most offshore located measurement point in the model area and use this value as SWASH

input. The most offshore located point is used as it is least influenced by set-up and set-down due to wave action.

The way tide induced alongshore currents are implemented in the model was described in Section 5.1. The only thing necessary for all cases is the time averaged alongshore water level gradient. This is obtained from two tidal gauges, Petten Zuid and IJmuiden, located respectively 19 kilometres to the north and 16 kilometres to the south of the area of interest. The gradient is calculated by dividing the vertical water level difference by the horizontal distance between the two gauges. Because the length of the tidal wave propagating through the North Sea is still hundreds of kilometres long the alongshore water level gradient over 35 kilometre can be assumed to be uniform.

As can be seen in Figure 6.4 there is a clear relation between the alongshore water level gradient and the alongshore velocity (at outer bar) due to the tide. After analysing the signals it was found that a time lag of approximately one hour is observed between the two signals. This means that peaks in velocity occur one hour later than peaks in the water level gradient. This time lag can be ascribed to a combination of inertia and friction of the flow (Bosboom and Stive, 2012). To take this lag into account the alongshore water level gradient of one hour earlier than the considered case is used as input for the simulations.

Section 5.3 described the importance of an initial velocity field to prevent excessively long spin-up time. This is taken care of by generating an initial velocity field based on local depth and the pseudo alongshore water level gradient.

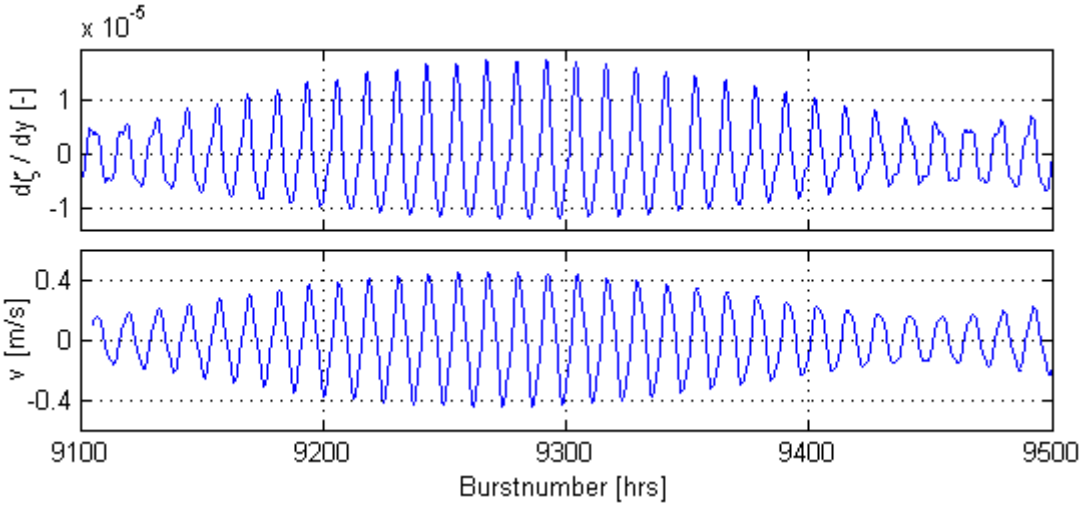

FIGURE 6.4: Tide induced alongshore water level gradient (upper panel) and tide induced alongshore current at outer bar (lower panel). Signals are processed with Matlab function ttide, therefore only tidal contributions are taken into account

6.4 Selected cases

Based on the requirements listed in Section 6.1 cases were selected for calibration and validation simulations. These are listed in Table 6.1. The wave characteristics are obtained from SWAN output spectra at the location of the SWASH wave maker boundary.

	Run	Burst	H_{m0} (m)	T_p (s)	θ (°)	σ_θ (°)	Tide
Calibration	**C1**	9307	1.5	6.7	25	25	Slack flow
	C2	9330	2.1	7.4	26	24	Flood flow
Validation	**V1**	9280	1.7	7.4	17	23	Flood flow
	V2	9305	1.6	7.4	14	24	Flood flow
	V3	9274	1.4	6.1	44	28	Ebb flow
	V4	9286	1.6	6.7	41	27	Ebb flow
	V5	9311	1.0	6.7	25	29	Ebb flow
	V6	9225	1.6	7.4	-15	26	Ebb flow
	V7	9231	1.3	8.1	-15	27	Flood flow

TABLE 6.1: COAST3D cases

6.5 Conclusions

The main findings of this section are summarised below:

- Even with a data set of almost 1000 hours it is still difficult to find useful cases to calibrate and validate the model. This is due to the large number of requirements for the simulations.
- Unfortunately, no local spectral wave data is available. Therefore, a JONSWAP wave spectrum is assumed, based on bulk parameters (H_{m0}, T_p, θ) from the DIWAR buoy located 5 kilometres offshore.
- For directional spreading input, a North Sea SWAN model is used to propagate spreading data from IJmuiden towards the DIWAR buoy.
- A local SWAN model is used to transform wave spectra from the DIWAR buoy (5km offshore) to the 10m depth contour, where the SWASH boundary is located (1.5km offshore).
- The tidal alongshore velocity is very well related to the tidal alongshore water level gradient. A time lag of approximately one hour was observed between the two signals, this will be accounted for in the model input.

Chapter 7

Calibration and validation

This chapter describes the calibration and the validation process of the model. Firstly, the set-up of model simulations is described in Section 7.1. Then the method to compare model predictions and measurements is presented in Section 7.2. In Section 7.3 the wave breaking and friction parameters are calibrated. Afterwards in Section 7.4 the SWASH model will be validated with COAST3D cases. Conclusions of this chapter can be found in Section 7.5. Figures visualising model results with respect to observations are presented at the end of this chapter. Furthermore, more detailed figures per transect can be found in Appendix K.

7.1 General model set-up

Based on all previously described researches, a general model set-up is used for all calibration and validation simulations. This set-up is dicussed in this section.

A computational domain of 1300m in cross-shore and 1100m in alongshore direction is used. The cross-shore distance results from the distance to the 10m depth contour where the numerical wavemaker is located. Bottom levels at the northern and southern boundary should be equal to avoid discontinuities at the cyclic boundaries. Therefore, 700m of the model represents actual measured Egmond bathymetry, whereas a linear transition in bottom level is applied for the remaining 400m.

Grid dimensions follow from the introduced wave spectrum. To ensure 75 grid cells per peak wave length in both cross- and alongshore direction $\Delta x = 0.5m$ and $\Delta y = 1.0m$. Explicit schemes are used for time integration, so the time step is limited by the CFL condition. This led to $\Delta t = 0.02s$.

The way wave and tide input were obtained, was already defined in Chapter 6. Similar numerical settings will be used as described in Sections 3.2.1 and 4.2.1. Finally, wave breaking and friction parameters will be determined by calibration.

7.2 Comparison method

7.2.1 Considered quantities

At locations 7a (near outer bar), 1a-1d and 7b (near inner bar), pressure sensors were located. Both raw measurement data and model data are processed in an identical way. Significant wave height and peak period are obtained from the wave spectrum. To get the short wave direction from raw data, u and v signals were transformed in high frequency velocity signals by applying frequency filters. Then wave direction is determined by linear regression through all u and v points.

Velocities were measured at locations 2 and 18a-b near the outer bar and locations 1a-d, 13a-b, 14a-b and 15 near the inner bar. Model output is only generated at two heights, in the middle of the lower layer and the top layer. Besides, it is debatable how accurate the vertical velocity distribution is when SWASH is applied with only two layers. Therefore, it is decided to use the depth averaged velocity for comparison. Unfortunately measurement velocity data is only available at a limited number (1-3) of heights above the bed. The method used to transform measurement velocities to depth averaged velocities is described in Appendix I.

As can be observed in Figure 2.1, not all measurement equipment was located in the same transect. From north to south transects are referred to as the North, Middle-North, Main, Middle-South and South transect.

7.2.2 Error metrics

To quantify differences in measurements and model results use is made of two error metrics. These present a score averaged over all active measurement locations. The Root Mean Squared Error is computed by $RMSE = \sqrt{\langle (Q_{SWASH} - Q_{C3D})^2 \rangle}$ and the Skill factor by $Skill = 1 - \sqrt{\langle (Q_{SWASH} - Q_{C3D})^2 \rangle / \langle Q_{C3D}^2 \rangle}$. $< ... >$ indicates averaging over all active locations.

A skill factor of 1 indicates a perfect match between model and measurements. A skill factor of 0 shows that the deviation between model and measurements is similar as the deviation between measurements and zero. If the skill factor becomes negative it

means that the model deviates more from measurements than the deviation between measurements and zero.

7.3 Calibration

In this section model parameters are calibrated. Firstly, wave breaking parameters will be calibrated for two cases in Subsection 7.3.1. Afterwards, the friction parameter will be calibrated with one case in Subsection 7.3.2. The cases which will be used are described in Table 7.1.

Run	H_{m0} **(m)**	T_p **(s)**	θ **(°)**	**Tide**
C1	1.5	6.7	25	Slack flow
C2	2.1	7.4	26	Flood flow

TABLE 7.1: COAST3D calibration cases

7.3.1 Wave parameters

As discussed in detail, correct modelling of wave transformation is essential for this study. Proper wave dispersion and transformation are taken into account by taking an appropriate grid resolution in both horizontal and vertical direction. The only thing which needs to be calibrated are wave breaking parameters α and β (see Sections 3.3.4 and B.1.3).

Cases C1 and C2, defined in Table 7.1, are used to check on wave transformation and in particular dissipation in case of wave breaking. Model and measurement data are compared at two transects. The main transect, with locations 1a-1d and a transect approximately 300m north where wave poles 7a and 7b were located, now referred to as the north transect. For both transects and both cases wave height normalised by the target wave height at the boundary is shown in Figure 7.1, including measured wave heights.

Firstly, clear differences in wave transformation can be observed between the north and main transect. These are seen in both model and measurement data and caused by bathymetric non-uniformities. Comparison of the bathymetry at both transects showed that the inner bar crest is significantly lower at the north transect resulting in less wave dissipation at this location.

In both cases, wave energy dissipation is at the correct location. At the main transect modelled wave energy seems to be slightly overestimated for case C1 and underestimated for case C2. These differences are small and could be a result of many model settings like

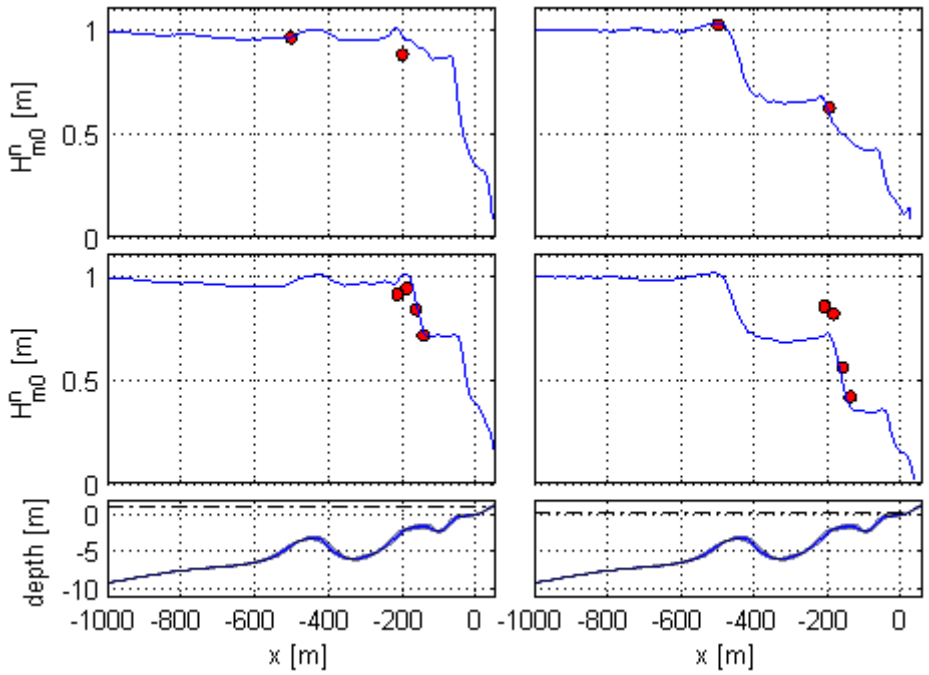

FIGURE 7.1: Comparison between measured and modelled wave height normalised by the target input wave height. Figures at the left side represent case C1 and at the right side C2. From top to bottom figures present normalised wave height for the north transect, normalised wave height for the main transect and bottom level. The shaded area in the bottom level plot represents standard deviation of the bottom level in alongshore direction.

wave input and the boundary error amongst wave breaking parameters. In conclusion, it can be said that the model performs rather well with standard breaking parameters $\alpha = 0.6$ and $\beta = 0.3$. Therefore, there is no reason to change these and to use some other values.

7.3.2 Friction parameter

Bottom friction is the main counteracting force for time averaged velocities. It depends on many things like sediment type, diameter, bed forms, ripples and processes in the boundary layer near the bed. Therefore, it is the final calibration parameter before validation can be performed. As can be read in this subsection, it appeared to be less straightforward than just varying friction terms and concluding which one performs best. This is complicated by the fact that the magnitude of the alongshore current is also dependent on the tidal forcing, wave direction and horizontal mixing terms. Ideally, one would use at least ten cases with varying friction terms to calibrate for bottom friction. Unfortunately, this is impossible due to computational time restrictions. Therefore, a reasonable friction parameter should be determined with running only few simulations. The way this is done is described in this subsection.

For this research the logarithmic wall law is used for bottom friction. The input parameter for this law is the roughness height. Initially, this parameter was estimated by 2.5 times the nominal grain diameter, which is a frequently appearing estimation in literature.

From first simulations it was observed that velocities are over predicted by the model. This implies that bottom friction is underestimated, especially as this was in regions only influenced by the tide. So a larger roughness height should be applied.

When looking into literature, many formulations for the roughness height were found. The above mentioned first estimation is an approximation for flat beds when the viscous sublayer is only a result of the sediment particles. When ripples are present or when the sublayer is larger due to wave turbulence, this approximation is a clear underestimation. Roughness height can then be one or two orders of magnitude larger.

No clear formulation for the roughness height in the surf zone was found in literature. Therefore, it is decided to use the Manning friction value 0.019 and re-write this to a roughness height. This Manning value is used in SWASH by default. This led to a roughness height of 0.01m. The underlying formulae, assumptions and sensitivity of this value on velocities are elaborated on in Appendix J.

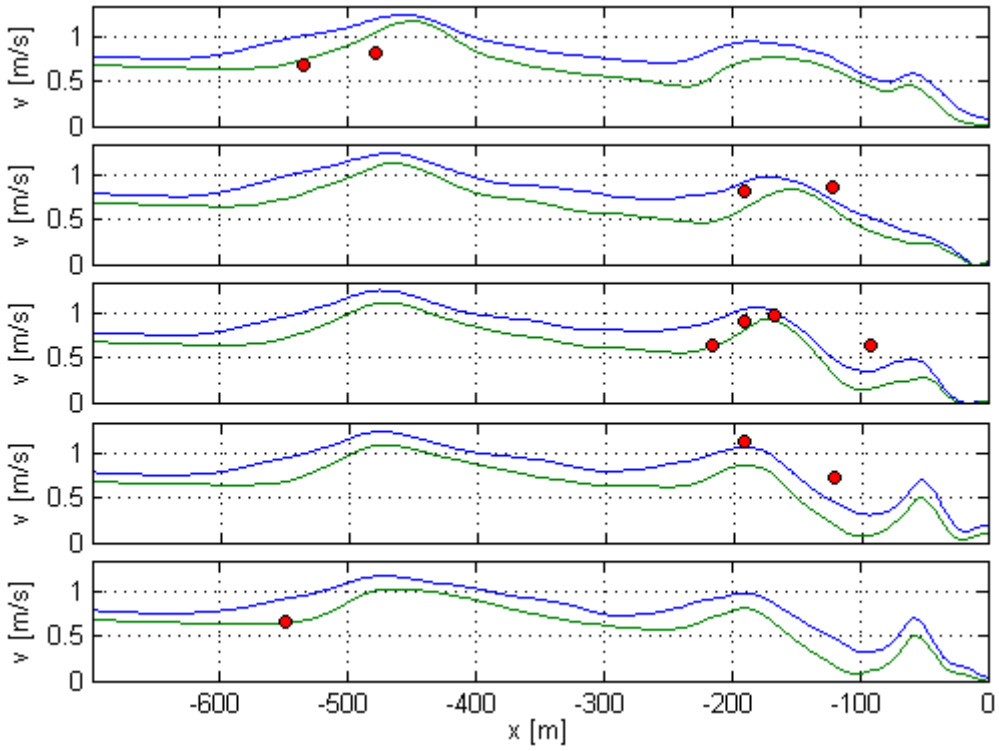

FIGURE 7.2: Modelled alongshore current for case C2 at five transects for $k_r = 0.00075$ (blue lines) and $k_r = 0.01$ (green lines). From top to bottom the north-, middle-north-, main-, middle-south- and south transect are shown. Red dots represent depth averaged measured velocities.

As can be seen, results of using a higher roughness height are twofold. On the one hand, velocities near the outer bank, which are mainly tidally induced, are predicted much better. On the other hand, predictions near the inner bar, which are induced by waves and tide, are not necessarily better with the higher roughness height. In Subsection 7.3.3 it will be described that the correctness of wave input is arbitrary for these simulations, as conditions at the boundary have changed due to the presence of an ambient current. At locations where wave influence is marginal, the balance between friction and velocity is in well agreement with measured data. Besides the roughness height of 0.01m is a more realistic value and is based on previous successful model results in the surf zone. Therefore, it is decided to use this as roughness height for subsequent validation simulations. Preferably, more calibration runs would have been performed. But due to limited computational time it is decided to stick with this value.

7.3.3 Note on wave input

Due to the presence of an alongshore tidal current in vicinity of the wavemaker boundary, an error is made when imposing a wave spectrum in the default way. Unfortunately, this only came to attention during the last calibration runs. Therefore, changes in boundary conditions, described in this subsection, were only effective in the validation simulations. Necessary conclusions until then are assumed to be still valid, despite of this error at the boundary. Two adjustments had to be made to correctly impose waves in the model:

1. According to Holthuijsen (2007), a distinction should be made between the relative (σ) and absolute frequency (ω) when an ambient current is present. The absolute frequency is measured by an observer at a fixed location like a wave pole. The relative frequency is measured by an observer moving with the ambient current.

   Without a current ω and σ are equal and wave number k follows from the linear dispersion relation (Equation 7.1). However, in presence of an ambient current, a frequency shift occurs which also influences k. This shift can be calculated with Equation 7.2, which reduces to Equation 7.3 when the current is directed parallel to the boundary as is the case here. U_n is the component of the ambient current in the direction of wave propagation.

$$\sigma = \sqrt{gk \tanh kh} \tag{7.1}$$

$$\omega = \sigma + kU_n \tag{7.2}$$

$$\omega = \sigma + kv \sin\theta \tag{7.3}$$

Orbital velocities imposed by SWASH as a boundary condition are a function of relative angular frequency σ and the corresponding relative wave number k_σ. The linear dispersion relationship is valid in a moving frame of reference. So when relative frequencies are given to SWASH, it will calculate the correct wave number and orbital velocities. Therefore, it is of importance to use a spectral input file with relative frequencies to correctly introduce waves at the boundary when a current is present. This is taken care of by re-running SWAN simulations with addition of the tidal current and both input and output spectra in relative frequency.

2. By default, velocities in the first velocity grid points at the wavemaker boundary, are solely orbital velocities as calculated by the wavemaker in SWASH. Apart from this row all other active velocity grid cells are influenced by the alongshore water level gradient, which results in a current velocity of order $1m/s$. To prevent a shear between the first and second row of grid cells, the tidal current should also be added in the first row. Therefore, an adjustment is made in the SWASH source code. This calculates the tidal velocity at the boundary as a function of depth, alongshore water level gradient and roughness height according to Equation 5.3. It then adds this to the orbital velocities calculated by the wavemaker.

7.4 Validation

This section will elaborate on results of seven validation simulations listed in Table 7.2. Unfortunately, instabilities were observed in five of them. The origin of these instabilities and reliability of the model output is discussed in Subsection 7.4.1. Subsequently, results of successful validation cases V1 and V2 are given in Subsection 7.4.2. Finally, results of cases V4 and V7 are discussed in Subsection 7.4.3. Although in these cases instabilities were observed, these were not that distinct. So results can be discussed with caution.

Run	H_{m0} **(m)**	T_p **(s)**	θ **(°)**	**Tide**
V1	1.7	7.4	17	Flood flow
V2	1.6	7.4	14	Flood flow
V3	1.4	6.1	44	Ebb flow
V4	1.6	6.7	41	Ebb flow
V5	1.0	6.7	25	Ebb flow
V6	1.6	7.4	-15	Ebb flow
V7	1.3	8.1	-15	Flood flow

TABLE 7.2: COAST3D validation cases

Modelled and measured wave height and alongshore velocity are visualised in Figures 7.3 to 7.6. To give a clear overview, measurement data of different transects are presented in one figure. Blue lines show the prediction averaged over the alongshore domain and its

standard deviation is represented by the blue cloud. When analysing results, it should be kept in mind that the red dots, representing measured data, have a considerable uncertainty. Additionally, modelled results and measurement data per transect can be found in Appendix K. Finally, results of the simulations are quantified with error metrics in Table 7.3.

7.4.1 Instabilities

All simulations with one or two forcing terms (wave and tide) in southern direction showed instabilities. So, disturbances were observed in simulations V3 to V7. These instabilities propagate in alongshore direction and disturb the originally imposed wave field. The magnitude and consequences of these instabilities varied per case. For cases V3, V5 and V6 the instabilities grew so large that it contained more energy than the imposed wave field. For cases V4 and V7 the instabilities were not that big but clearly visible, certainly at the end of the simulation. A note on these instabilities, including snapshots of surface elevation and v-velocity at the end of the simulations are given in Appendix L.

Initially, it was suspected that some error with the cyclic boundary conditions could be present in the SWASH model when velocities leave the southern boundary. Eventually, a bug was found in the source code. This bug was not in the cyclic boundary conditions but in the higher order approximation of the horizontal advective terms. For negative values of the instantaneous v velocity inaccuracies occurred due to this bug. These instabilities grew in time and remained in the model domain because of the cyclic boundary conditions. The research to find the bug is summarised in Appendix N. This bug was only observed in the final stage of this thesis research. Therefore, model results of validation cases V3 until V7 unfortunately do not give reliable results.

For cases V1 and V2 the flood tide provided a positive background current. Therefore, the instantaneous velocity is positive most of the time, although orbital velocities are also negative. For these cases, only 1% of the wet grid cells showed a negative instantaneous velocity during the entire simulation. This is the reason why for these runs no disturbances can be observed and results are thus better.

It is useless to analyse results of cases V3, V5 and V6 as these are dominated by the instabilities. To be able to say something about alongshore current modelling when not all forcing is northerly directed, cases V4 and V7 are analysed. It should be noted that it is unclear to what extent these two simulations are influenced by the disturbances. Therefore, conclusions should be drawn with caution.

7.4.2 Results V1 and V2

For cases V1 and V2 wave height predictions agree very well with measurement observations. It should be noted that slightly too much energy is added to the model as compensation for the boundary error made by SWASH. Therefore, the wave height prediction is slightly too high at the boundary. Although V1 is slightly better than V2, wave peak period prediction is overall good. Differences in wave direction are more distinct. This can probably be attributed to errors in measuring instantaneous velocities and inaccuracy in calculating corresponding short wave directions.

Modelled velocities near the outer bar match very well with measurement data. As this region is mostly influenced by the tide it shows that the tidal forcing is well represented. Also near the inner bar, where the current is relatively more induced by waves, predictions are good, although in both cases the model seems to be slightly underestimating velocities in this region. In general, it can be concluded that there is good agreement between measured and modelled alongshore currents. This is confirmed with skill scores of 0.85 and 0.87 and RMSE values around 10cm/s.

7.4.3 Results V4 and V7

For both simulations it can be observed that, despite the instabilities, wave characteristics are well predicted. In Table 7.3 it can be seen that error metrics are the same order of magnitude for wave characteristics as for cases V1 and V2. Alongshore current results are less good. Root mean squared error values for the v comparison are two to three times as high as for case V1 and V2. Part of this could be due to the instabilities. Nevertheless, as disturbances were minor, results will be analysed to see whether physical explanations could be found for disagreements between measured and modelled results.

It should be noted that according to Van Rijn et al. (2002) time-averaged velocities below 0.15m/s may have an inaccuracy up to 100%. Besides, the skill value is a bit biased as it is very sensible when measurement data is near zero. This is more the case for simulations V4 and V7 as wave and tide induced currents are in opposing directions.

7.4.3.1 Results case V4

Case V4 is a simulation with ebb tidal forcing to the south and wave induced currents to the north. Wave height prediction is quite good. The modelled alongshore current, on the other hand, is predicted too much to the south. At the inner bar modelled

velocities are more southward than measurements. However, the distinction is less clear as observed at the outer bar. Changes in wave energy are marginal near the outer bar, so wave related causes for the differences in velocity predictions can be excluded. Three other possible causes for this distinction are discussed below:

1. Alongshore water level gradients can be a driving force for alongshore velocities. In the present study only time averaged water level gradients due to the tide are taken into account. So an additional gradient, which was not taken into account could be the cause of a flow component in southern direction. This would mean that there was a difference in set-up outside the model domain.

   Although this could have some influence, it is probably not the main cause. Mean water level variations in the alongshore, apart from the tide, occur mainly due to set-up differences. As only negligible set-up is observed near the outer bar, it is unlikely that this caused the velocity differences.

2. Processes in the boundary layer are different when wave propagation is in the same direction as a current than in the opposite direction. As bottom friction is calibrated without flow and with flood flow, this could mean that bottom friction is underestimated in case of ebb flow. An underestimation of bottom friction could be the cause of too high velocities in the model.

3. Tidal forcing is implemented in the model by imposing a time-averaged and spatially uniform alongshore water level gradient with its equilibrium current field as initial velocity. This means that the tide is seen as a stationary forcing and thus inertia is neglected. The momentum balance for a tidal wave propagating along a shore, described by Equation 2.8, shows that tidal forcing is balanced by inertia and bottom friction. In deep water friction can be neglected and in shallow water friction dominates inertia (Bosboom and Stive, 2012). An approximation of the order of magnitude of friction and inertia terms shows that inertia can almost be as high as friction in 10m water depth. It also shows that inertia does influence the tidal movement and can only be neglected in depths below 1m. Furthermore, two experimental SWASH simulations indicate that time necessary to develop equilibrium velocity might be longer than halve a cycle time, certainly for ebb forcing. A description of the hand calculations and simulations to approximate these terms can be found in Appendix M. Influence of inertia seems to affect the ebb flow more than the flood flow. Due to tidal asymmetry the ebb tidal forcing is more gentle than the flood tidal forcing, resulting in a longer time to reach equilibrium velocity. Therefore, it is debatable whether the ebb tidal water level gradient is capable of fully reaching its equilibrium velocity before forcing has changed direction again.

7.4.3.2 Results case V7

Case V7 is a simulation with flood tidal currents to the north and wave induced currents to the south. However, wave and current results are not that good in the main transect. Wave height is overpredicted by the model and the alongshore current is too northerly, implying that tidal forcing is too strong or wave forcing too weak. This might be caused by wave current interaction or boundary layer processes when waves and tide oppose each other. On the other hand, it could very well be possible that differences are caused by the instabilities as well.

7.4.4 Results summarised

Root Mean Squared Error and Skill values are presented in Table 7.3. It should be noted that for simulations C1 and C2 the adjusted wave input, as described in Subsection 7.3.3, was not included. Besides, tidal forcing was incorrectly introduced in case C1, resulting in low scores for alongshore velocity. Unfortunately, not all results are reliable due to the bug, which came to attention during the finishing phase of this thesis. Cases influenced by instabilities, will be simulated again and results will be added to this thesis by means of an addendum.

	C1	C2	V1	V2	V4	V7
RMSE H_{m0}	0.07	0.20	0.09	0.06	0.08	0.11
RMSE T_p	0.8	0.5	1.3	0.4	1.4	0.9
RMSE θ	7.8	2.0	5.5	9.0	4.5	8.2
RMSE v	0.21	0.27	0.10	0.10	0.30	0.20
Skill H_{m0}	0.94	0.87	0.94	0.97	0.93	0.90
Skill T_p	0.89	0.93	0.80	0.94	0.81	0.89
Skill θ	0.56	0.82	0.64	0.47	0.66	0.42
Skill v	0.38	0.68	0.87	0.85	-0.04	0.31

TABLE 7.3: RMSE and Skill values for calibration and validation cases

A considerable deviation can be seen between observed and modelled short wave direction. Another method was used to compute the short wave direction from a 2D spectrum of water level, u-velocity and v-velocity time series. Error metrics, however were of the same order of magnitude. It is unknown whether these discrepancies are caused by uncertainty in velocity measurements, the methods to calculate short wave direction or due to inaccuracies in correctly modelling wave and current induced refraction.

7.5 Conclusions

Main conclusions of the calibration and validation studies are listed here.

Calibration:

- Calibration of a 3D model is difficult when only a limited amount of cases can be considered due to limited computational time.
- Simulations C1 and C2 showed good results for wave breaking dissipation with default wave breaking parameters. Other model settings, like wave input, could also cause the minor differences observed between model predictions and measurements. Therefore, it was decided not to change the wave breaking parameters. It should be noted that results are good for this spatial resolution with two layers and $\Delta x = 0.5m$ and $\Delta y = 1.0m$. In Chapter 3, however, it was shown that this is grid size dependent, so it can not be concluded that results are similarly good when a different grid resolution is used.
- For surf zone applications a roughness height estimation of 2.5 times the median grain diameter leads to an underestimation of bottom friction.
- Conversion from a Manning value of 0.019 leads to a roughness height between 0.005 and 0.015m depending on local depth. Variation between these values only marginally influences current velocities (Appendix J). In this study a roughness height of 0.01m is applied.

Wave input:

- When a current is present at the boundary, attention should be paid to the difference in absolute and relative frequency. If relative frequencies are provided to SWASH, the model correctly calculates the wave number and orbital velocities. Furthermore the ambient current should be added to the orbital velocities calculated by the numerical wavemaker, in the boundary velocity grid cells.

Validation:

- Instabilities were observed for cases V3 to V7. They were caused by a bug in the source code. Due to this bug, higher order approximations of horizontal advective terms led to instabilities. Disturbances grew so large for cases V3, V5 and V6 that they dominated the originally imposed wave field. Therefore, results of these cases are useless, and thus not presented.

- For cases V1 and V2, which are not or negligibly influenced by the instabilities, good agreement was found between measurements and modelled predictions for the alongshore current. At deeper water, the mainly tidally induced current is predicted very well by the model. Near the inner bar, where wave induced currents are dominant, the velocity magnitude seems to be slightly underpredicted by the model.

- Cases V4 and V7 are influenced by the instabilities. These, however, did not dominate the imposed wave field. Results are analysed with caution as it is unknown to what extent results are influenced by the instabilities. Distinctions in alongshore currents were observed between observation and model. Potential physical causes could be:

  - Boundary layer processes which are different when waves and tide oppose each other. This could lead to inaccuracies in the used bottom friction.
  - Inertia of the tidal wave is not taken into account by the model. This has to do with the implementation of tidal forcing, which is assumed to be time averaged and spatially uniform.

- For all considered cases, results for wave height and period are very good with skill scores above 0.9 and 0.8, respectively.

- For short wave direction less agreement was found between measured and modelled values. This might be due to inaccuracies in measurements or the methods to compute the short wave direction. It is recommended to further analyse this.

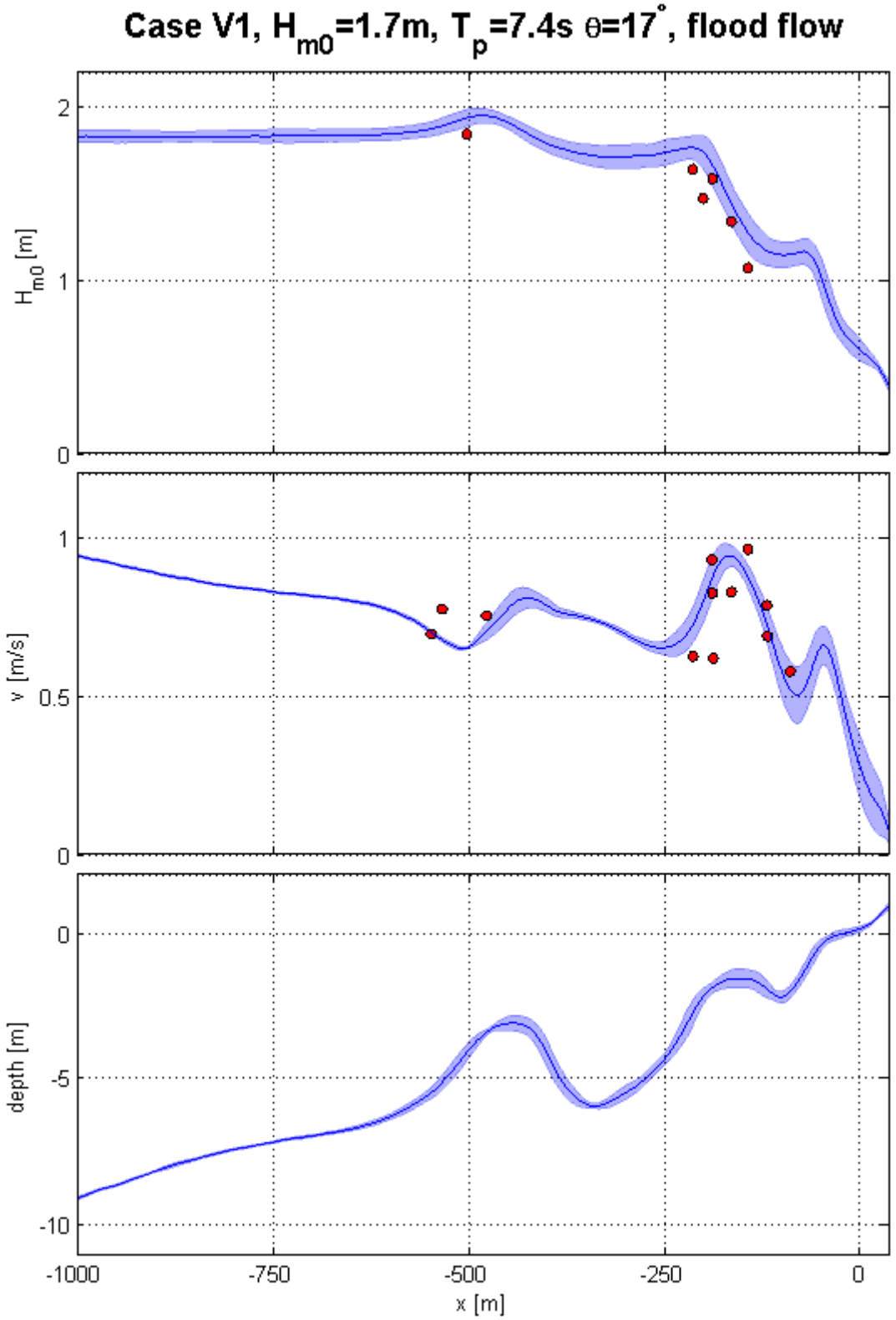

FIGURE 7.3: Results case V1. From top to bottom modelled values (blue lines) and observations (red dots) are plotted for spectral wave height, alongshore current and bottom level. The shaded area represents the standard deviation of results in alongshore direction.

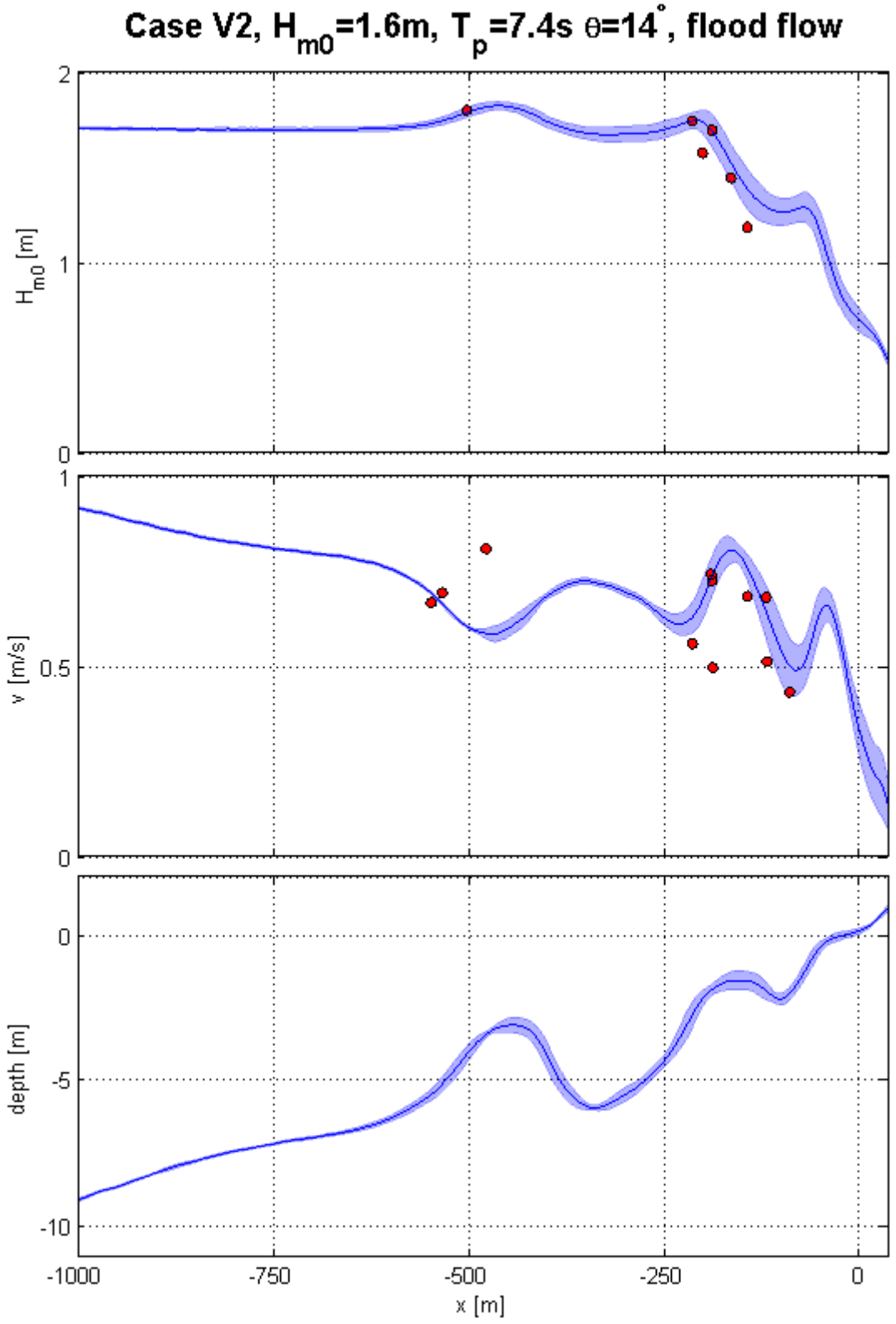

FIGURE 7.4: Results case V2. From top to bottom modelled values (blue lines) and observations (red dots) are plotted for spectral wave height, alongshore current and bottom level. The shaded area represents the standard deviation of results in alongshore direction.

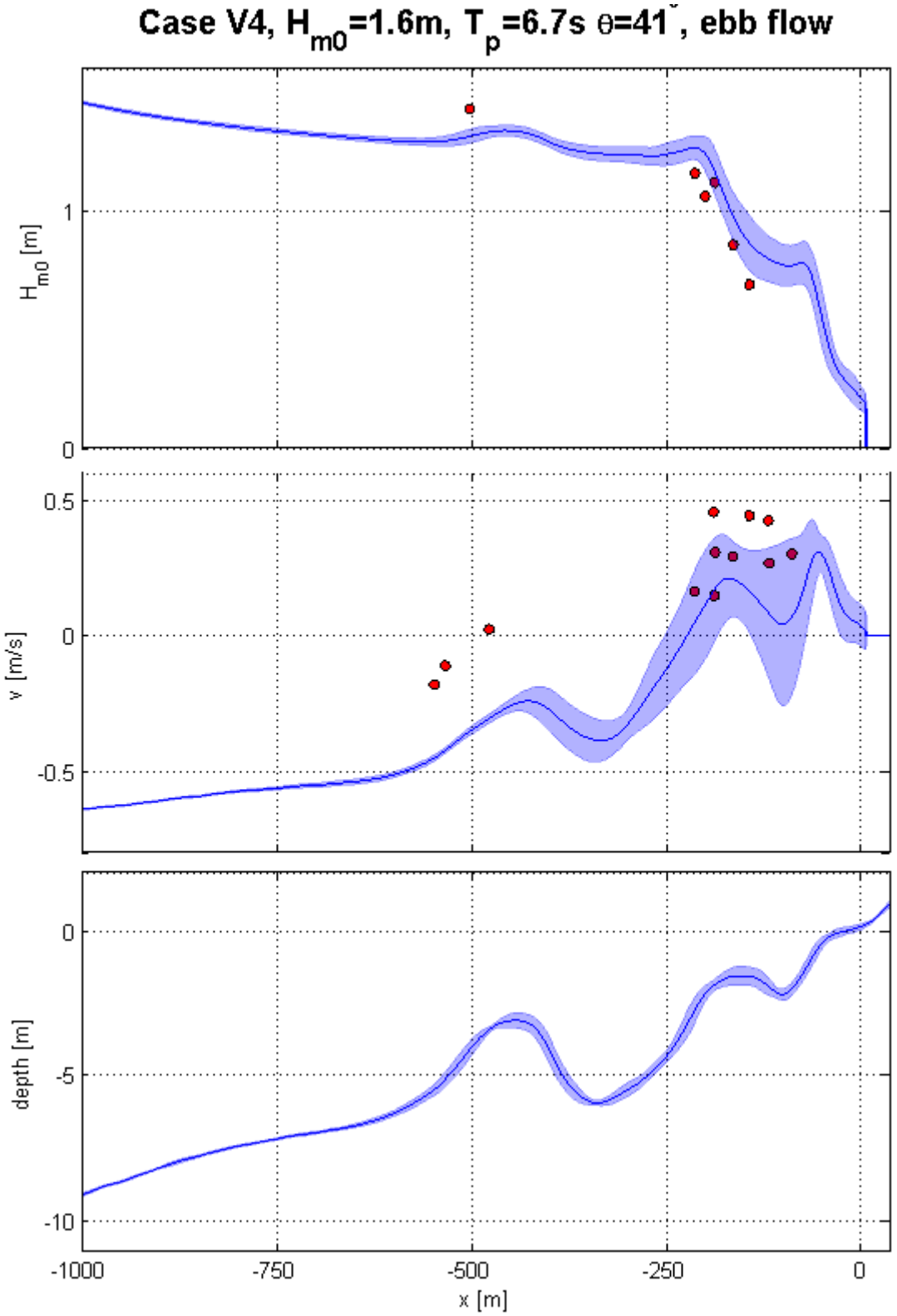

FIGURE 7.5: Results case V4. From top to bottom modelled values (blue lines) and observations (red dots) are plotted for spectral wave height, alongshore current and bottom level. The shaded area represents the standard deviation of results in alongshore direction.

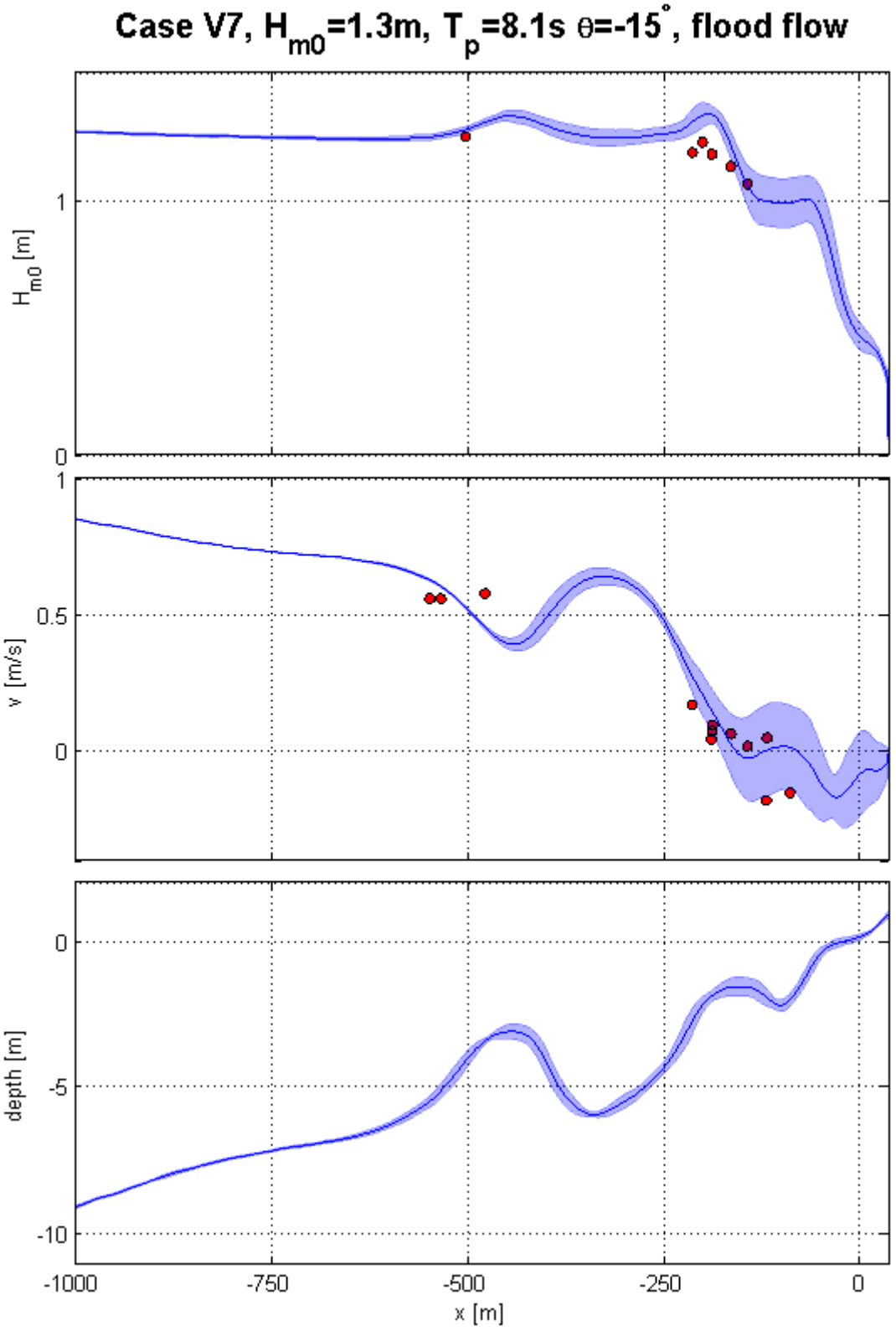

FIGURE 7.6: Results case V7. From top to bottom modelled values (blue lines) and observations (red dots) are plotted for spectral wave height, alongshore current and bottom level. The shaded area represents the standard deviation of results in alongshore direction.

Chapter 8

Discussion

During the course of this thesis a number of topics of interest have come up which are open for discussion. These will be presented in this chapter. Firstly, in Section 8.1 some issues and overall performance related to wave modelling are discussed. Subsequently, the implementation of the tidal forcing and its assumptions are described in Section 8.2. Section 8.3 elaborates on the uncertainty in data from the COAST3D data set. Finally, Section 8.4 discusses alongshore current results and the influence of inertia.

8.1 Wave modelling

Although the main research question of this thesis is related to currents, considerable effort and time was spent on wave modelling. This is necessary since a main part of surf zone dynamics is determined by wave action. This section discusses findings, shortcomings and assumptions of the 2DV wave transformation study (Chapter 3) and wave modelling issues of subsequent studies.

During the first study, model simulations were performed with one horizontal dimension to define which model settings result in proper wave transformation. A limitation of this study is that model data is not compared to laboratory or field experiments, but to other model results instead. The correctness of wave transformation is determined by the grid resolution. The accuracy of frequency dispersion, so the speed of propagating waves, is specified by the number of layers applied. The horizontal grid resolution determines to what extent waves are represented well. Comparable results were found for both horizontal and vertical resolution as in previous studies (eg. Brinkkemper (2013); Rijnsdorp (2015)).

Wave breaking is taken care of by the wave breaking model, a detailed description of which can be found in Smit et al. (2013) and Smit et al. (2014). This model sets non-hydrostatic pressure to zero when wave steepness is above a certain threshold value. During this research considerable differences in water level set-up kept occurring for varying model settings. Numerous potential causes were considered and eventually the final attempt resulted in a dependency which identifies the underlying reason. A clear correlation was found between the set-up and non-hydrostatic pressure integrated over the surf zone. This suggests that the local cut-off of non-hydrostatic pressure under wave crests results in exclusion of onshore directed impulse, which then leads to an under estimation of set-up. It might be worth to consider cutting off non-hydrostatic pressure over a bigger region, for instance one wave length, as applied in Tissier et al. (2012).

While investigating the above mentioned issue the performance of wave breaking parameters was evaluated. Smit et al. (2014) and the SWASH Manual state that default α and β work well under all conditions, and are thus not subject to calibration. This study, however, showed that these parameters clearly depend on grid size as they are steepness induced, whereas steepness calculated by the model is a function of the grid size. The calibration study with default values, on the other hand, showed good agreement between modelled predictions and measured observations, giving no reason to change these default values. Rijnsdorp (2015) concluded similarly, so it is reasonable to conclude that when horizontal grid resolution is fine enough default values work well. When using a coarse grid it is advisable to check on the performance of these parameters. For calibration and validation simulations good agreement was observed between modelled predictions and measured observations. Therefore it was concluded that SWASH is very well capable of predicting bulk wave parameters.

8.2 Implementation of the tide

To include tidal alongshore currents a new method has been implemented in the source code. Alongshore tidal velocities are forced by a time averaged water level gradient in alongshore direction. To properly model wave induced currents cyclic boundary conditions should be used at the lateral boundaries. This, however, is in conflict with the alongshore water level gradient as cyclic boundaries require water levels to be equal at the northern and southern boundary. That is why the pseudo alongshore water level gradient is introduced. To satisfy continuity, it is decided to not include the time averaged water level gradient in the alongshore momentum balance, but instead the pressure gradient which results from the water level gradient. As this water level gradient is not

actually present in the model, but is used as input parameter, it is referred to as the pseudo alongshore water level gradient. By including the pressure gradient in the momentum equation the resulting velocity is added to the equation. Test results showed that the method is very accurate in predicting the correct velocity. An advantage of this method is that it adds a forcing term instead of a velocity field. The latter namely, leads to errors as velocity and forcing terms are not linearly related to each other. For the present study, the tide is simplified by a number of assumptions. These and their consequences are discussed below. Besides, further suggestions for improving the method are provided.

- **Actual water level difference is not present in the model**
  Due to the way the tide is implemented, the actual tidal water level gradient is not accounted for by the model. Nevertheless, mean tidal elevation and alongshore velocities are taken into account. As the alongshore domain length is O(1km) the water level difference between northern and southern boundary is maximum O(1cm). This difference is negligible so it is safe to assume that the error in local water level is small and will not influence wave transformation.

- **The pseudo alongshore water level gradient is assumed to be spatially uniform**
  Tidal waves propagating through the North Sea have a wave length which is O(100km). As this is two orders of magnitude longer than the alongshore domain length, it is reasonable to assume that the water level gradient is constant over the domain.

- **The pseudo alongshore water level gradient is assumed to be time averaged**
  Whereas above two assumptions are not expected to influence model results, this one might. Due to the semi-diurnal tide encountered in the North Sea the tidal wave has a period of 12.4 hours. So in approximately six hours the tide changes from flood to ebb. Model output is generated for one hour, which is a considerable fraction of this time. Therefore the alongshore water level gradient is most likely not constant during this time. For the cases considered a maximum mismatch of 15% was observed in data with respect to the inputted alongshore tidal water level gradient. As $v_{tide} \sim \sqrt{\partial\zeta/\partial y}$, this could result in maximum velocity errors of 4%. This is still within reasonable limits, but for longer simulations or more accuracy, it is advisable to implement a time varying pseudo alongshore water level gradient in the model.

In addition to the slight inaccuracy in tidal forcing another model discrepancy can probably be related to the time averaged pseudo alongshore water level gradient. This topic will be further elaborated on in Section 8.4.

8.3 Uncertainty in measurement data

When evaluating a models accuracy based on measured observations, uncertainty of measurement data should be treated with caution. This section discusses inaccuracies in wave input and the uncertainty of depth and time averaged velocity signals used for comparison. Both are obtained from the COAST3D data set.

Wave input for the SWASH model was obtained with spectral wave model SWAN. Input for this SWAN model was hourly averaged wave characteristics (H_{m0}, T_p and θ) from the DIWAR buoy (5km offshore, 16m depth) and directional spreading from a global North Sea SWAN model. As considerable variations in wave characteristics were observed at the DIWAR buoy between consecutive hours it is questionable whether wave input is representative for an entire case of one hour. Besides, some inaccuracy might have been induced by using the SWAN model to transform waves from the DIWAR buoy to the SWASH boundary. Nevertheless good agreement was observed for wave height and period for all calibration and validation simulations, indicating that wave input must have been quite good.

For model velocity output almost no difference is observed between the upper and lower layer. This is in accordance with the expectation that SWASH is not well capable of modelling the vertical flow structure when a course vertical resolution is applied. In measurement data at location 2, on the other hand, current meters at three different heights show that there clearly is a velocity variation over depth. Therefore, it was decided to convert measured velocities to depth averaged velocities so that a comparison between model and observations could be made. As was shown in Appendix I this conversion involves errors up to 15%. This error is caused by the fact that the height above the bed of measurement equipment is not exactly known as this was only reported at the beginning of the measurement campaign. Furthermore the current meters itself have a certain degree of inaccuracy which is elaborated on in Appendix A. Altogether it can be concluded that there is a significant degree of uncertainty in depth averaged velocity from measurements used to evaluate the model.

8.4 Alongshore current modelling

The main subject of this research was combining wave and tide induced currents. Shortcomings of the calibration study and validation results are discussed in this section.

Due to the fine grid resolution and corresponding small time step computational effort per simulation was considerable. Ideally wave breaking and friction parameters would be calibrated for a number of cases under varying conditions and a number of values per parameter. Eventually, an overall best-fit would than determine values which should be used. Unfortunately, this was not feasible due to computational limitations. Within the scope of this thesis, reasonable values for wave breaking and friction parameters were obtained through three simulations and a number of hand-calculations. However, in the end more calibration would lead to better optimised values, improving model results. Furthermore, it is worth considering a spatially varying bottom friction as in reality it is also a function of local water depth.

Due to instabilities, induced by a bug in the source code, not all results were reliable to analyse. Cases V1 and V2 with flood currents and waves from the southwest were not or negligibly influenced by these instabilities. For these cases the validation study showed that modelled alongshore currents are in good agreement with observed values. Certainly when we take inaccuracies, described in the previous section, into account.

However, other cases, which contain one or two forcing terms to the south, are influenced by the instabilities. Therefore, it is doubtful to what extent disagreements between observation and model were due to these instabilities or due to physical causes. Two cases, which were least influenced by the disturbances were analysed. These were case V4 with ebb currents and waves from the southwest and case V7 with flood currents and waves from the northwest. For case V7, currents were quite low as northward tidal forcing opposes the southward wave forcing. Alongshore current predictions are not very good. The direction and order of magnitude, however, is correctly predicted. It is hard to say whether measurement inaccuracies, model instabilities or physical reasons cause the disagreement between model and observations. For case V4, the alongshore current seems to be predicted to much southward by the model. The mismatch with observations is most distinct at the outer bar, where currents are mainly driven by the tide for this case. A plausible explanation is inertia of a tidal wave, which is not taken into account by the way tidal forcing is implemented in the model. According to Bosboom and Stive (2012), in shallow regions inertia can be neglected and the tidal wave is represented by a balance between forcing and friction. On the contrary, as shown in Appendix M, inertia is of the same order of magnitude as friction in 10m water depth and also at depths between 2 and 5m, where velocities are measured, it can not be neglected. Due to

absence of inertia, the model treats the tide as a stationary process with an equilibrium tidal velocity which is constant throughout the entire simulation. In reality, however, when forcing changes inertia of the body of water results in a time lag for velocity to respond. Firstly, the tidal velocity has to be decelerated and subsequently accelerated in opposing direction. The reason that influence of inertia is more pronounced for ebb flow than for flood flow is that water level gradients are more gentle so more time is needed for the flow to turn around and reach equilibrium flow velocities. This is supported by SWASH simulations with flood and ebb tidal forcing, described in Appendix M.

To verify whether the lack of inertia really leads to inaccurate wave results, firstly simulations have to be performed with a source code without bugs. Subsequently, multiple cases should be simulated. If the ebb tidal velocity is consistently overpredicted by the model, this points towards a shortcoming in the way inertia is taken into account by the model. Solutions which could then be considered to include the effect of inertia in the model are:

- Use an initial velocity field which is not the equilibrium velocity (based on forcing) but instead the velocity which is present at $t = 0$ of the simulation. The latter velocity field is hard to obtain from measurements. Therefore, it might be a good solution to firstly run a simulation with tidal forcing only for a complete tidal cycle. This can be performed with a very coarse grid and time step, as tidal wave length and period are O(100km) and O(12hrs), respectively. Thereafter a velocity field can be obtained from this simulation to be used as initial velocity in the subsequent simulation with wave forcing. To make this possible the pseudo alongshore water level gradient should be implemented time varying.
- Decrease tidal forcing by a factor to compensate for the influence of inertia. As influence of inertia is depth dependent, this factor will also be a function of depth. Therefore the pseudo alongshore water level gradient will not be uniform over the model domain so should be implemented spatially varying.

Chapter 9

Conclusion and recommendation

9.1 Conclusion

The main research question of this Master of Science Thesis was:

What is the validity of the non-hydrostatic model SWASH
in predicting alongshore currents in the surf zone?

This research confirms findings of previous publications that SWASH is very well capable of modelling inner surf zone wave transformation. Therefore wave induced currents are well predicted. Furthermore, surf zone vortices, spreading the current through the surf zone, are well captured by the model.

During this thesis a method was developed and implemented in the source code to expand SWASH by including the forcing of tidal alongshore currents in the momentum equations and solve tidal velocities on the same temporal and spatial scales as short waves.

The potential of this implementation and the capability of SWASH to solve combined short wave and tidal forcing was shown with the validation studies. For cases with flood tidal forcing and waves from the southwest, which were not disturbed by instabilities, good correlation was found between model predictions and measured observations, despite the uncertainty of measured velocities. For other cases results contained inaccuracies due to a bug in the source code. Despite these instabilities, it seems for the weaker ebb tidal forcing, that the model over predicts tidal velocities. This probably has to do with inertia, which was not yet implemented.

9.2 Recommendation

This section provides recommendations which came up during this thesis. They are separated in two parts. Firstly, recommendations are provided which concern this research. Secondly, some recommendations are given for further development of the SWASH model to improve its capability of surf zone modelling.

Present research:

- A number of grid cells per wave length was assumed which is used for the simulations. In hindsight, this may have been a bit conservative, but the grid size was chosen to prevent having to say in the end that a finer grid size would have improved results. Computational time is inversely proportional to the third power of grid size. Therefore it is important to optimise this parameter for future studies.
- It is advisable to perform more calibration simulations to achieve bottom friction values with more certainty. It would be good to extend this study to other field experiments and investigate depth varying bottom friction. In this way more knowledge is obtained on which values for roughness height suit surf zone modelling best.
- To finish the present research, simulations should be performed with the new source code without bugs. Subsequently conclusions can be drawn without the uncertainty of the influence of the instabilities on model results.
- It would also be good to perform more validation simulations to validate SWASH under a wider range of wave conditions.
- Discrepancies were observed between modelled and observed short wave direction. It is recommended to verify whether the origin of these discrepancies is in the model, measurement observations or method to calculate the short wave direction.
- Validation study results showed that the inclusion of inertia might be necessary to improve model results. It should be investigated whether the lack of inertia really influences the model results. If this is the case, it is recommended to extend the method presented in this thesis with one of the possibilities provided in Section 8.4.

Model development:

- Investigate the boundary error which is made at the numerical wavemaker. An alternative is to quantify the error as a function of model settings (eg. grid size,

number of layers, wave height). In this way the extra amount of energy added to compensate for the boundary error can be estimated more accurately.

- The differences in set-up which were described in Subsection 3.3.5 should be studied. This can be done according to laboratory measurements to see whether a solution can be found.

- Include wave breaking induced turbulence in the model. Presently some extra spreading is provided by the Smagorinsky horizontal mixing model in presence of velocity gradients. When wave breaking induced turbulence is included this would better represent reality and spreading of currents would be improved.

- The final recommendation is to include the pseudo alongshore water level gradient in the next version of SWASH as it provides the possibility to more accurately model surf zones when ambient currents are present.

List of Figures

List of Tables

Abbreviations

1D	**1 D**imensional
2DH	**2 D**imensional **H**orizontal
2DV	**2 D**imensional **V**ertical
3D	**3 D**imensional
C3D	**C**OAST**3D**
DIWAR	**DI**rectional **WA**ve **R**ider buoy
DGPS	**D**ifferential **G**lobal **P**ositioning **S**ystem
HFA	**H**ydrostatic **F**ront **A**pproximation
EMF	**E**lectro **M**agnetic **F**lowmeter
RANS	**R**eynolds **A**veraged **N**avier **S**tokes
RMSE	**R**oot **M**ean **S**quared **E**rror
SWAN	**S**imulating **WA**ves **N**earshore
SWASH	**S**imulating **WA**ves till **SH**ore
WESP	**W**ater **E**n **S**trand **P**rofiler

Symbols

a	wave amplitude	m
C	Chézy constant	$m^{1/2}/s$
c	wave phase celerity	m/s
c_g	wave group celerity	m/s
d	bottom level (positive downwards)	m
E	wave energy	J
f	wave frequency	1/s
g	gravitational acceleration	m/s^2
h	total water depth	m
H_{m0}	wave height based on spectral analysis	m
H^n_{m0}	normalised wave height based on spectral analysis	m
H_{rms}	Root mean squared wave height	m
k	wave number	1/m
k_r	roughness height	m
L	wave length	m
N	number of layers	-
p	pressure	Pa
p_h	hydrostatic pressure	Pa
p_{nh}	non-hydrostatic pressure	Pa
p_{tide}	tidal pressure	Pa
S_{xx}	radiation stress of x-momentum in x-direction	N/m
S_{xy}	radiation stress of x-momentum in y-direction	N/m
S_{yy}	radiation stress of y-momentum in y-direction	N/m
S_{yx}	radiation stress of y-momentum in x-direction	N/m
t	time	s

T_p	peak wave period	s
U_{10}	wind speed at 10 meters height	m/s
U_n	ambient current velocity	m/s
u	flow velocity in x-direction	m/s
v	flow velocity in y-direction	m/s
v_{tide}	tidal alongshore velocity	m/s
w	flow velocity in z-direction	m/s
x	horizontal location perpendicular to coastline (positive towards shore)	m
y	horizontal location parallel to coastline (positive to north)	m
z	vertical location (positive upwards)	m
Δt	time step	m
Δx	grid size in x-direction	m
Δy	grid size in y-direction	m
α	breaking onset parameter	-
β	breaking offset parameter	-
ζ	free water surface (positive upwards)	m
θ	wave direction	$\circ$
$\nu_{t,h}$	horizontal eddy viscosity	m^2/s
$\nu_{t,v}$	vertical eddy viscosity	m^2/s
ρ	density of water	kg/m^3
σ	relative angular wave frequency	1/s
σ	directional spreading	$\circ$
τ_b	bottom shear stress	Pa
τ_w	wind shear stress	Pa
Ω	vorticity	1/s
ω	absolute angular wave frequency	1/s

Appendix A

COAST3D

Measurements were performed at Egmond aan Zee, which is located along the Dutch North Sea coast. Hydrodynamic measurements were carried out at several locations in an area of approximately 500 x 500 m^2, of which an overview is given in Figure 2.1. It concerns a dissipative sandy beach with two alongshore bars. The tidal range varies between 1.4 and 2.0m, at neap and spring tide respectively. The yearly-averaged wave height is about 1 m, but during storms conditions wave heights up to 5m might occur.

A.1 Available data

Most current and water level measurements were located in the main transect. Wind velocities and directions are available at locations 7a. Wave conditions are obtained from a directional wave rider buoy, located 5 km offshore at a depth of 16 m (not on this picture). Also on locations 7A, 7B, 7D and 7E wave data is available which is useful for validation.

The topic of this MSc thesis will concern currents. Therefore the flow data reported during the COAST3D project is of great interest. A summary of the available flow data is given below:

- location 1A to 1D: four tripods [1] with EMF's [2] at two heights over inner bar

[1] Tripod is a structure on three poles containing measurement devices
[2] EMF is an abbreviation for Electro Magnetic Flow meter

- location 2: one tripod with at three heights an EMF at the outer bar
- locations 13, 14 and 15: frames with a single EMF in the surf zone
- locations 18a to 18c: frames with a single EMF at the outer bar

At all locations listed above the cross-shore and alongshore components of the velocity are measured for six weeks with a frequency of 2 Hz. (van Rijn et al., 2002)

A.2 Equipment inaccuracies

This data is extracted from the paper Van Rijn et al. (2002), which is part of the COAST3D book. In this paper the accuracy of the several measurement instruments is elaborated. This can be useful to know to which extent the data is reliable and which error ranges are acceptable when validating. Below a short summary is given for the accuracy of relevant parameters and instruments.

Velocity

The velocities at interesting locations are all measured by electromagnetic velocity meters.

- Peak orbital velocities have an uncertainty of maximum 15%
- Time-averaged velocities smaller than $0.05 m/s$ have an uncertainty up to 100 %
- Time-averaged velocities from 0.15 to $0.30 m/s$ have an uncertainty up to 30 %
- Time-averaged velocities above $0.50 m/s$ have an uncertainty up to 15%

Wave height

Wave height and water depth have been measured by pressure meters. The uncertainty is in the range of $10 - 15\%$. The inaccuracy in water depth is due to the uncertainty of height above the bed of the pressure sensor.

Bathymetry

The bathymetry has been measured in three ways:

- Bed level soundings with a ship-mounted echo sounder. A inaccuracy of 0.1-0.15m in vertical height is found in water depths larger than 6m. In shallower water the uncertainty can be as large as 0.25m.
- Bed level soundings with a DGPS [3] on the WESP [4] vehicle have a vertical inaccuracy of 0.1-0.15m.
- Beach level soundings by a DGPS receiver have a vertical uncertainty of 0.05 to 0.1m.

[3] DGPS is an abbreviation for Differential Global Positioning System

[4] WESP is a dutch abbreviation saying: Water And Beach Profiler, which is a vehicle able to measure bed levels above and below water

Appendix B

SWASH model

B.1 Boundary conditions

B.1.1 Numerical wavemaker

At the seaward boundary, waves are generated by a numerical wavemaker which specifies the horizontal normal velocities based on linear wave theory. However, if the command ADDBOUNDWAVE is used, the velocity components of the bound sub harmonics (bound infragravity waves) are additionally included. The super harmonics are not included in the current version of SWASH 3.14. These sub and super harmonics are generated as a result of nonlinearity. They are called bound waves as they travel with the same speed as the primary wave and are a result of the difference and sum interaction of the linear waves, respectively. It is assumed that the lack of super harmonics does not significantly influence the model results. Therefore the inputted waves can be assumed to be according to weakly nonlinear wave theory (second order Stokes wave). So the depth, wave height and wave period should be such that the inputted waves are within linear or weakly nonlinear wave theory. In this thesis the nonlinearity is quantified by the Ursell number $N_{Ursell} = \frac{HL^2}{d^3}$. According to Holthuijsen (2007) this number should be below 10 for waves for the weakly nonlinear wave theory to be valid.

B.1.2 Dispersion accuracy

SWASH improves its frequency dispersion by increasing the number of layers. Table B.1 shows the dimensionless water depth ($= kd$) range required to solve the normalised wave celerity ($= c/\sqrt{gd}$) within an error range of 1% for one to three layers K.

K	kd range
1	$kd \leq 0.5$
2	$kd \leq 7.7$
3	$kd \leq 16.4$

TABLE B.1: Frequency dispersion error below 1% (SWASH-User-Manual, 2015)

The value of kd usually highest and thus critical at offshore boundary in coastal models, due to the largest water depth. For this location kd should be small enough for the number of layers applied to correctly solve dispersion in the model. Figure B.1 can be used to quickly see the kd value as a function of the frequency and water depth. For a given depth and frequency the point should be below the limit for SWASH to accurately solve the frequency dispersion.

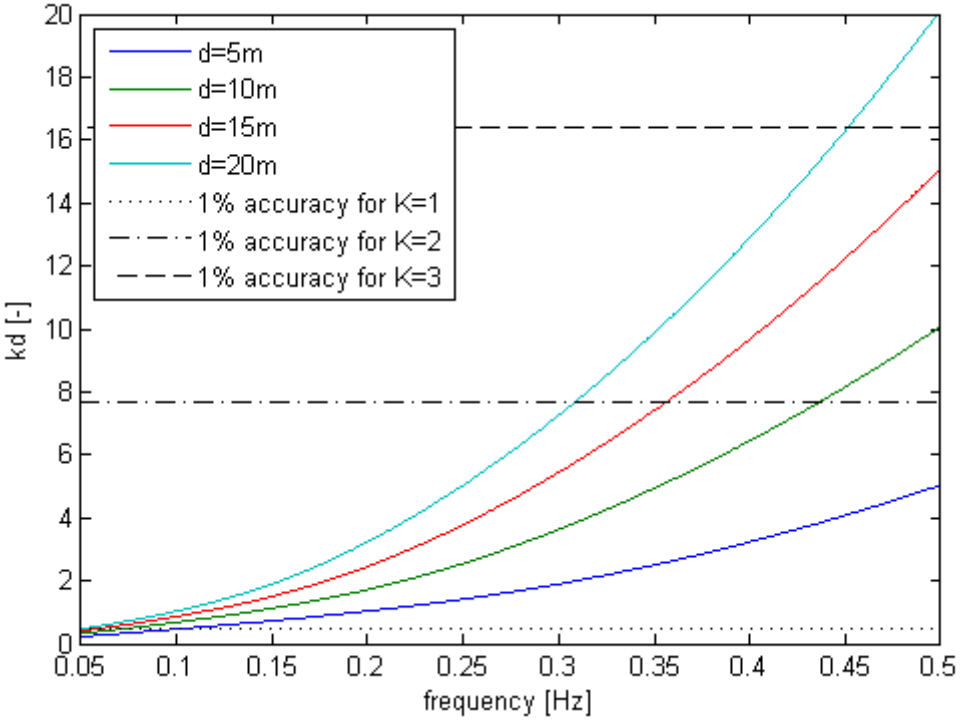

FIGURE B.1: kd as a function of frequency and water depth

B.1.3 Evanescent modes

When SWASH generates waves by using a spectrum, evanescent modes might be included as well. These modes are a result of the underlying model equations. Because it is undesirable to have these evanescent waves in the model all wave components above the so-called cut-off frequency are removed by SWASH. This is the frequency where these evanescent modes are generated, which depends on the local water depth and the number of layers. If too much wave components above the cut-off frequency are removed also energy of the wave spectrum is not taken into account leading to errors. Therefore it is wise to choose the number of layers, water depth and wave period at the boundary in such a way that no components are removed. SWASH will only give a warning if more than 10% of wave components are removed. The cut-off frequency is given by:

$$f_{cut-off} = \frac{K}{\pi}\sqrt{\frac{g}{d}}$$

in which: K is the number of layers, $g = 9.81 m/s^2$ is the gravitational acceleration and d is the water depth at the boundary in m. Because SWASH generates wave components between $0.5 f_p$ and $3 f_p$, the maximum peak frequency f_p to not have components removed should be:

$$f_{p,max} = \frac{f_{cut-off}}{3}$$

and the corresponding minimum wave peak period:

$$T_p = \frac{1}{f_{p,max}} = \frac{3}{f_{cut-off}}$$

The minimum wave peak period to avoid removed components is plotted as a function of water depth for one, two, three and four layers in Figure B.2.

B.2 Wave breaking

SWASH can accurately model energy dissipation due to wave breaking in the surfzone when a high vertical resolution (10 layers or more) is applied (Smit et al., 2013). When less layers are used the particle velocities near the surface are underestimated, postponing the wave from getting more asymmetrical and consequently delays wave breaking.This implies that in this region the non-hydrostatic pressure is overestimated. Smit et al.

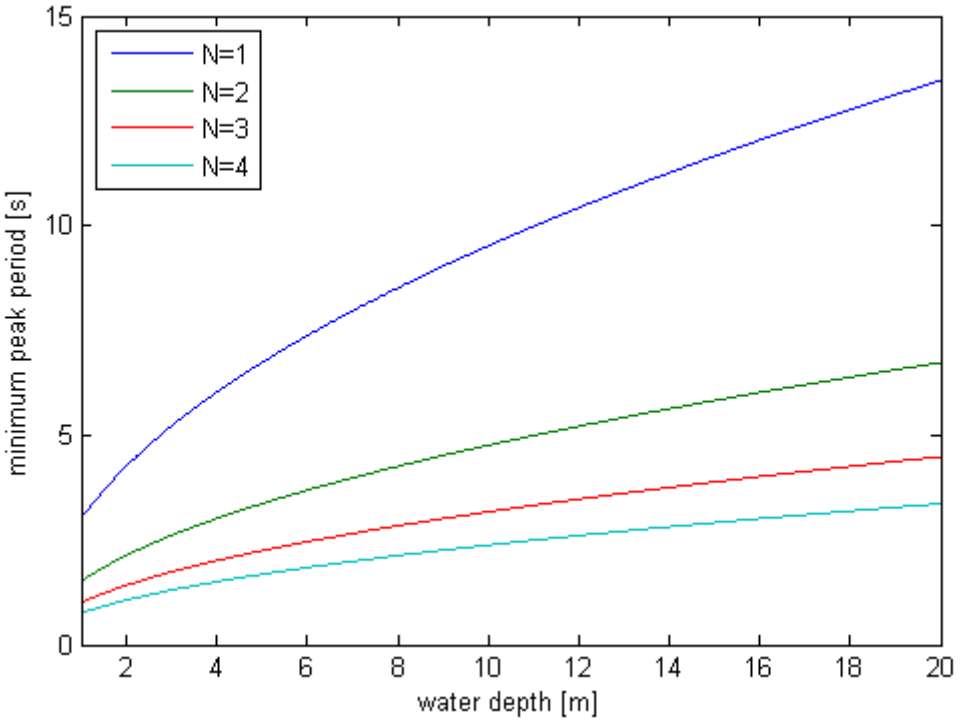

FIGURE B.2: Minimum wave peak period to avoid evanescent modes

(2013) developed the BREAKing command in SWASH which can initiate the onset of wave breaking by approximating hydrostatic pressure at the wave front when it becomes too steep. This happens when the vertical speed of the free surface exceeds a certain threshold value α. When this parameter in neighbouring grid points becomes below value β the hydrostatic front approximation (HFA) will be switched off again.

The only values found in literature for the parameters for onset and offset of breaking α and β are described by Smit et al. (2014). These are for two and six layers and shown in Table B.2

N	α	β
2	0.6	0.3
6	1.0	0.3

TABLE B.2: α and β values

For other numbers of layers no values are available. As these values are only calibrated with laboratory experiments this parameter should be calibrated to accurately present wave breaking in the model.

Appendix C

Radiation stresses

The transport of wave induced momentum ρu is equivalent to a stress, which is called radiation stress (Longuet-Higgins and Stewart, 1964). Wave momentum is transported by the orbital velocities (u_x and u_y) and by the wave induced dynamic pressure p_{wave} (Holthuijsen, 2007). The radiation stresses can be written as [1]:

$$S_{xx} = \overline{\int_{-d}^{\eta} (\rho u_x u_x + p_{wave}) dz} \tag{C.1}$$

$$S_{yy} = \overline{\int_{-d}^{\eta} (\rho u_y y_x + p_{wave}) dz} \tag{C.2}$$

$$S_{xy} = \overline{\int_{-d}^{\eta} (\rho u_x u_y + \tau_{xy}) dz} \tag{C.3}$$

$$S_{yx} = \overline{\int_{-d}^{\eta} (\rho u_y u_x + \tau_{yx}) dz} \tag{C.4}$$

The wave forcing in x-, and y-direction as a result of these radiation stresses are:

$$F_x = -\frac{\partial S_{xx}}{\partial x} - \frac{\partial S_{xy}}{\partial y} \tag{C.5}$$

$$F_y = -\frac{\partial S_{yy}}{\partial y} - \frac{\partial S_{yx}}{\partial x} \tag{C.6}$$

[1] The first subscript defines whether it is x or y momentum and the second one in which direction it is transported.

Included in the alongshore uniform, depth and wave period averaged momentum balances this leads to the following equation for x-momentum (Svendsen et al., 2006) and y-momentum (Ruessink et al., 2001):

$$\underbrace{\frac{\partial S_{xx}}{\partial x}}_{\text{wave forcing}} = - \underbrace{\rho g h \frac{\partial \zeta}{\partial x}}_{\text{water pressure}} - \underbrace{\tau_b}_{\text{bottom shear stress}} \tag{C.7}$$

S_{xx} = radiation stress of x-momentum in x-direction

$\frac{d\zeta}{dx}$ = cross-shore water level gradient

τ_b = bottom shear stress

$$- \underbrace{\frac{1}{\rho}\frac{dS_{yx}}{dx}}_{\text{wave forcing}} + \underbrace{\frac{\tau_y^w}{\rho}}_{\text{wind forcing}} - \underbrace{g h \frac{d\zeta}{dy}}_{\text{tidal forcing}} = \underbrace{c_f \langle |\overrightarrow{u}| v \rangle}_{\text{bottom stress}} - \underbrace{\frac{d}{dx}\left(\nu \frac{d\overline{v}}{dx}\right)}_{\text{lateral mixing}} \tag{C.8}$$

S_{yx} = radiation stress of y-momentum in x-direction

τ_y^w = alongshore wind stress

$\frac{d\zeta}{dy}$ = alongshore water level gradient

c_f = friction coefficient

ν = eddy viscosity

The wave forcing can be described by:

$$\frac{dS_{yx}}{dx} = -\frac{sin(\theta)}{c} D_r \tag{C.9}$$

Appendix D

Wave model results

This appendix provides additional visualisations of the performed wave transformation study.

D.1 Assumption N is 10 layers $\approx N$ is 20 layers

As can be seen in Figure D.1 almost no difference can be observed between similar simulations with 10 and 20 layers. The maximum error for mean water level and wave height prediction is $O(1mm)$ and $O(1cm)$, respectively. Therefore it is concluded that the assumption that using 10 layers gives approximately similar results as 20 layers. So 10 layers is sufficiently accurate to be used as reference simulation for other runs. Additionally, it is shown in Figure D.2, that differences in numerical approximation for the non-hydrostatic pressure term are negligible.

D.3 Assumption Δx $0.25m \approx \Delta x$ $0.125m$

Instabilities were observed at a number of computations with $\Delta x = 0.125m$. All together it can be concluded that $\Delta x = 0.125m$ is too small and leads to instabilities. This is probably caused by the fact that using a smaller grid size means that shorter wave components are taken into account which result in problems. These components can be eliminated by using a more dissipative numerical scheme for the advective terms. However, this leads to less reliable results. Because results with $\Delta x = 1m$ and $\Delta x =$

$0.5m$ already strongly converged towards the $\Delta x = 0.25m$ it is assumed that decreasing the grid size even further is not necessary.

To support this assumption the successful runs with $\Delta x = 0.125m$ will be compared to their similar runs with $\Delta x = 0.25m$. This comparison will be based on two parameters, namely the relative root-mean-squared error of predicted spectral wave height as well as mean water level. The values can be found in Table D.1.

H_s [m]	N [-]	$E_{RMS}(H_{m0})$ [%]	$E_{RMS}(MWL)$ [%]
1	2	0.02	0.25
1	3	0.02	0.25
1	4	0.01	0.30
1	5	0.02	0.21
2	2	0.03	0.28
2	3	0.02	0.22
2	4	0.03	0.38
3	2	0.04	0.37
3	3	0.05	0.50

TABLE D.1: Relative RMS error for spectral wave height and mean water level prediction between $\Delta x = 0.25m$ and $\Delta x = 0.125m$

As can be seen in Table D.1 the errors are small for all comparisons. Relative errors for water level are significantly higher than those for wave height prediction. This is because the mean value which it is averaged over is close to zero for the mean water level and much higher for the mean wave height. So the assumption, that decreasing the grid size further than $\Delta x = 0.25m$ is unnecessary, is valid as relative errors are small.

D.5 Determination number of layers

In this section error metrics and figures are presented which where used to determine the number of layers. Tables D.2 until D.7 provide the relative root mean squared error for wave height and mean water level prediction. This is done for all three wave climates. Model simulations are compared to a 10 layer reference run and comparisons were only made in the pre-breaking region. Figures D.3, D.4 and D.5 visualise comparisons for above mentioned simulations.

Number of layers	1	2	3	4	5
dx=1m	0.08%	0.04%	0.03%	0.03%	0.02%
dx=0.5	0.06%	0.05%	0.04%	0.03%	0.03%
dx=0.25m	0.05%	0.05%	0.03%	0.03%	0.03%

TABLE D.2: Relative RMS error for wave height prediction of low wave climate (H=1m, T=6s) compared to 10 layer reference run

Number of layers	1	2	3	4	5
dx=1m	11.6%	1.7%	1.5%	1.3%	1.0%
dx=0.5	12.8%	1.6%	1.5%	1.3%	1.1%
dx=0.25m	12.6%	1.9%	1.5%	1.3%	1.3%

TABLE D.3: Relative RMS error for mean water level prediction of low wave climate (H=1m, T=6s) compared to 10 layer reference run

Number of layers	1	2	3	4	5
dx=1m	0.05%	0.06%	0.05%	0.04%	0.03%
dx=0.5	0.05%	0.07%	0.05%	0.05%	0.04%
dx=0.25m	0.05%	0.07%	0.07%	0.06%	0.06%

TABLE D.4: Relative RMS error for wave height prediction of medium wave climate (H=2m, T=7s) compared to 10 layer reference run

Number of layers	1	2	3	4	5
dx=1m	13.1%	1.0%	0.8%	0.5%	0.9%
dx=0.5	13.4%	0.6%	0.8%	0.8%	0.7%
dx=0.25m	14.2%	1.2%	1.2%	1.2%	1.2%

TABLE D.5: Relative RMS error for mean water level prediction of medium wave climate (H=2m, T=7s) compared to 10 layer reference run

Number of layers	1	2	3	4	5
dx=1m	0.05%	0.05%	0.04%	0.03%	0.02%
dx=0.5	0.04%	0.05%	0.05%	0.04%	0.03%
dx=0.25m	0.03%	0.05%	0.05%	0.04%	0.04%

TABLE D.6: Relative RMS error for wave height prediction of high wave climate (H=3m, T=8s) compared to 10 layer reference run

Number of layers	1	2	3	4	5
dx=1m	7.5%	0.9%	1.1%	1.0%	0.8%
dx=0.5	7.6%	1.0%	1.2%	1.2%	0.9%
dx=0.25m	7.8%	1.2%	1.4%	1.4%	1.4%

TABLE D.7: Relative RMS error for mean water level prediction of high wave climate (H=3m, T=8s) compared to 10 layer reference run

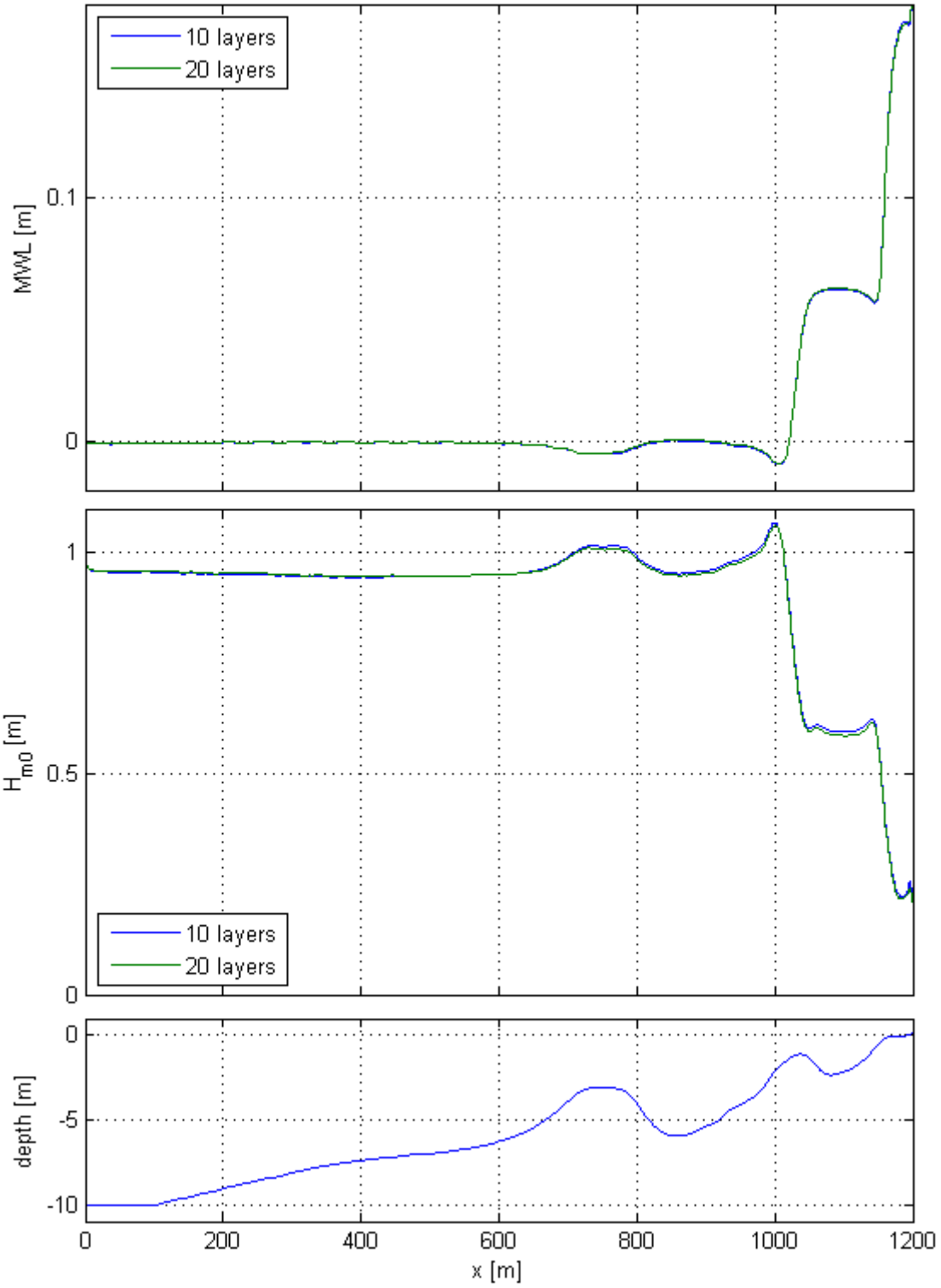

FIGURE D.1: Comparison for mean water level and wave height prediction between 10 and 20 layers

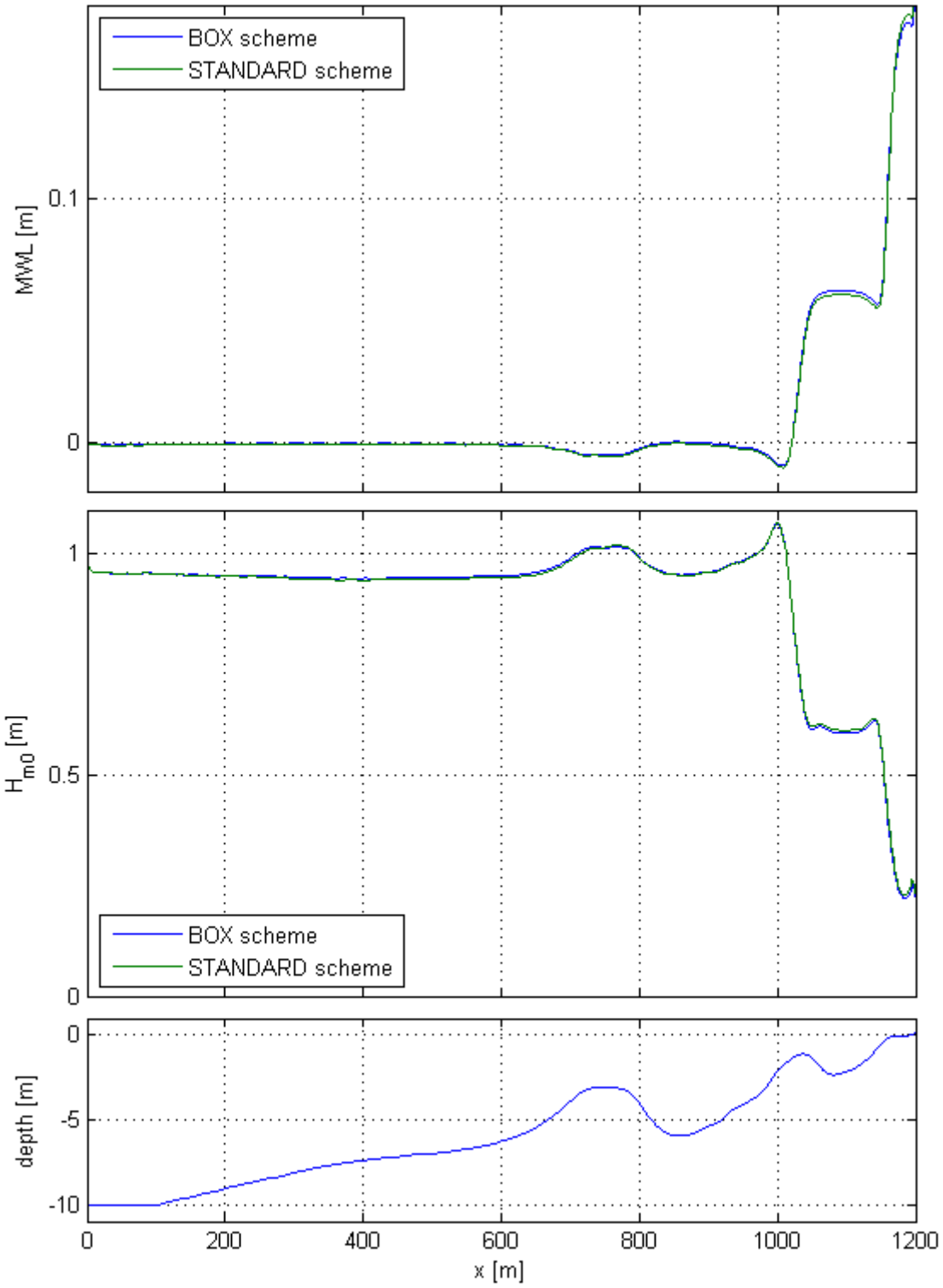

FIGURE D.2: Comparison for mean water level and wave height prediction between 10 and 20 layers

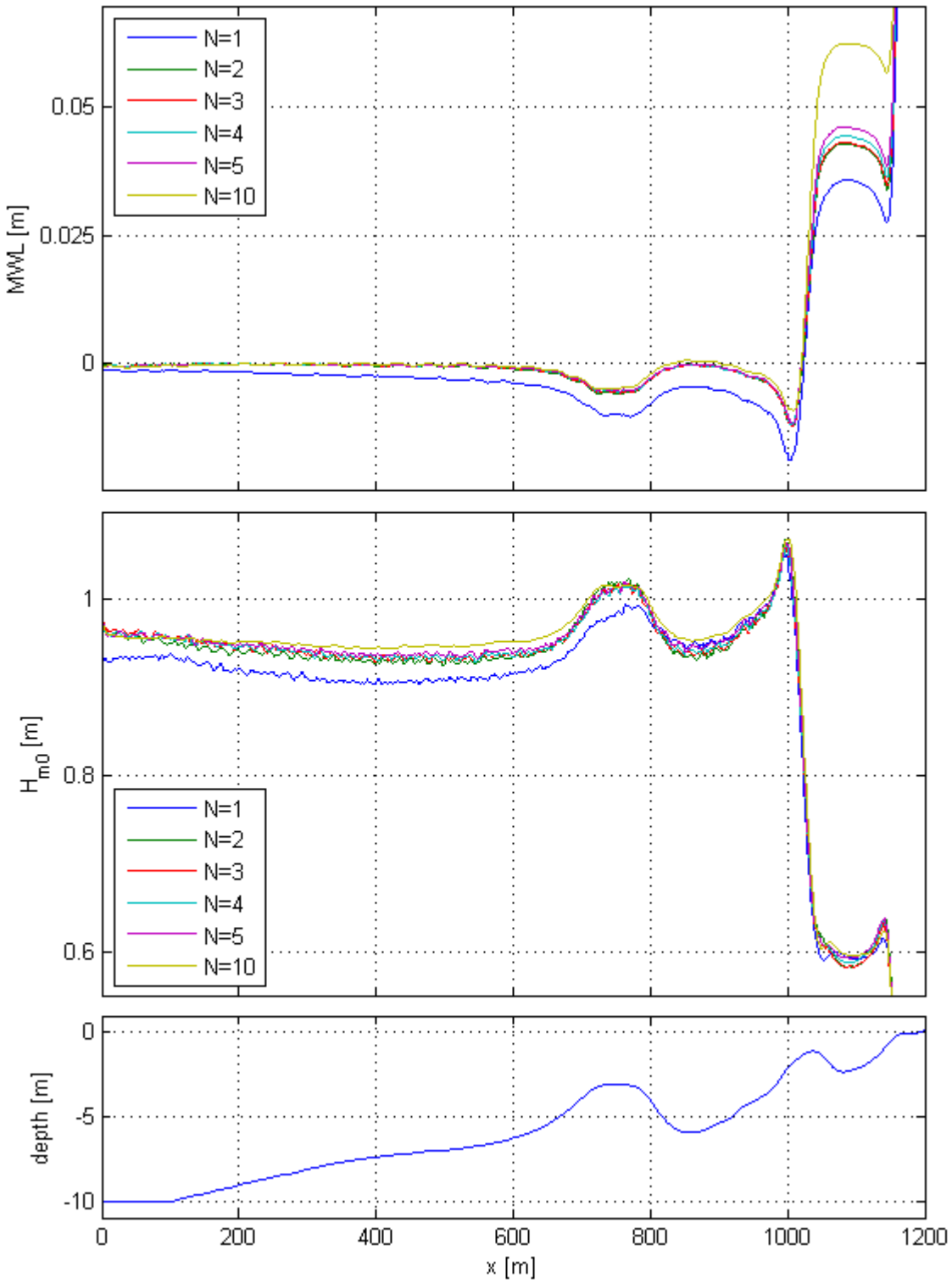

FIGURE D.3: Mean water level and wave height prediction in shoaling zone with low wave climate for different number of layers and $\Delta x = 0.5m$

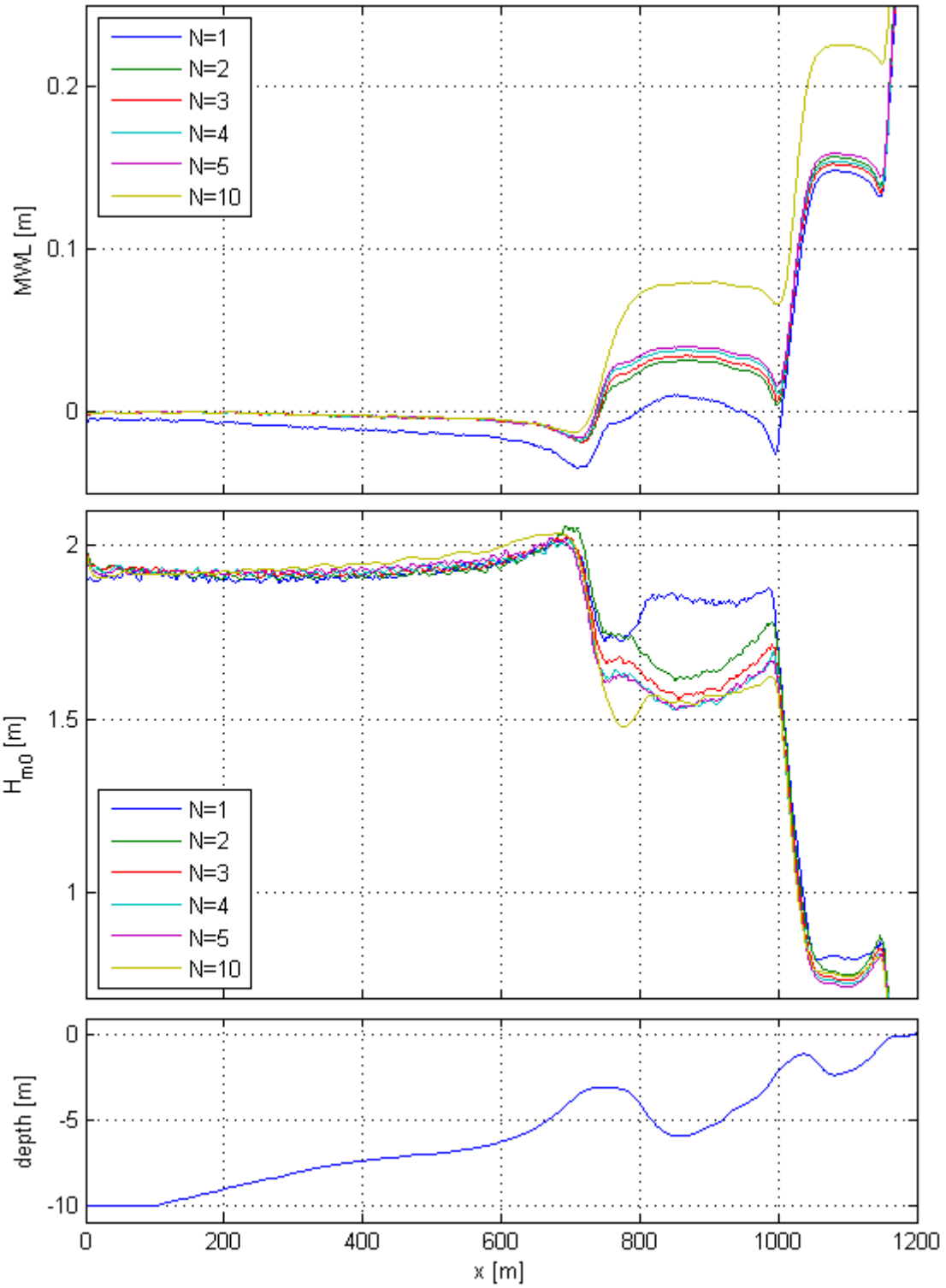

FIGURE D.4: Mean water level and wave height prediction in shoaling zone with medium wave climate for different number of layers and $\Delta x = 0.5m$

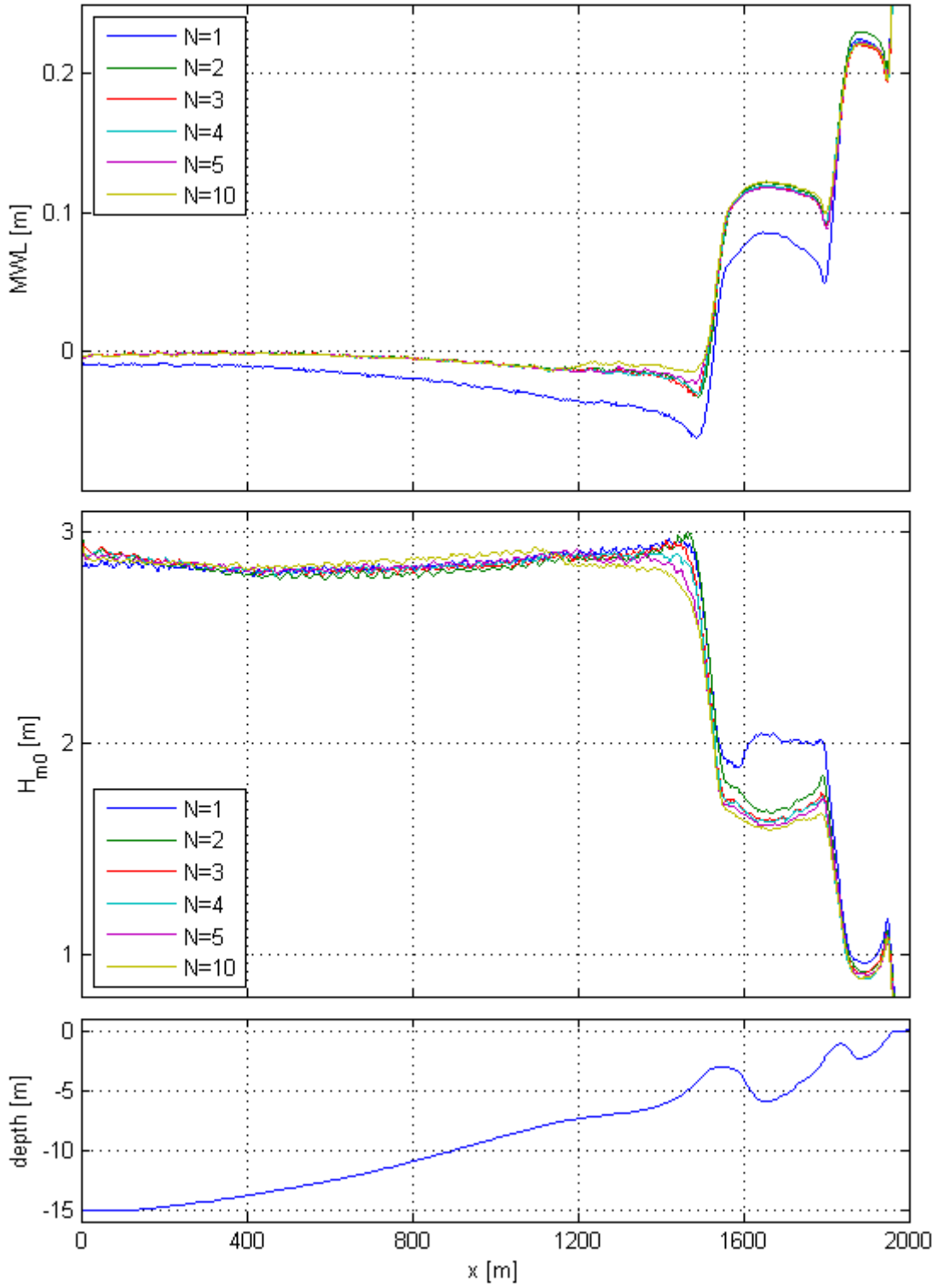

FIGURE D.5: Mean water level and wave height prediction in shoaling zone with high wave climate for different number of layers and $\Delta x = 0.5m$

D.7 Determination grid size

This section presents error metrics and figures which were used to determine the grid size. Table D.8 presents the relative root mean squared error for wave height and water level predictions. Figure D.6 shows corresponding plots of wave height distribution over the pre-breaking zone.

H_s [m]	Δx [m]	$E_{RMS}(H_{m0})$ [%]	$E_{RMS}(MWL)$ [%]
1	1	0.06	1.53
1	0.8	0.04	0.61
1	0.65	0.02	0.64
1	0.5	0.01	0.68
1	0.25	0.01	0.31
2	1	0.02	1.77
2	0.8	0.02	1.01
2	0.65	0.01	1.16
2	0.5	0.02	1.05
2	0.25	0.01	0.49
3	1	0.02	0.48
3	0.8	0.02	0.53
3	0.65	0.03	0.60
3	0.5	0.01	0.34
3	0.25	0.01	0.16

TABLE D.8: Relative RMS error for spectral wave height and mean water level prediction for runs with 2 layers and varying grid size. It is the RMSE with respect to simulations with extreme fine grid size ($\Delta x = 0.125m$).

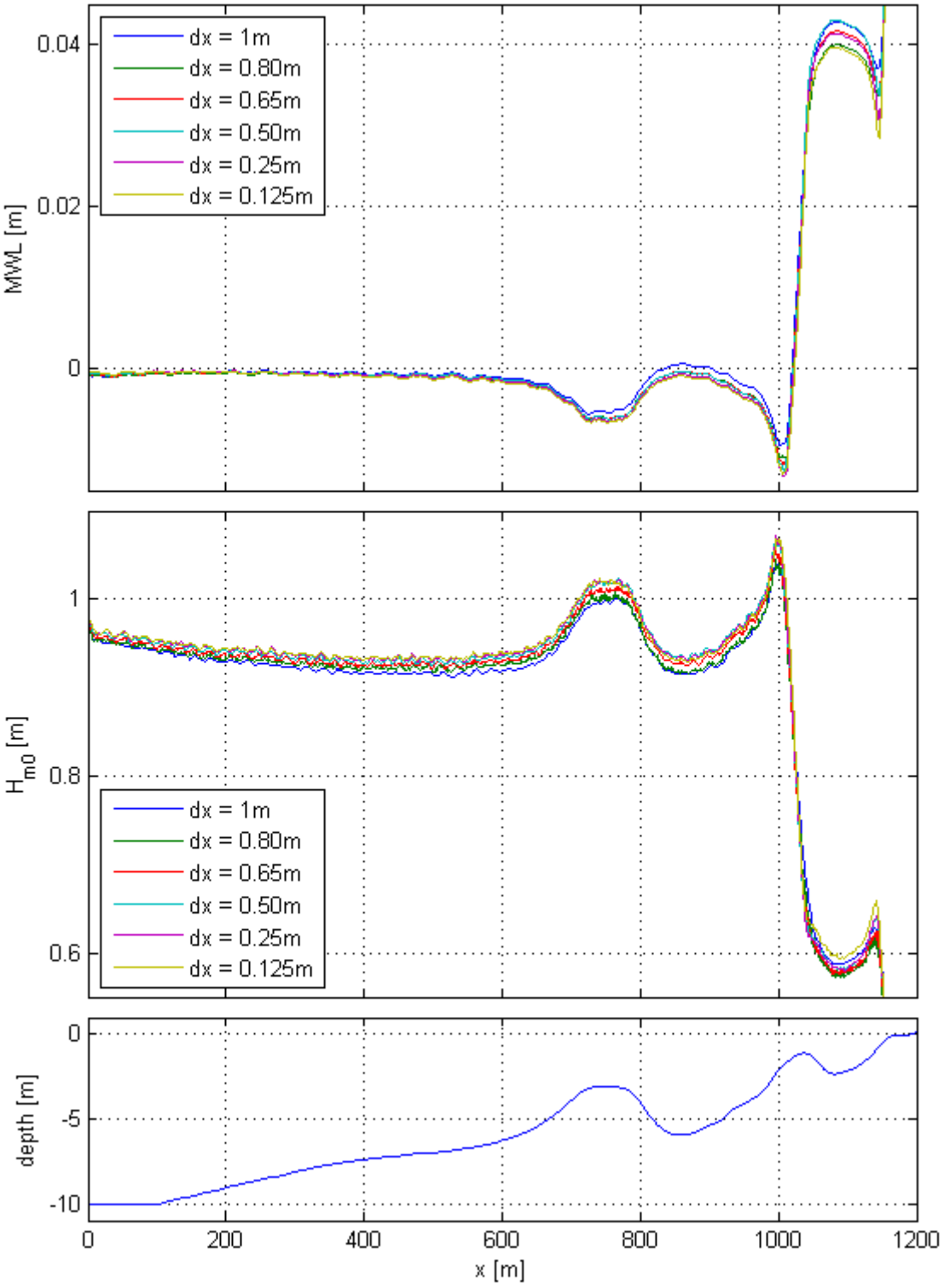

FIGURE D.6: Wave height prediction in the shoaling zone for low wave climate (upper figure), medium wave climate (middle figure) and high wave climate (lower figure)

D.9 Skewness and asymmetry

Dimensionless skewness and asymmetry were calculated with the following formulae applied to the time series.

$$Sk = \frac{<\zeta^3>}{\sigma^3} \tag{D.1}$$

$$As = \frac{<H(\zeta)^3>}{\sigma^3} \tag{D.2}$$

In which σ is the standard deviation and H represents the imaginary part of the Hilbert transform of the time series (Elgar, 1987). For the low wave climate this dimensionless skewness and asymmetry is shown in D.7 for:

- 2 layers and $\Delta x = 0.5m$
- 2 layers and $\Delta x = 0.125m$
- 10 layers and $\Delta x = 0.5m$

Differences between predicted skewness and asymmetry are small for the above described model simulations. Therefore, it is concluded that using 2 layers and a grid size in the order of $\Delta x = 0.5m$ is enough to accurately predict skewness and asymmetry of waves.

D.10 Sensitivity friction parameter

Variations have been made in the Nikuradse roughness height k_r. This is the only variable in the formulation of the LOGLAW friction command. For similar runs the following values have been considered: $1.0e^{-4}$, $2.5e^{-4}$, $5.0e^{-4}$, $7.5e^{-4}$, $1.5e^{-3}$, $3e^{-3}$. Figure D.8 shows the resulting graphs for mean water level and wave height prediction. As can be seen the differences are marginal. The only area where the influences of friction can be observed is in very shallow water O(0.1m). This area has been plotted in D.9. What can be seen is that higher friction leads to slightly more wave height

dissipation and a small increase in set-up. Still, differences are very small as a factor 30 in friction factor only leads to a difference of O(0.01m).

D.12 Sensitivity breaking parameters

To check the sensitivity of breaking parameters α and β, simulations were performed with varying configuration of these parameters. α values of 0.55, 0.6 and 0.65 were considered and β values 0.28, 0.30 and 0.32, resulting in a total of 9 runs. For the physical background of these parameters is referred to Appendix B.1.3.

Figure D.10 shows the result of varying α and β in the upper and lower graph, respectively. As can be seen, with higher values of α, the onset of wave breaking is delayed and therefore it takes longer for the wave height to drop. For higher β values, on the other hand, the offset of breaking start earlier.

D.14 Set-up differences when breaking

This section provides additional figures for the explanation of differences in observed set-up. In Figure D.11 it is visualised why a coarser grid leads to a lower maximum steepness internally calculated by SWASH. Figure D.12 shows that, for some reason, the boundary error was considerably larger for the simulation with $\Delta x = 1.0m$ than for $\Delta x = 0.5m$ or $\Delta x = 0.25m$.

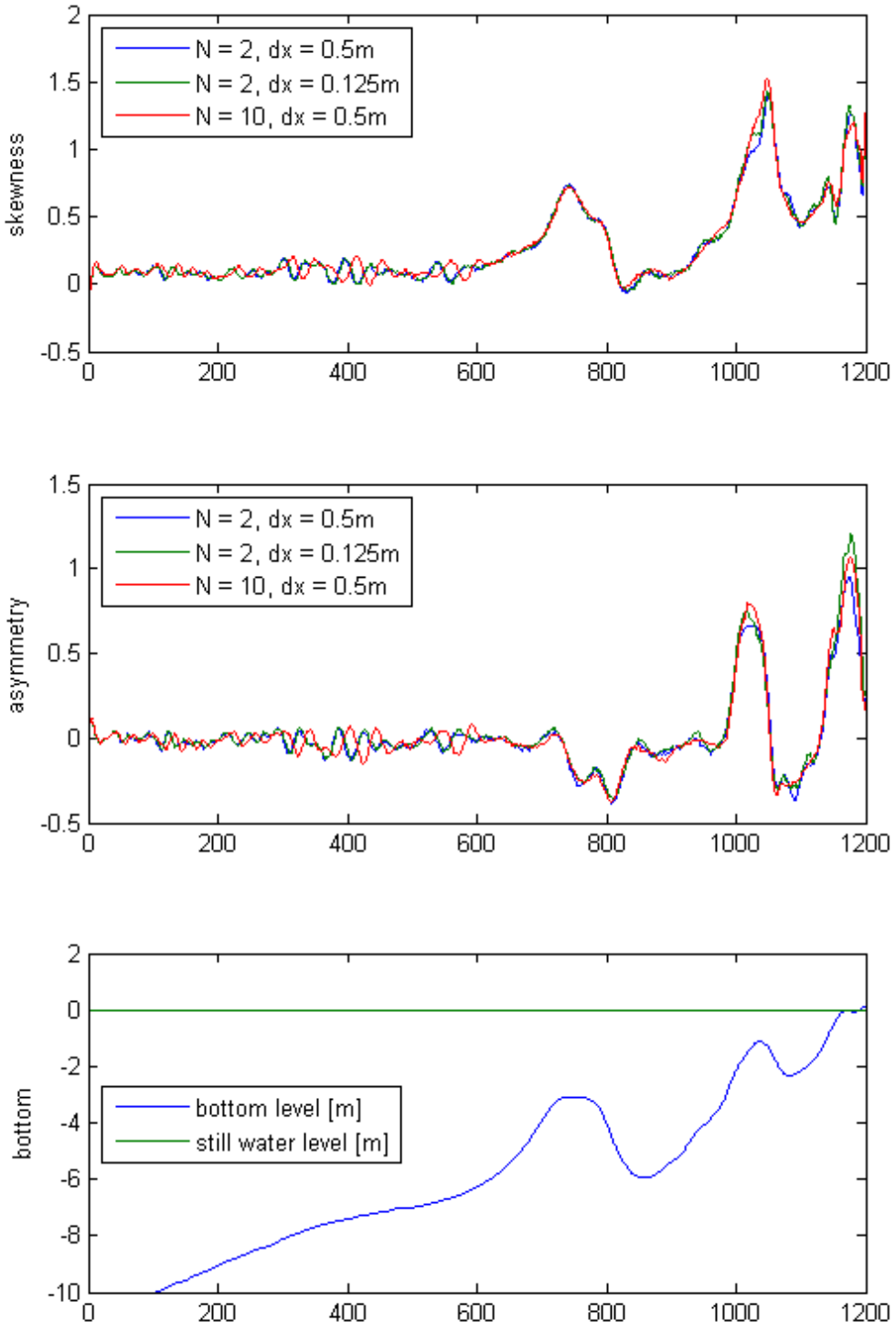

FIGURE D.7: Dimensionless skewness and asymmetry accompanied by bathymetry for three different runs

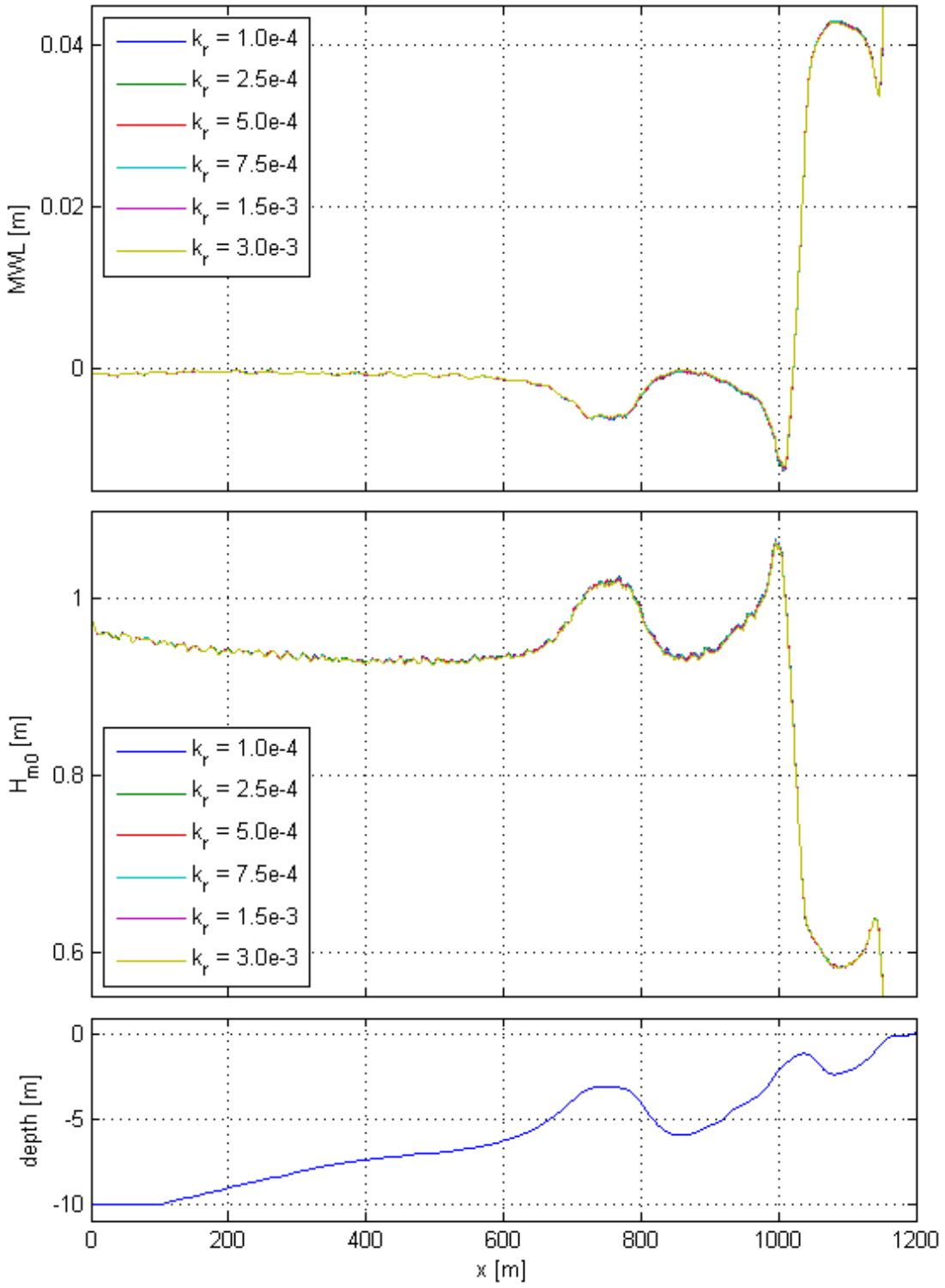

FIGURE D.8: Sensitivity friction for entire domain

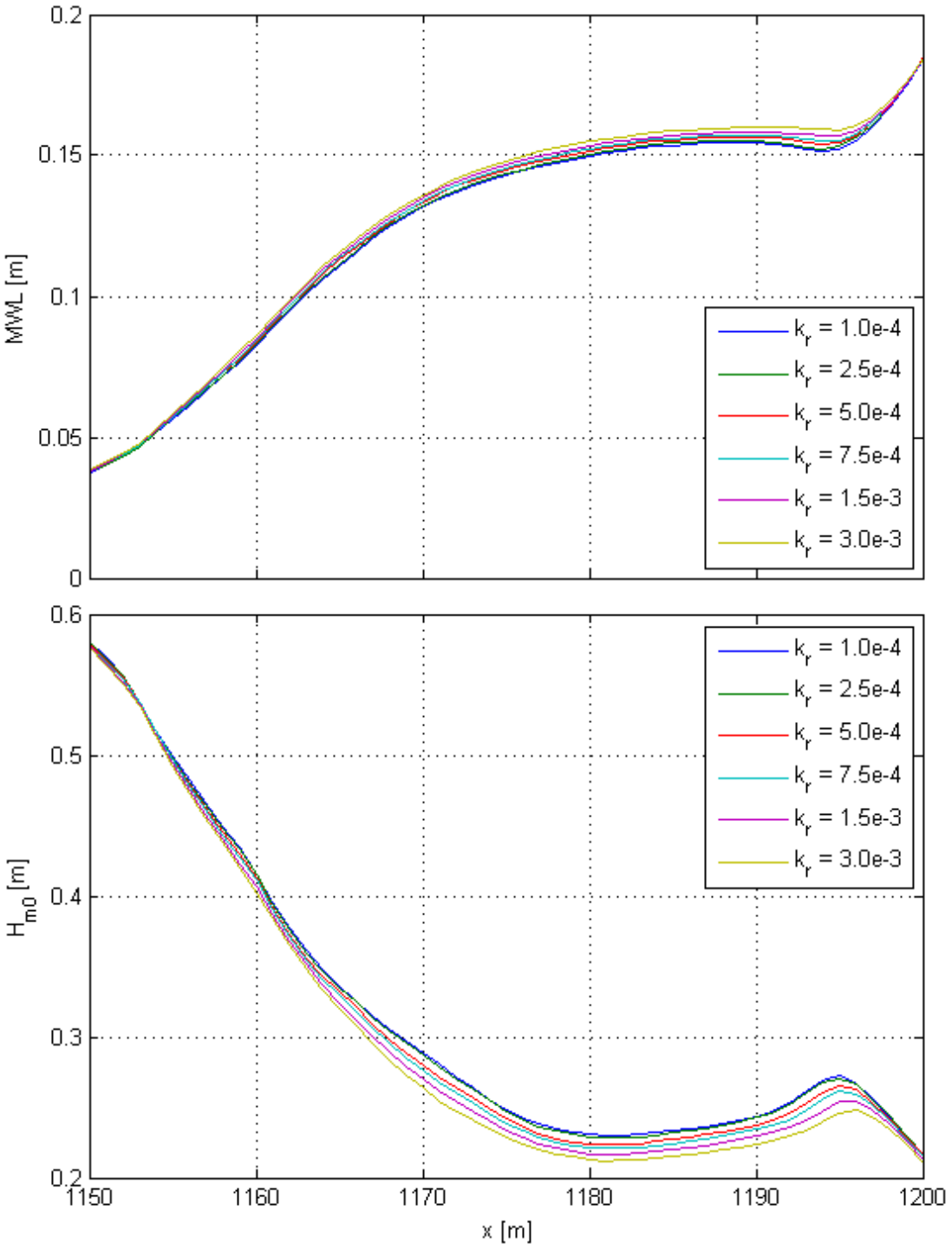

FIGURE D.9: Sensitivity friction in very shallow region

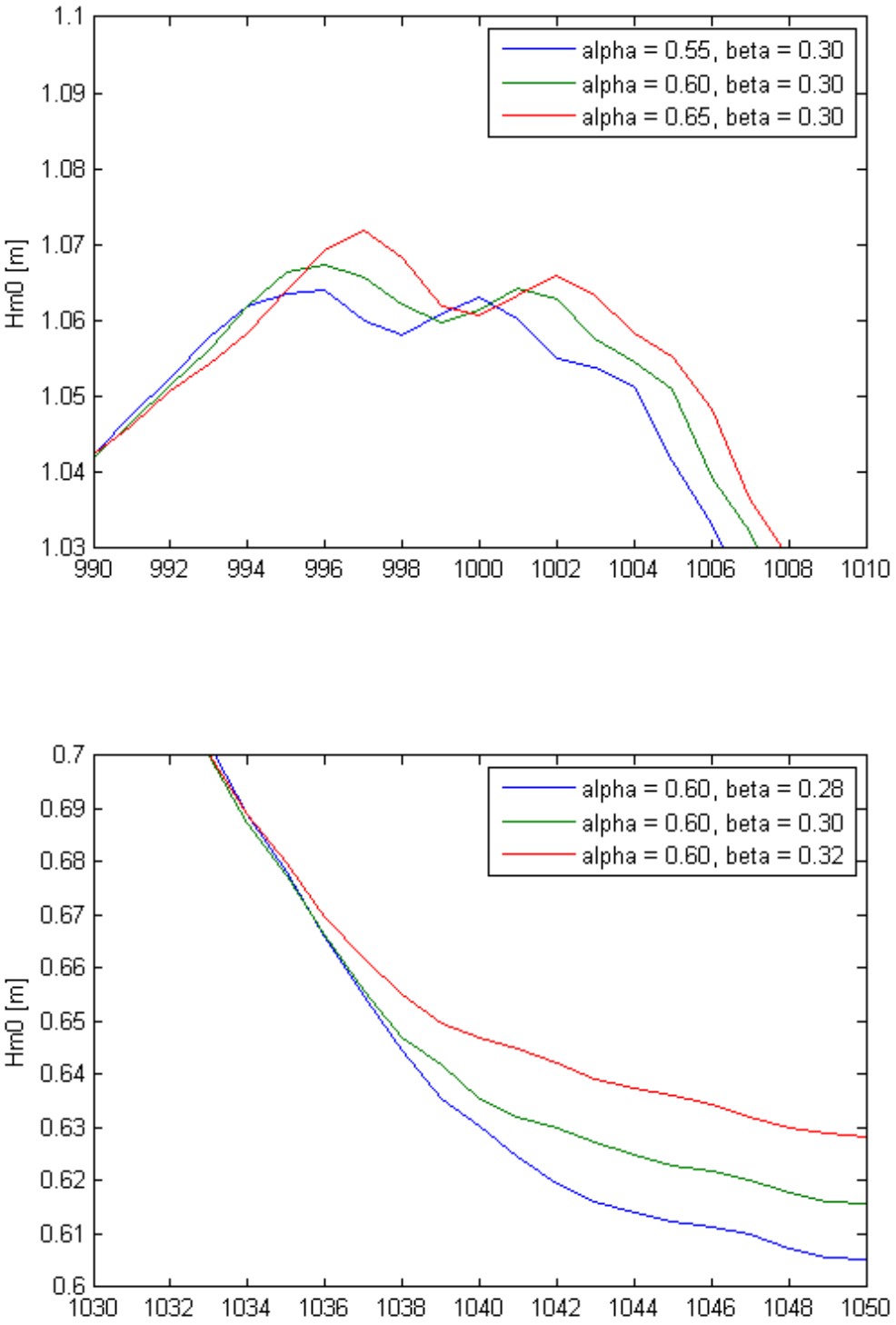

FIGURE D.10: Upper: varying values for breaking parameter alpha
Lower: varying values for breaking parameter beta

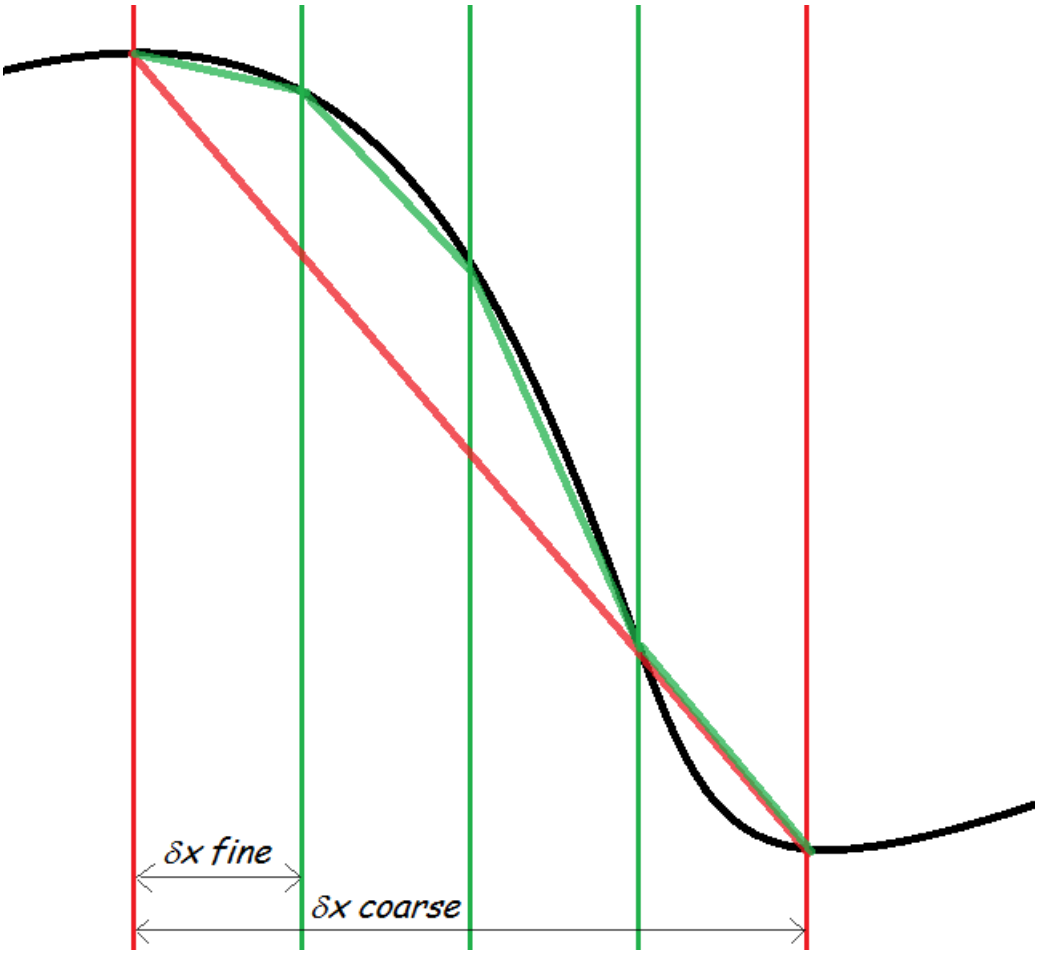

FIGURE D.11: Sketch explaining different steepness calculation in SWASH for different grid size

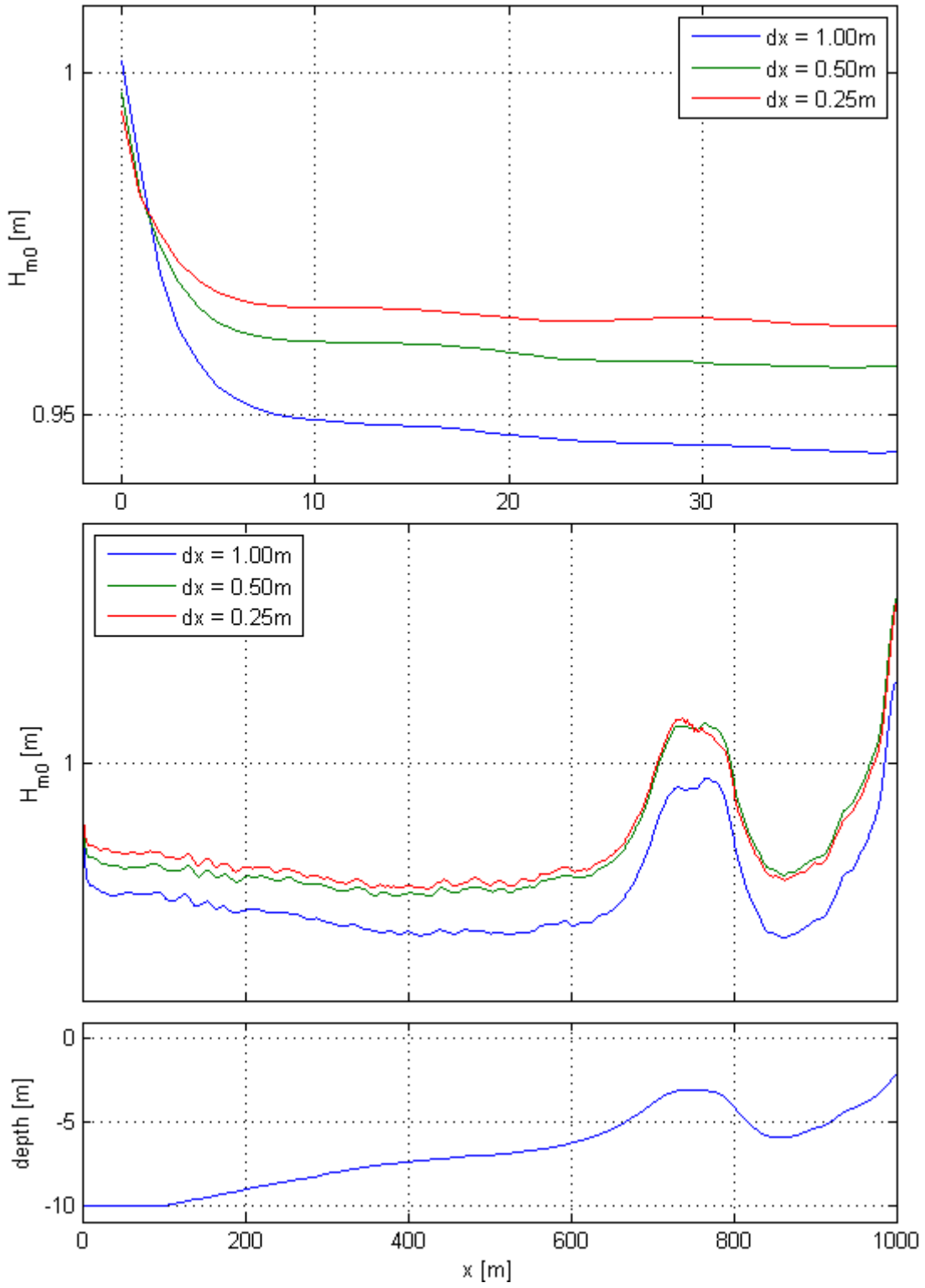

FIGURE D.12: Error at boundary for 20 layer simulations

Appendix E

Wave induced current results

E.1 Sensitivity wave direction

Tables E.1 and E.2 give the error which is induced by SWASH changing directions when using cyclic boundary conditions.

TABLE E.1: Relative error in direction due to alongshore domain length for $T_p = 6s$

Direction	**30**		**20**		**10**		**5**	
Spreading	**20**	**10**	**20**	**10**	**20**	**10**	**20**	**10**
Ly=100m	n.p.	n.p.	2%	3%	16%	20%	20%	37%
Ly=200m	0%	0%	1%	2%	2%	3%	3%	17%
Ly=300m	0%	0%	0%	0%	1%	2%	2%	7%
Ly=400m	0%	0%	0%	0%	1%	1%	1%	2%
Ly=500m	0%	0%	0%	0%	0%	0%	0%	1%
Ly=800m	0%	0%	0%	0%	0%	0%	0%	1%
Ly=1000m	0%	0%	0%	0%	0%	0%	0%	0%

TABLE E.2: Relative error in direction due to alongshore domain length for $T_p = 8s$

Direction	**30**		**20**		**10**		**5**	
Spreading	**20**	**10**	**20**	**10**	**20**	**10**	**20**	**10**
Ly=100m	n.p.	n.p.	10%	10%	28%	33%	33%	55%
Ly=200m	2%	2%	2%	4%	8%	11%	11%	29%
Ly=300m	0%	1%	1%	1%	1%	4%	4%	16%
Ly=400m	0%	0%	0%	0%	1%	2%	2%	8%
Ly=500m	0%	0%	0%	0%	1%	1%	1%	3%
Ly=800m	0%	0%	0%	0%	0%	0%	0%	1%
Ly=1000m	0%	0%	0%	0%	0%	0%	0%	1%

E.2 Figures wave induced current

Figures E.1 until E.3 show alongshore velocity predictions for varying alongshore domain lengths. This is done for waves incident under an angle of 10, 20 and 30°, respectively. E.4 presents the wave height predictions for varying Δy, from this can be concluded that convergence is observed from $\Delta y = 1.5m$ and smaller.

Figure E.5 shows the sensitivity of wave direction and directional spreading on the alongshore current. The influence of directional spreading is investigated for an angle of incidence of 20°. Simulation results for the medium wave climate ($H_{m0} = 2m$ and $T_p = 7s$) for varying angles of wave incidence are shown in Figure E.6.

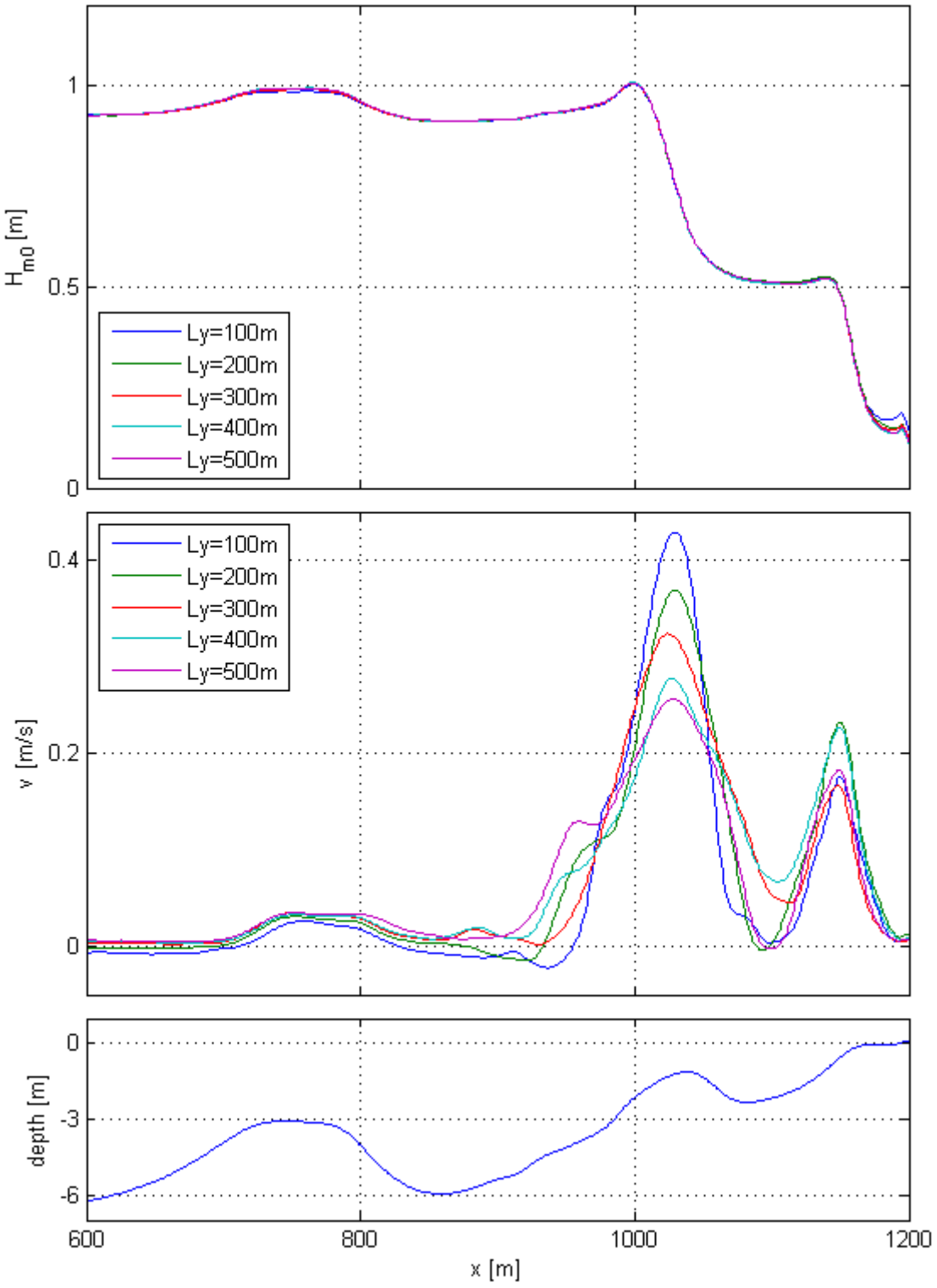

FIGURE E.1: Alongshore current for varying alongshore domain length for waves incident under an angle of 10 degrees

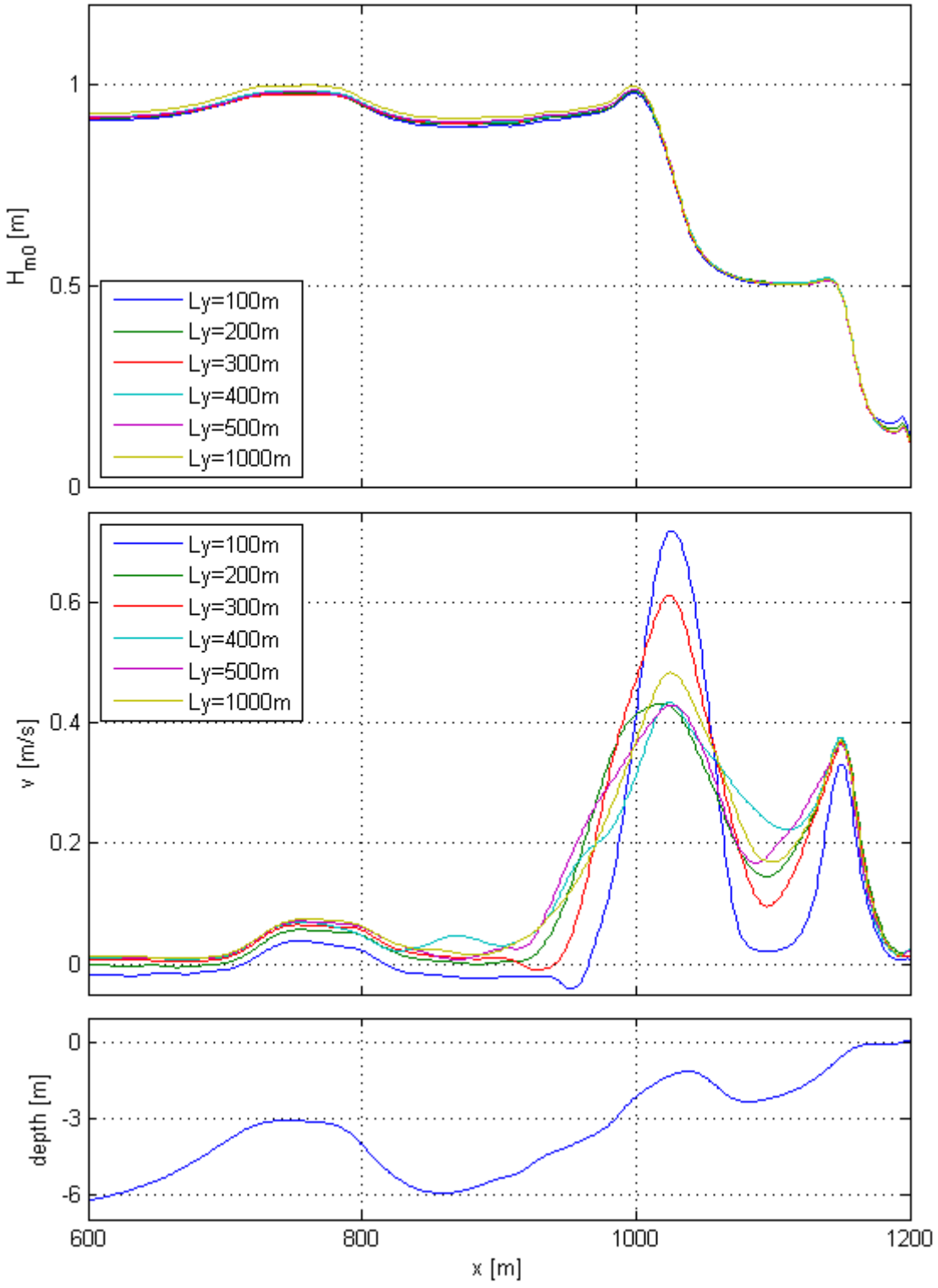

FIGURE E.2: Alongshore current for varying alongshore domain length for waves incident under an angle of 20 degrees

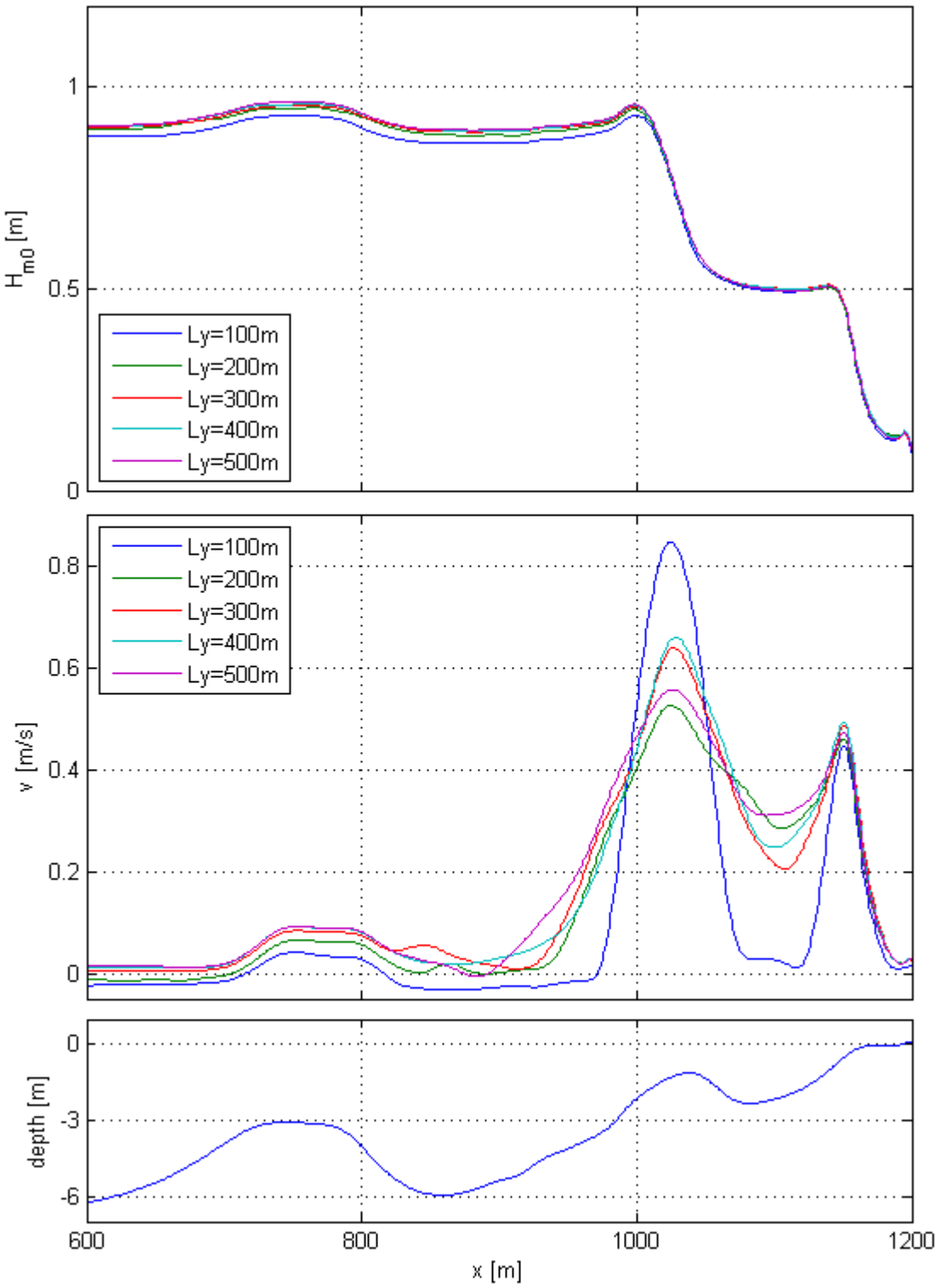

FIGURE E.3: Alongshore current for varying alongshore domain length for waves incident under an angle of 30 degrees

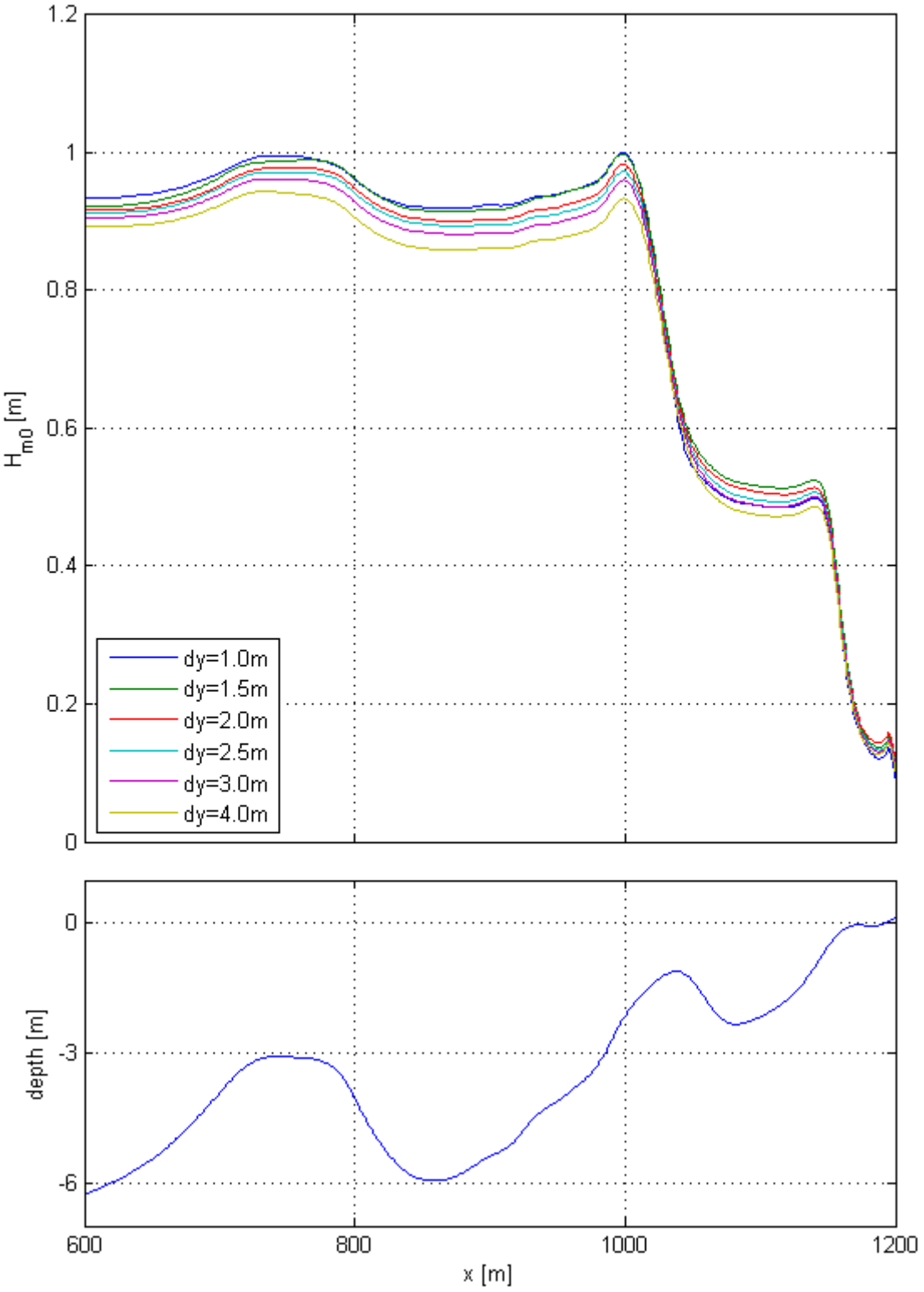

FIGURE E.4: Wave height for varying alongshore grid size

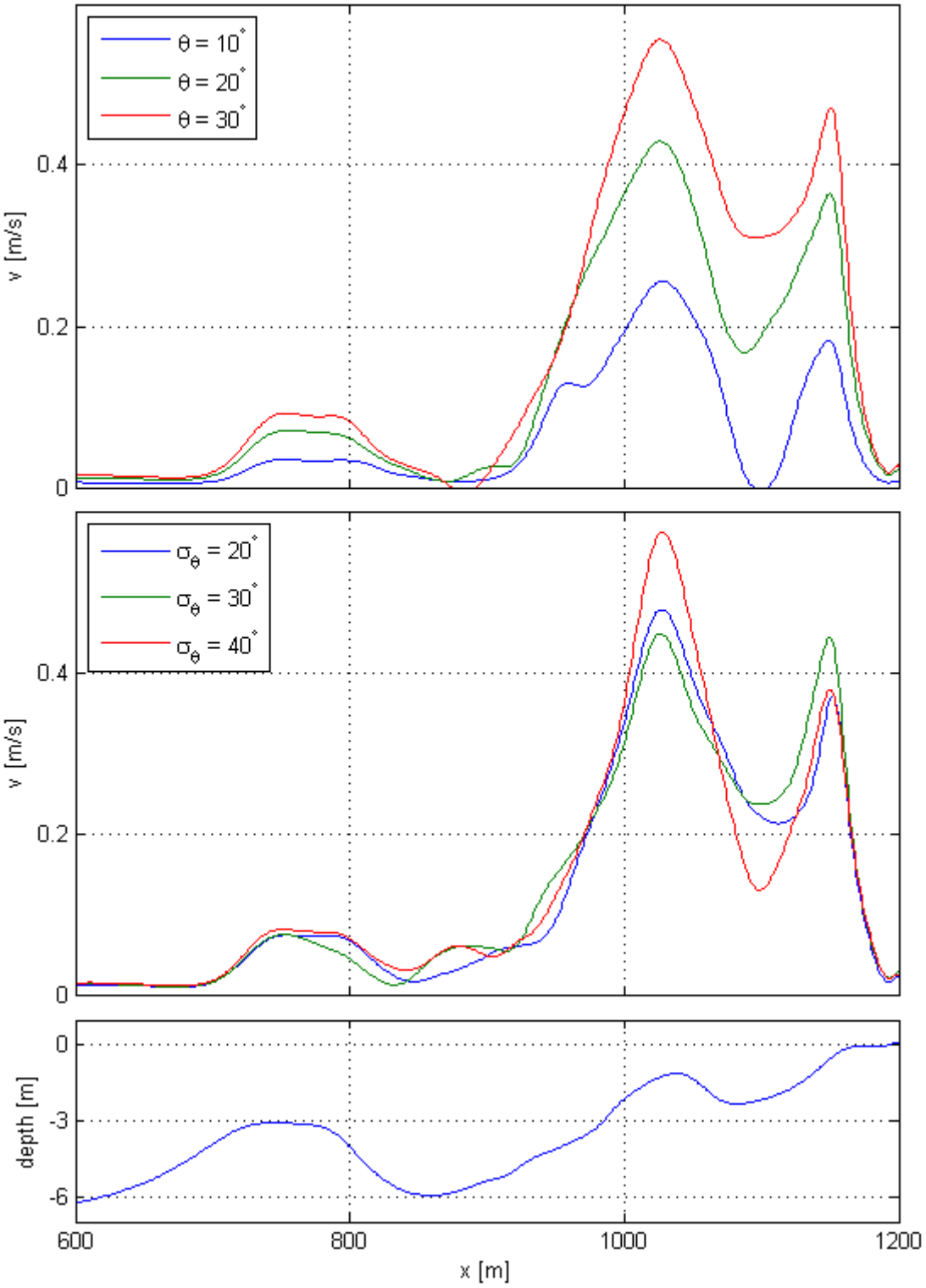

FIGURE E.5: Alongshore current for varying directions and directional spreading

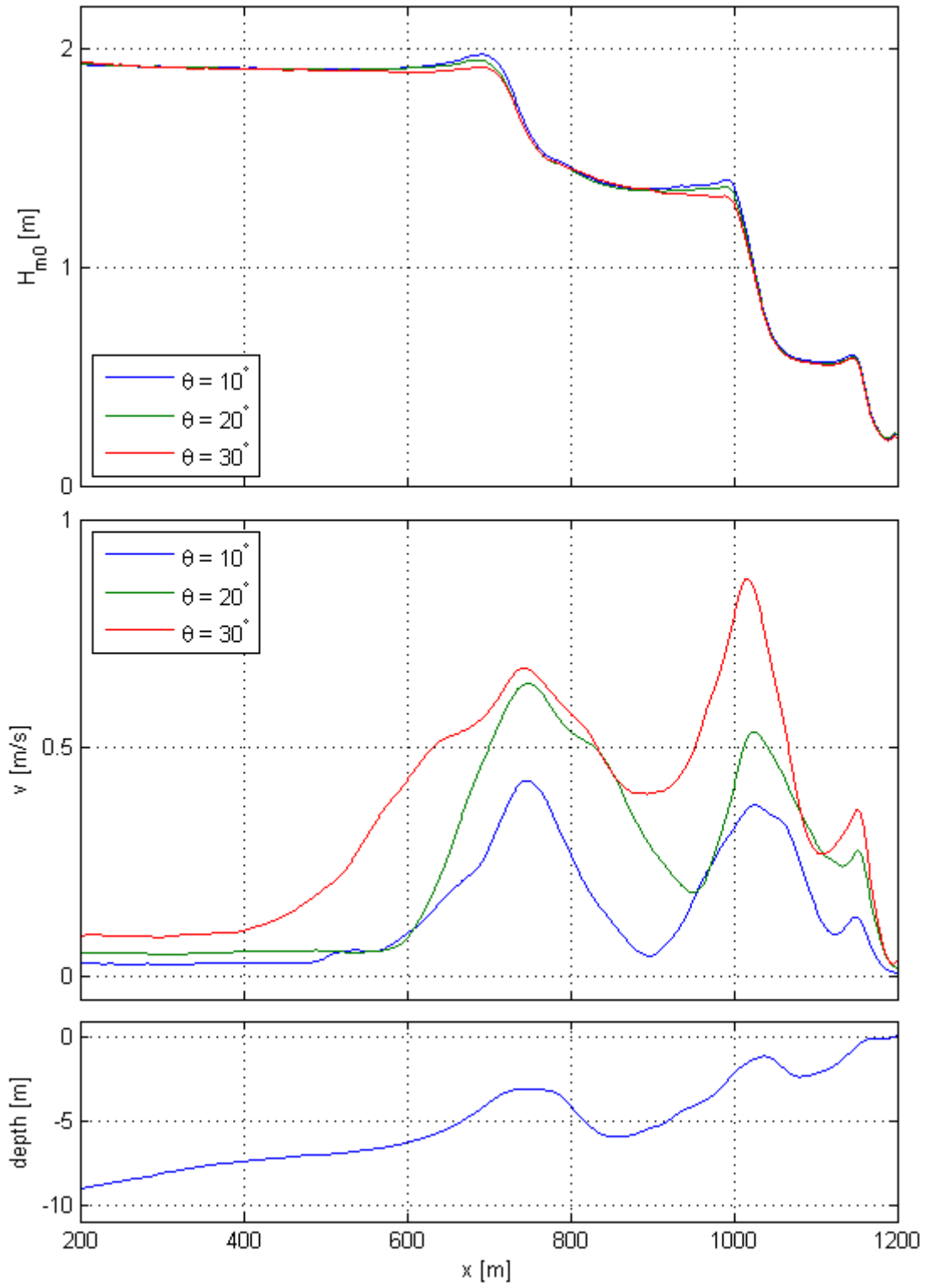

FIGURE E.6: Alongshore current for varying directions with medium wave climate

Appendix F

Implementation alongshore tide in SWASH

This appendix describes the changes which were made to the source code to implement an alongshore tidal velocity in combination with a cycling boundary condition.

SwashModule1.ftn90:

In this file the actual parameter is defined. Additions to the original file are in lines 414 and 415:

```
414   real    :: floris   ! the floris constant (time averaged
                              alongshore tidal water level gradient)
415                       ! =floris; set by command SET ...
                              [tidegradient] ...
```

SwashInit.ftn90:

An initial value of 0 is assigned to the parameter if not defined in the input file. This is in line 136:

```
136       floris = 0.0
```

SwashReadInput.ftn90:

A change has been made in line 454 of the read input file to make it able to read the [alongshoregradient] from the inputfile:

```
454   call INREAL ('TIDEGRAD',    floris, 'UNC', 0.)
```

SwashExpLay2DHflow.ftn90:

In this file the formulae for explicit calculation with multiple layers and two horizontal dimensions are described. Lines 2450 until 2465 add a term to the alongshore momentum balance:

```
2450      !
2451      ! implement pseudo alongshore tidal water level gradient
2452      !
2453      do m = mfu, ml
2454         do n = nsta(m), nend(m)
2455            !
2456            nm  = kgrpnt(m,n )
2457            !
2458            if ( vwetp(nm) == 1 ) then
2459               !
2460               rhsu(nm,:) = rhsu(nm,:) - grav * floris
2461               !
2462            endif
2463            !
2464         enddo
2465      enddo
```

Appendix G

Tide induced current results

This appendix provides additional figures concerned with the tide current experimental simulations.

G.1 Open channel

For the open channel experiment the velocity signals are compared for varying Chézy values with their corresponding equilibrium velocity. Figures G.1 and G.2 show results without and with additional dissipation by shore normal monochromatic waves.

G.2 Egmond bathymetry

Figure G.3 presents a colour plot of the equilibrium tidal alongshore current, after a simulation of 5 hours, for a gradient of $10^{-}5$. In the lower panel the corresponding bathymetry is plotted. Figure G.4 shows the equilibrium alongshore flow induced by varying pseudo water level gradients versus depth. Furthermore, black lines represent the equilibrium which would have been calculated by Equation 5.3.

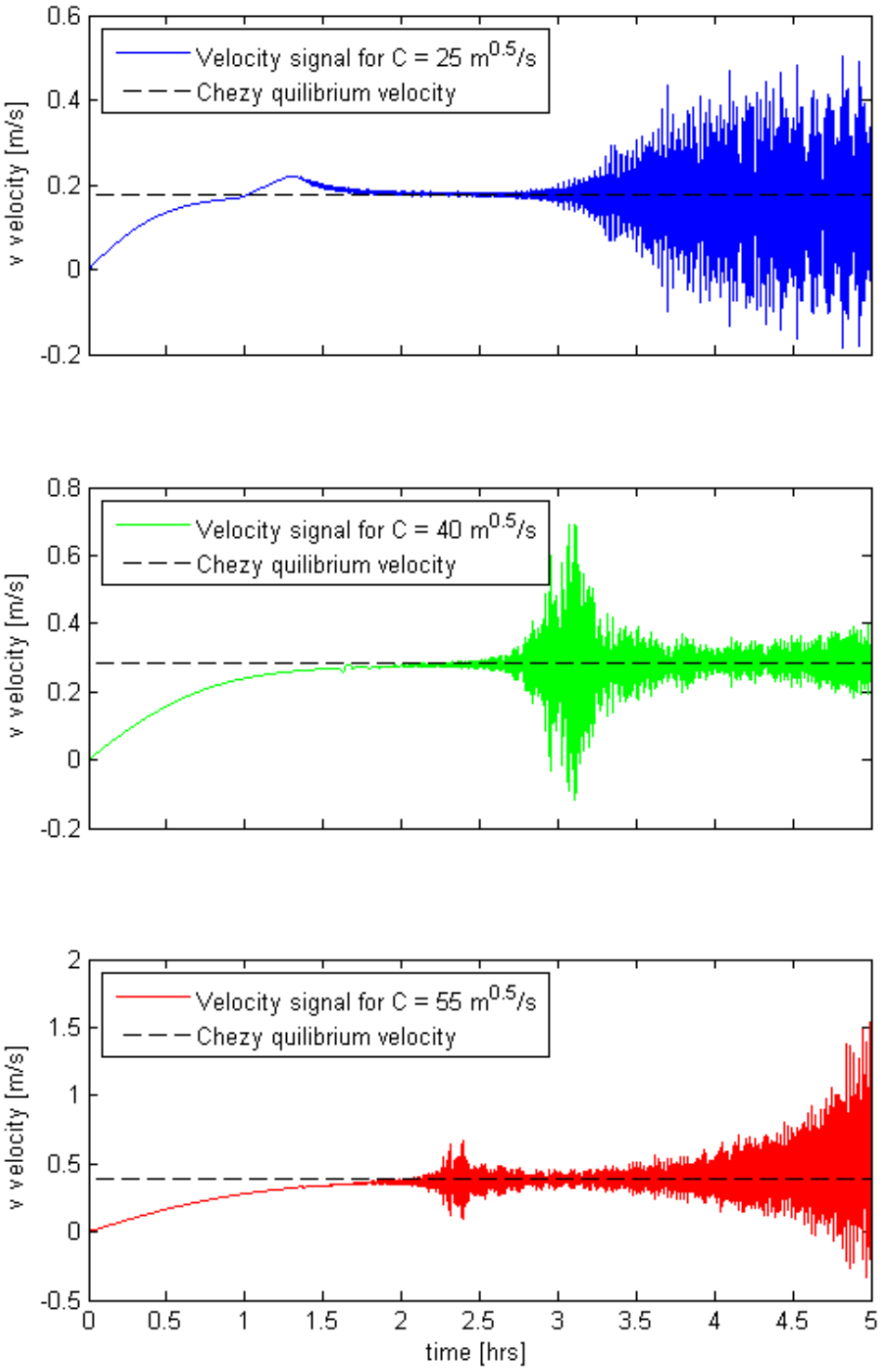

FIGURE G.1: Flow velocity through an open channel as a result of the pseudo water level gradient for different Chézy values and their corresponding equilibrium velocity without a dissipating mechanism

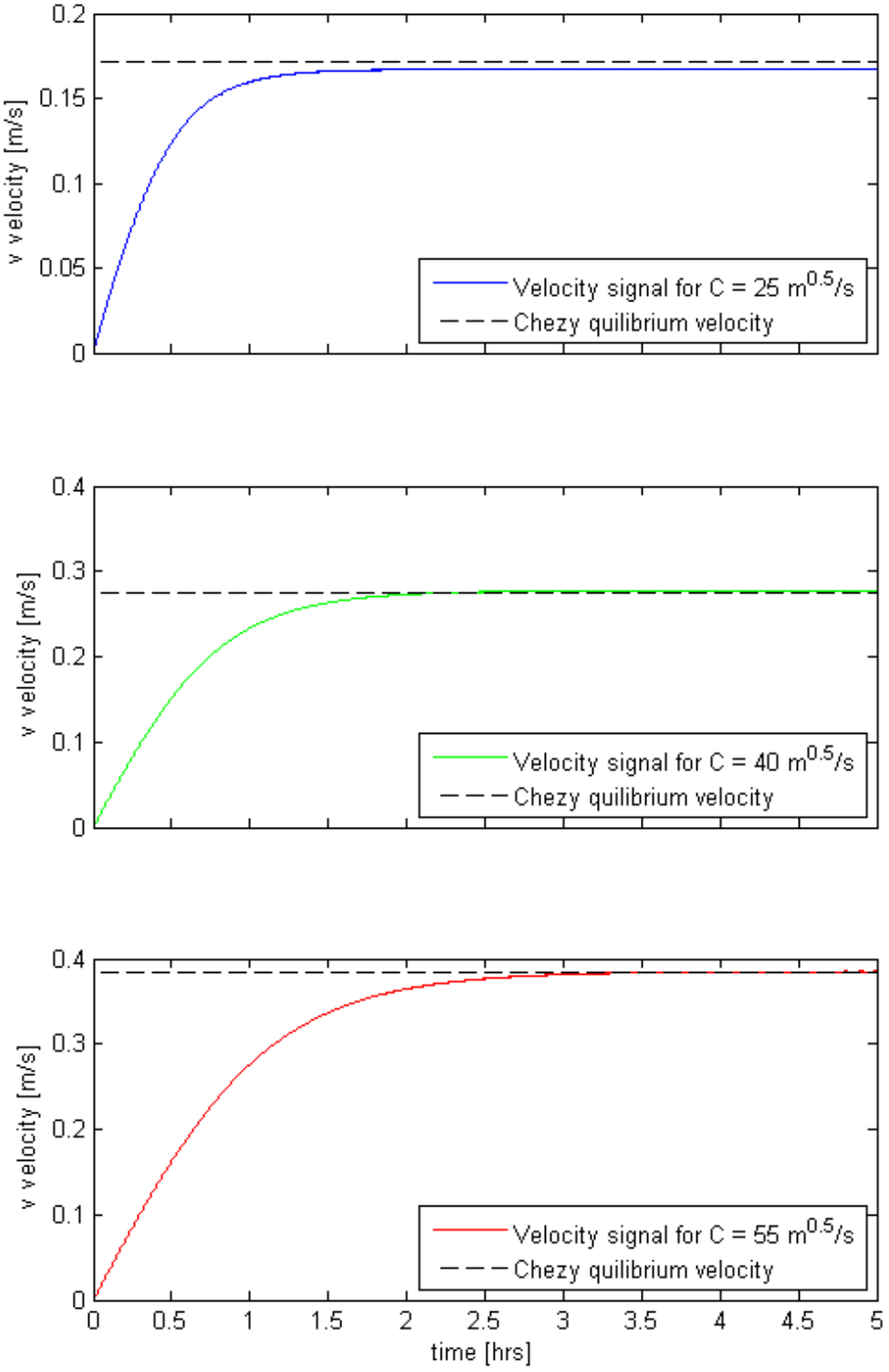

FIGURE G.2: Flow velocity through an open channel as a result of the pseudo water level gradient for different Chézy values and their corresponding equilibrium velocity with a dissipating mechanism

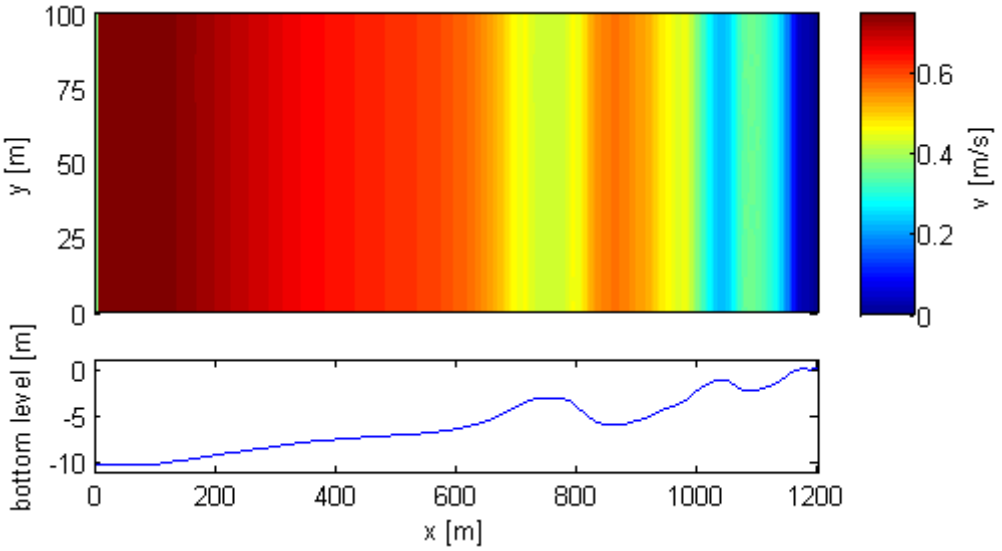

FIGURE G.3: Equilibrium alongshore flow induced by a pseudo water level gradient of 10^{-5} over alongshore uniform Egmond bathymetry

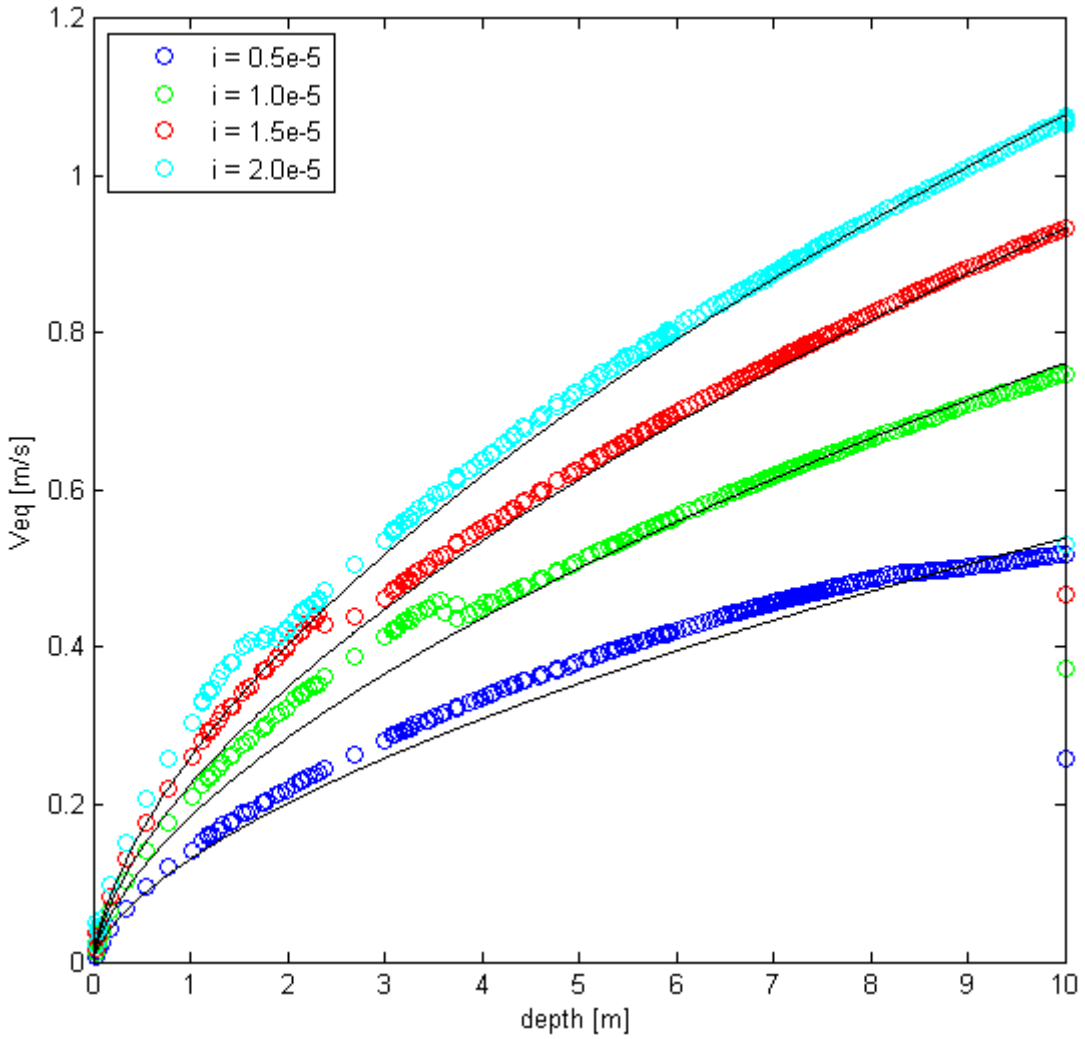

FIGURE G.4: Equilibrium alongshore flow induced by varying pseudo water level gradients versus depth. Black lines represent estimation with Equation 5.3

Appendix H

SWAN wave modelling

To obtain wave input data for the SWASH model use is made of two SWAN models. Firstly the North Sea SWAN model is used to propagate wave characteristics from IJmuiden towards the DIWAR buoy near Egmond. Of these characteristics only directional spreading is subsequently used for the second SWAN model. Input for this Local SWAN model are waves according to a JONSWAP model with Hs, Tp and direction from the DIWAR buoy with addition of the directional spreading from the North Sea SWAN model.

Both models make use of the same nested grids with corresponding bathymetries. The difference is that the Local model does not include the largest out of four grids. Nesting has been performed to get more accurate and recent bathymetric data with a finer grid resolution when approaching the coast. The following nested grids are used:

1. North Sea grid: 155 x 40 km (not used for Local model)
2. Vakloding grid 1999: 16 x 6 km
3. Jarkus grid 1998: 8 x 2.5 km
4. Local bathymetry 24 October 1998: 1300 x 800 m

H.1 North Sea SWAN model

As wave input for the North Sea SWAN model spectral data obtained from the Rijkswaterstaat permanent wave buoy at IJmuiden Munitiestortplaats is used. To check the accuracy, model results were compared to COAST3D measurement data at locations 7a (outer bank), 7b (inner bank) and 8 (DIWAR buoy). The correlation for H, T and dir is visualised in Figures H.1 to H.3. As described in Section 6.2, results with low or offshore wind conditions polluted the results. Similar results for a reduced data set (wind onshore directed and velocity higher than 5 m/s) are shown in Figures H.4 to H.6. Finally the root mean squared error and Skill score are shown in Tables H.1 and H.2 for both full and reduced data-set.

H.2 Local SWAN model

As input for the Local SWAN model use is made of the bulk parameters from the COAST3D data set with addition of directional spreading data from the North Sea SWAN model. As there is a lack of spectral shape data and for the considered cases the spectra at the outer bank were JONSWAP alike, a JONSWAP shape is considered. Spectral data is sent in to the local domain at the location of the DIWAR buoy and output is generated at a depth of 10m. Finally, these SWAN spectral output files will be used as wave input files for SWASH.

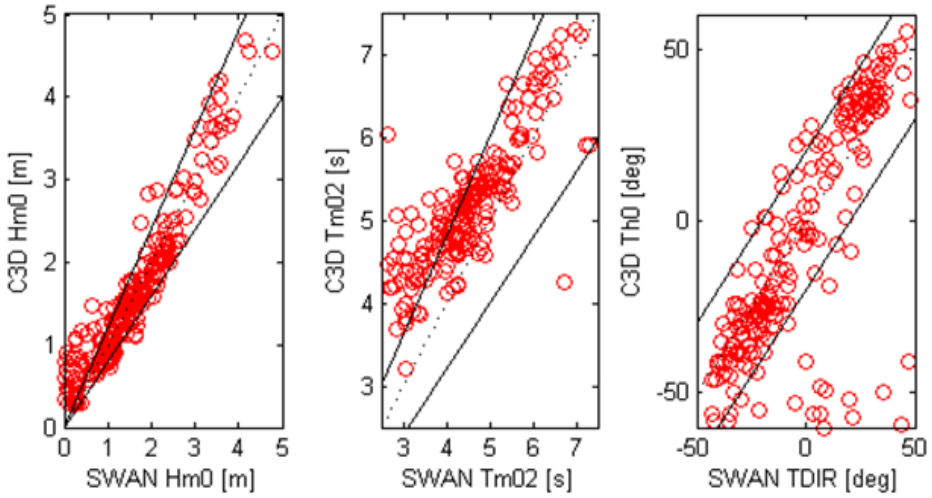

FIGURE H.1: Wave height, period and direction comparison between SWAN model and COAST3D results at location 8 (DIWAR buoy)

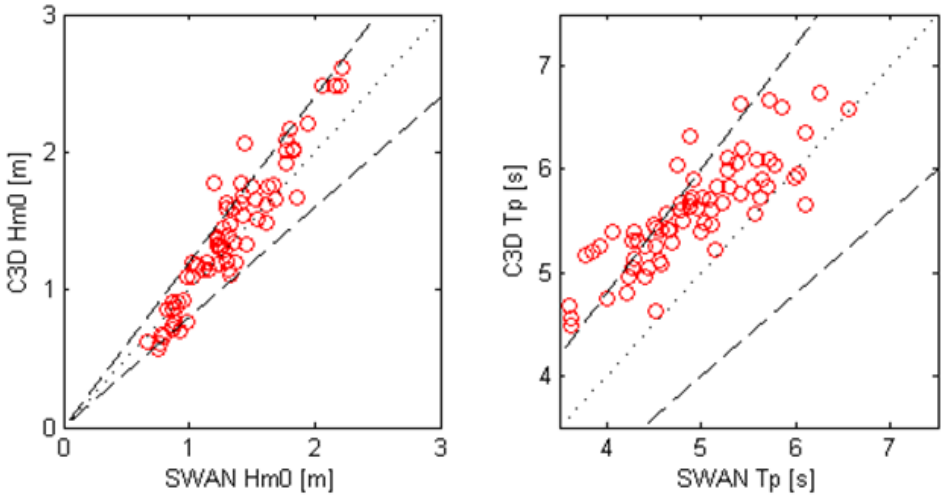

FIGURE H.2: Wave height and period comparison between SWAN model and COAST3D results at location 7a (Outer bank)

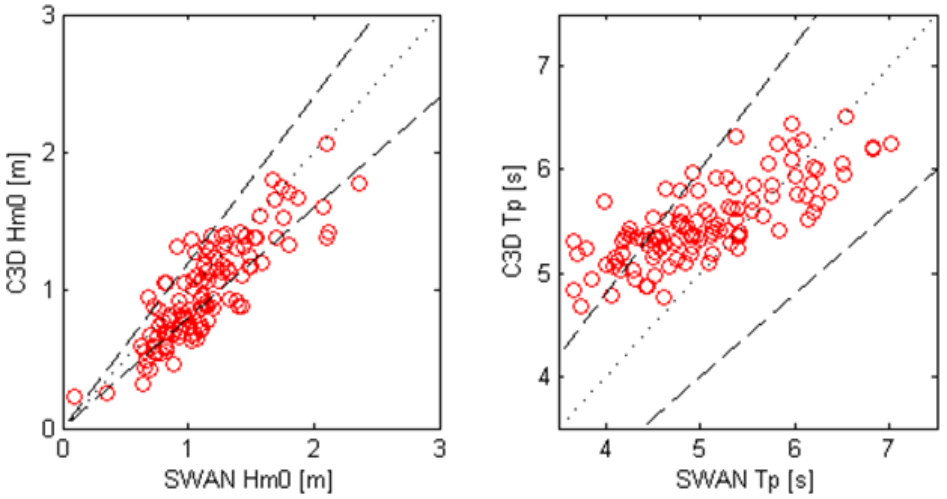

FIGURE H.3: Wave height and period comparison between SWAN model and COAST3D results at location 7b (Inner bank)

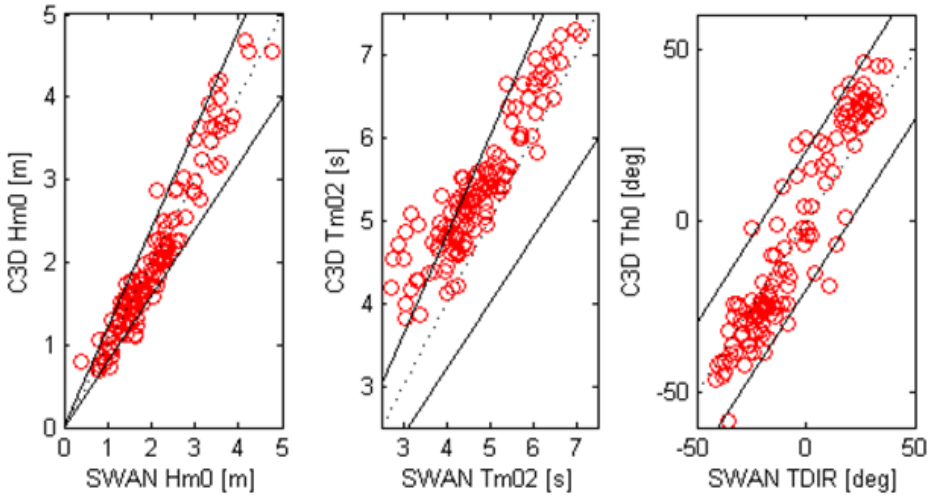

FIGURE H.4: Wave height, period and direction comparison between SWAN model and COAST3D results at location 8 for reduced data set (DIWAR buoy)

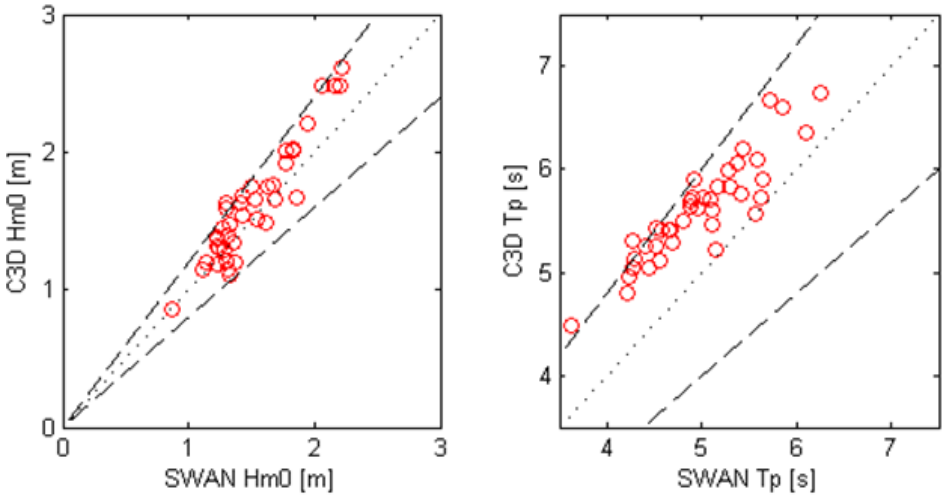

FIGURE H.5: Wave height and period comparison between SWAN model and COAST3D results at location 7a for reduced data set (Outer bank)

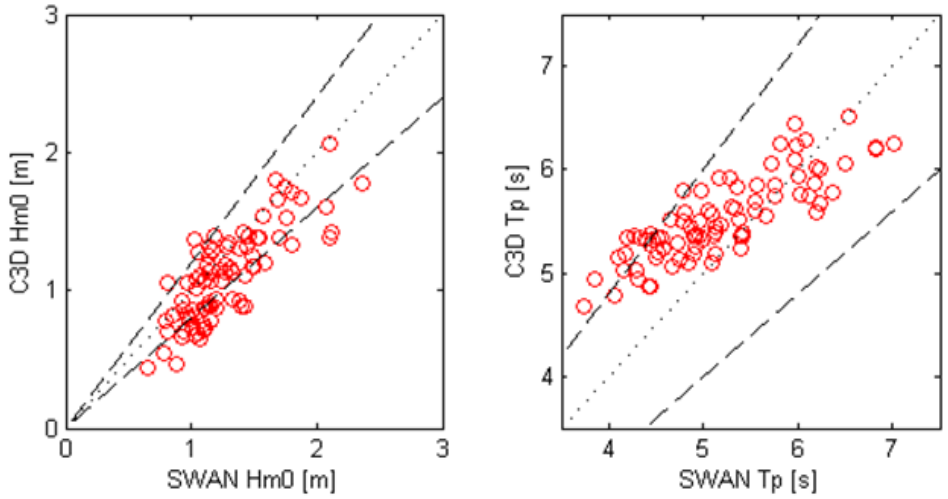

FIGURE H.6: Wave height and period comparison between SWAN model and COAST3D results at location 7b for reduced data set (Inner bank)

	DIWAR (loc. 8)	**Outer bar (loc. 7a)**	**Inner bar (loc. 7b)**
RMSE(H)	0.30	0.19	0.31
RMSE(T)	1.41	0.76	0.80
RMSE(θ)	40	N/A	N/A
Skill(H)	0.84	0.87	0.68
RMSE(T)	0.72	0.86	0.85
Skill(Dir)	0.62	N/A	N/A

TABLE H.1: Root mean square error and Skill factor of wave height, period and direction at three locations for the full data set. For quantity Q, the RMSE is computed as $RMSE = \sqrt{\langle (Q_{SWAN} - Q_{C3D})^2 \rangle}$ and $Skill = 1 - \sqrt{\langle (Q_{SWAN} - Q_{C3D})^2 \rangle / \langle Q_{C3D}^2 \rangle}$.

	DIWAR (loc. 8)	**Outer bar (loc. 7a)**	**Inner bar (loc. 7b)**
RMSE(H)	0.25	0.18	0.34
RMSE(T)	0.77	0.68	0.58
RMSE(θ)	11.5	N/A	N/A
Skill(H)	0.89	0.89	0.68
RMSE(T)	0.86	0.88	0.90
Skill(Dir)	0.62	N/A	N/A

TABLE H.2: Root mean square error and Skill factor of wave height, period and direction at three locations for the reduced data set. For quantity Q, the RMSE is computed as $RMSE = \sqrt{\langle (Q_{SWAN} - Q_{C3D})^2 \rangle}$ and $Skill = 1 - \sqrt{\langle (Q_{SWAN} - Q_{C3D})^2 \rangle / \langle Q_{C3D}^2 \rangle}$.

Appendix I

Determination depth averaged velocity

During the measurement campaign current meters were located at three different heights at location 2 (see Figure 2.1). This data is used to be able to predict a vertical velocity profile and depth averaged velocity at all locations where current meters were available. For this research only cases were taken into account where all three currentmeters measured velocities higher than a treshold value of 0.2m/s (Below this value current predictions contain a lot of uncertainty).

First a logarithmic curve fitting was applied through all three velocity points (green dots in Figure I.1), resulting in a vertical velocity profile (blue line). The depth averaged velocity is calculated from this velocity profile and represented by the blue dashed line.

Unfortunately, velocity data is only available at one or two depths in all other measurement locations. To estimate a vertical velocity profile at these locations the logarithmic wall law (referred to as loglaw) is used, shown in equation I.1.

$$u(z) = \frac{u_*}{\kappa} \ln \frac{z}{z_0} \tag{I.1}$$

With friction velocity u_*, $\kappa = 0.41$ the Von Karman constant, z the height above the bed and $z_0 = k_r/33$ is the distance from the bed where velocity is assumed to be zero, which is approximated by dividing roughness height by 33.

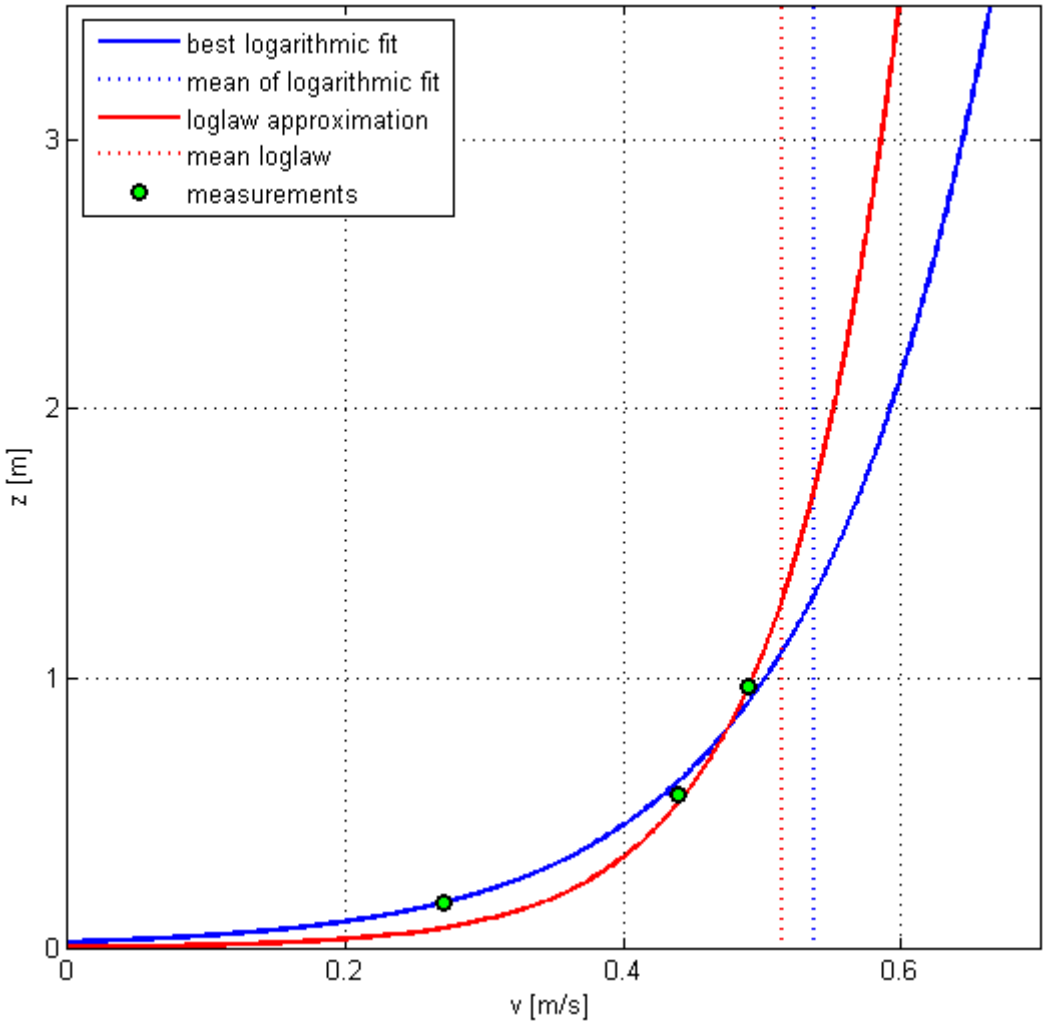

FIGURE I.1: Caption

To see how accurate this formula is it is applied to the data points at location two to compare the vertical velocity profile which was logarithmically fitted through three points and a loglaw profile fitted through one point at a single depth. For a certain case this is visualised in Figure I.1. The red lines represent the logarithmic wall law profiles whereas the dashed red lines represent theory equivalents. Green points are measurement points and blue lines represent logarithmic curve fitting again.

What can be seen is that loglaw profiles and especially depth averaged velocities agree quite well to the logarithmic curve fitting equivalents if the loglaw is applied to the higher located velocity points. However, when loglaw is applied to the lowest measurement point near the bed, predictions are much worse. This can also be concluded from Table I.1, which shows the mean and maximum error for fit curves through points at different height above the bed.

	mean error	**max error**
$\mathbf{h_{EFM}}$**=0.17m**	38%	104%
$\mathbf{h_{EFM}}$**=0.57m**	7%	15%
$\mathbf{h_{EFM}}$**=0.97m**	8%	15%

TABLE I.1: Relative error of mean velocity calculated by a Loglaw fit through one point with respect to a logarithmic fit through three points.

Eventually a Matlab routine was developed which calculates the depth averaged velocity as a function of measured velocity, measurement depth and total water depth.

Appendix J

Determination of the roughness height

Manning is related to Chézy as:

$$n = \frac{h^{1/6}}{C} \tag{J.1}$$

If the velocity profile is assumed to be logarithmic, Chézy can be written as a function of z_0 (WAQUA/TRIWAQ, 2012):

$$C = \frac{\sqrt{g}}{\kappa} \ln\left(\frac{h}{z_0 * e^1}\right) \tag{J.2}$$

Equations J.1 and J.2 can be combined as:

$$z_0 = h/e^{1+\frac{\kappa h^{1/6}}{n\sqrt{g}}} \tag{J.3}$$

The roughness height then follows from:

$$k_r = 33 * z_0 \tag{J.4}$$

With:

n = Manning friction coefficient

h = Total water depth

C = Chézy friction coefficient

$\kappa = 0.41$(=Von Karman constant)

z_0 = distance from the bed where velocity is assumed to be zero

k_r = roughness height

The roughness height is calculated for a varying depth and Manning coefficient with Equations J.3 and J.4. Result can be seen in Figure J.1. What can be observed is that the roughness height is quite sensitive for the Manning coefficient, and slightly less sensitive to the depth. As in previous studies a Manning coefficient of 0.019 has proven to give good results in the surf zone, this will be used here as well. The average depth of the velocity meters is 2.5 meters. To achieve best results at these locations it is decided to use the roughness height corresponding with this water depth, which results in a roughness height of 0.01m (see green line in Figure J.1).

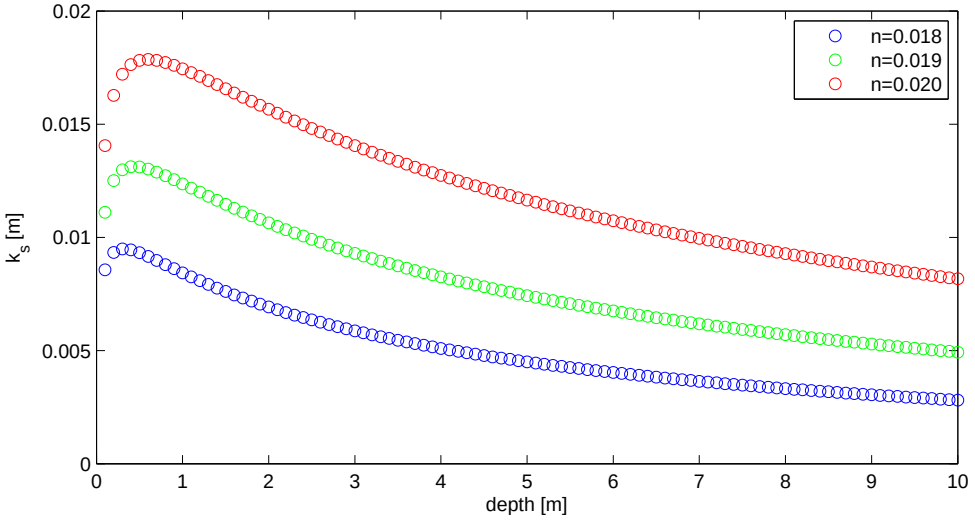

FIGURE J.1: Roughness height for varying depth and Manning friction coefficient

The calculated roughness height shows significant variation for varying depth and Manning coefficients. The equilibrium tidal velocity is calculated to investigate what the

effect of the varying roughness height is. This is done by using formulae which are implemented in the Unibest model from (Bosboom et al., 2000), namely:

$$\overline{v_{tide}} = C\sqrt{h\frac{dh}{dy}} \tag{J.5}$$

$$C = 18log(\frac{12h}{k_r}) \tag{J.6}$$

Resulting velocities are found in Table J.1. From this table can be concluded that results for $k_r = 7.5e^{-4}m$ substantially differ from the other values. This explains the over prediction of velocities in the first simulations. Furthermore, velocity differences are marginal in shallow water and tend to be a bit bigger in larger water depths (h>5m) for k_r between 0.005m and 0.020m.

k_r **[m]**	**7.5e-4**	**0.005**	**0.010**	**0.015**	**0.020**
d=1.0m	0.24	0.19	0.18	0.17	0.16
d=2.5m	0.41	0.34	0.31	0.30	0.29
d=5.0m	0.62	0.52	0.48	0.46	0.44
d=10m	0.94	0.78	0.73	0.70	0.68

TABLE J.1: Velocity in m/s calculated with equations J.5 and J.6 with an alongshore water level gradient of 10^{-5} as a function of depth and roughness height.

Appendix K

Calibration and validation results

In this appendix, figures show results of the calibration and validation simulations per transect. For all cases firstly comparison between model prediction and measurements is given for wave height at the North and Main transects. Subsequently velocity predictions are compared to measurement data at 5 transects. From top to bottom: North, Middle-North, Main, Middle-South and South. These transects correspond to the black lines seen in Figure 2.1.

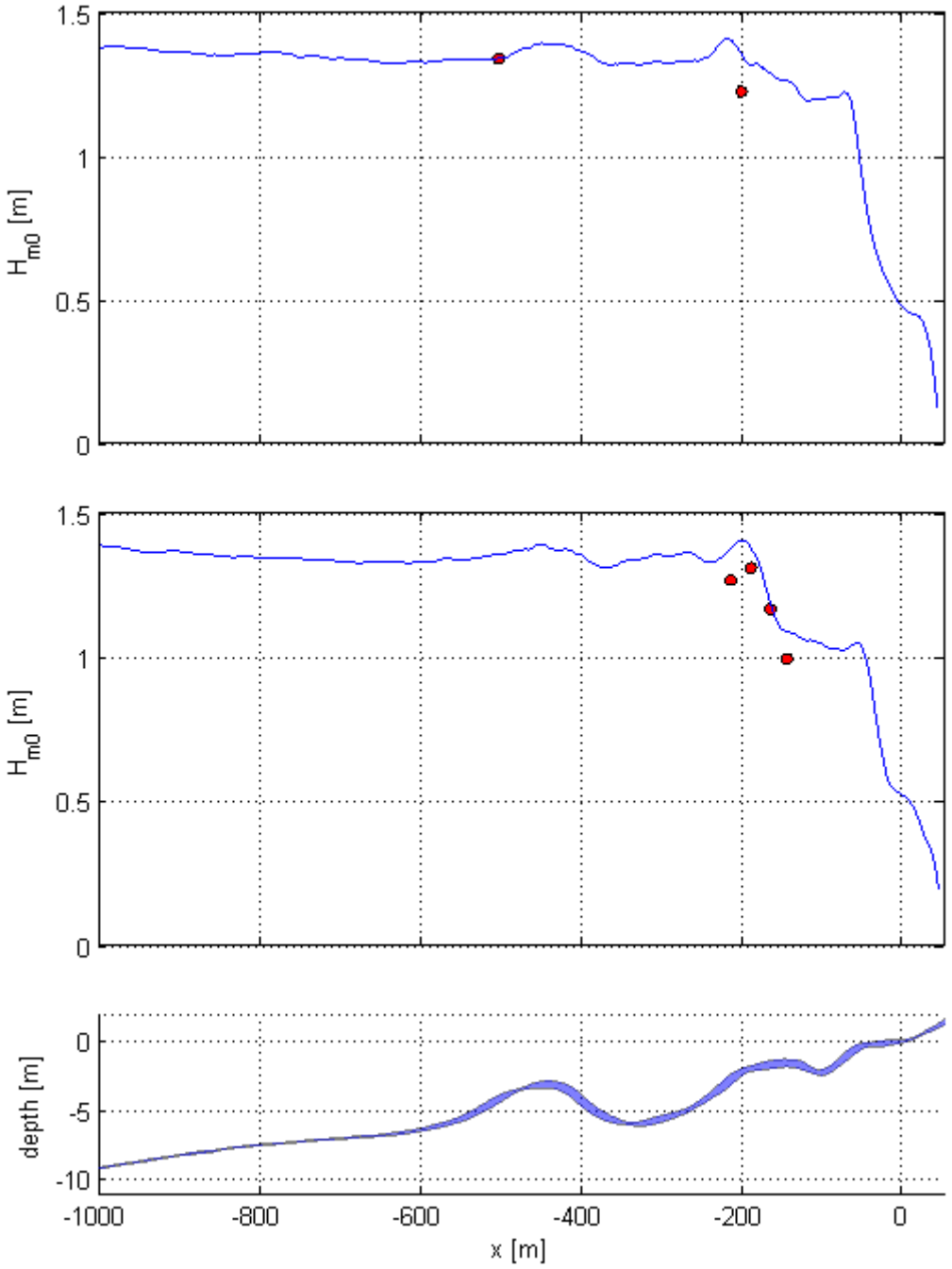

FIGURE K.1: Case C1; Wave transformation results for North transect and Main transect with corresponding depth

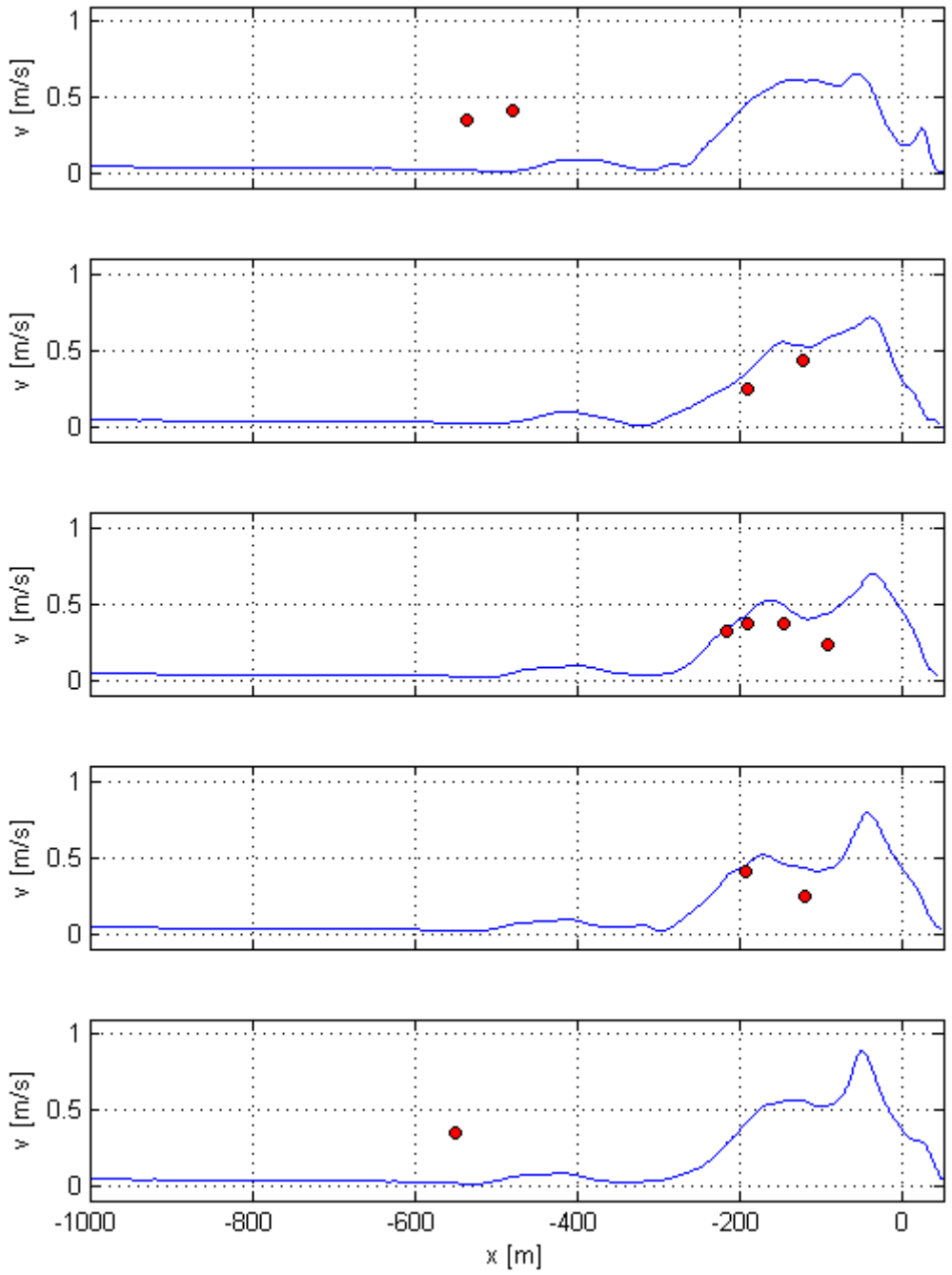

FIGURE K.2: Case C1; Velocity results for North-, Middle-North-, Main-, Middle-South and South transect

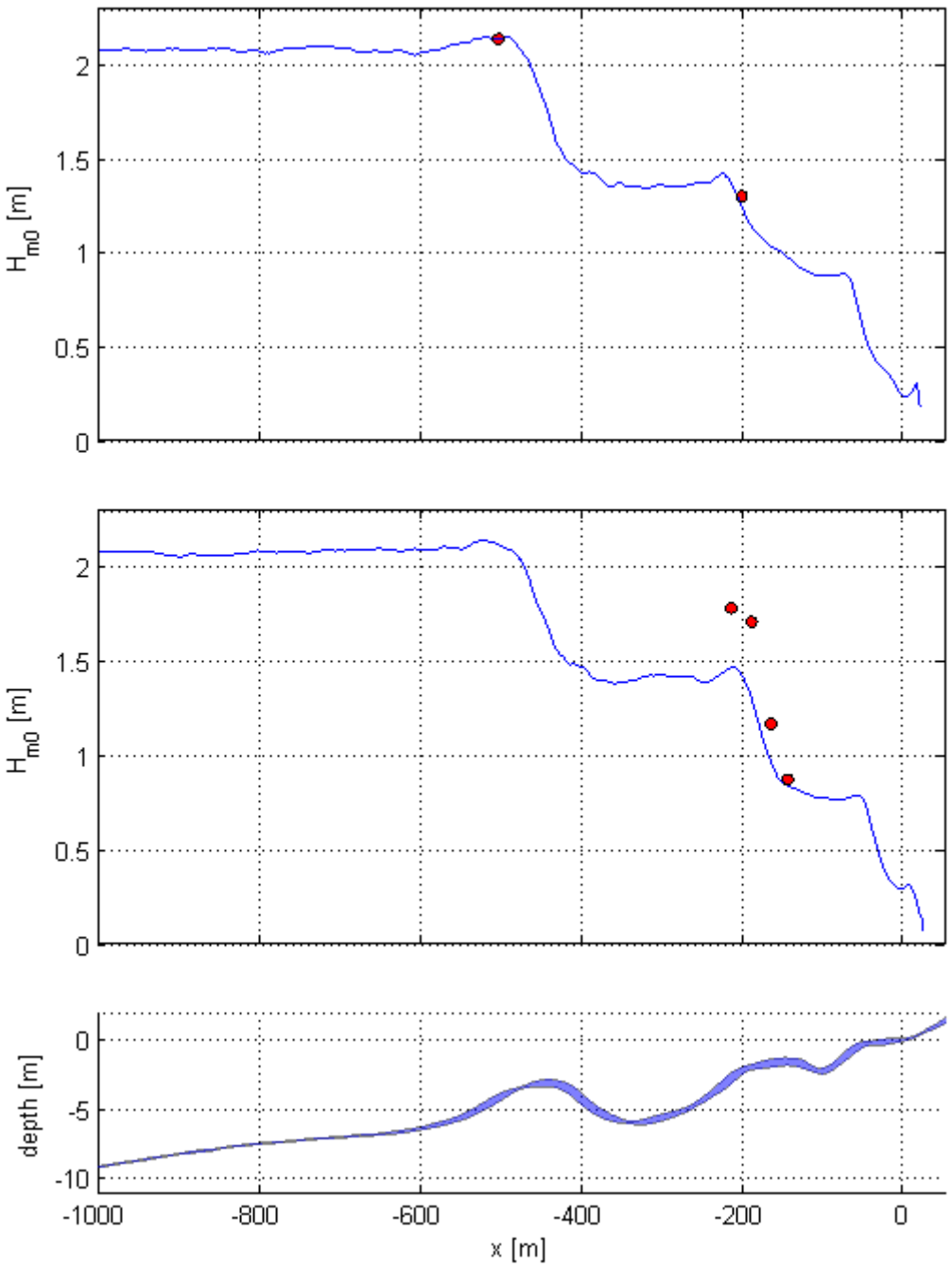

FIGURE K.3: Case C2; Wave transformation results for North transect and Main transect with corresponding depth

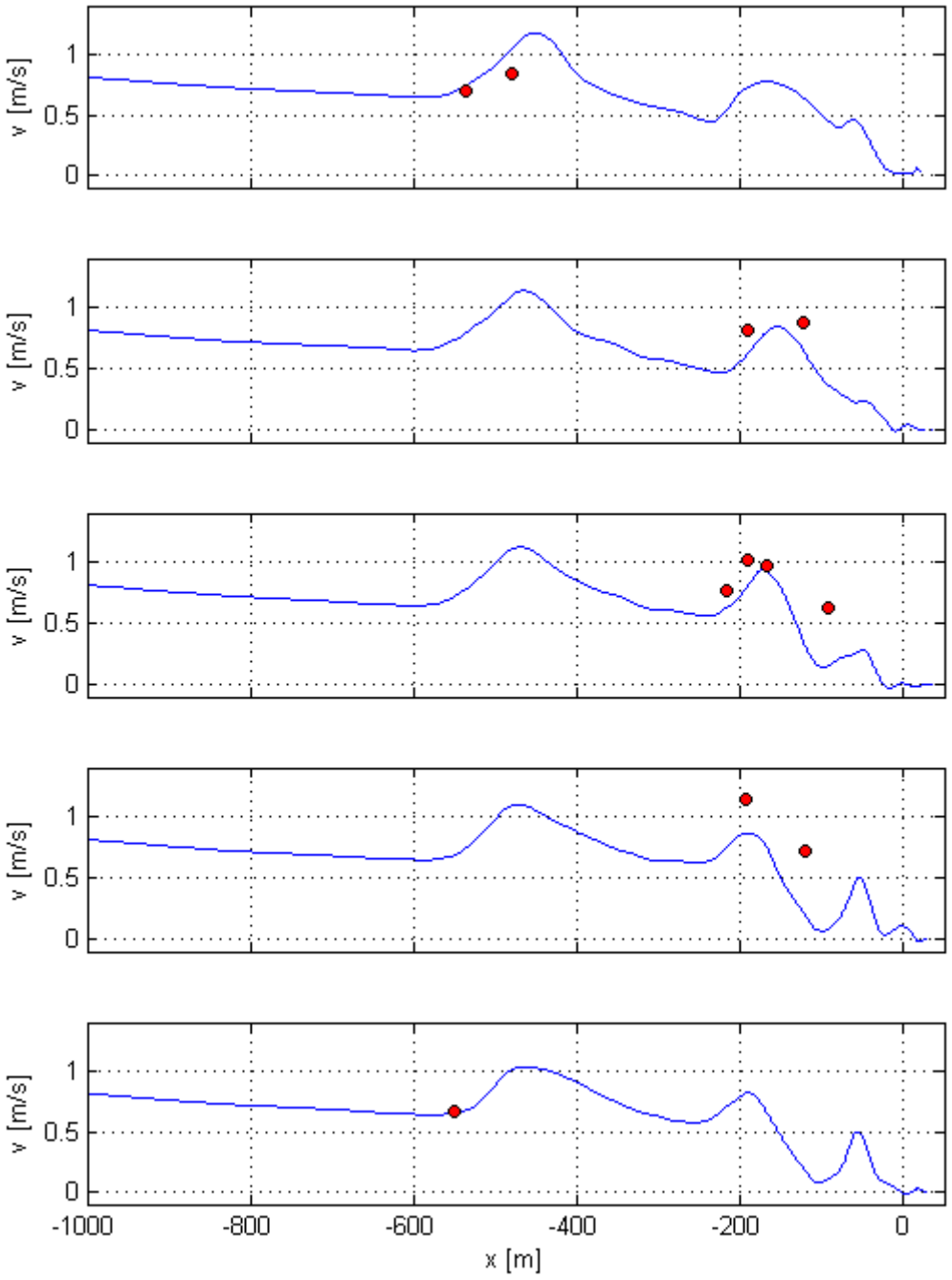

FIGURE K.4: Case C2; Velocity results for North-, Middle-North-, Main-, Middle-South and South transect

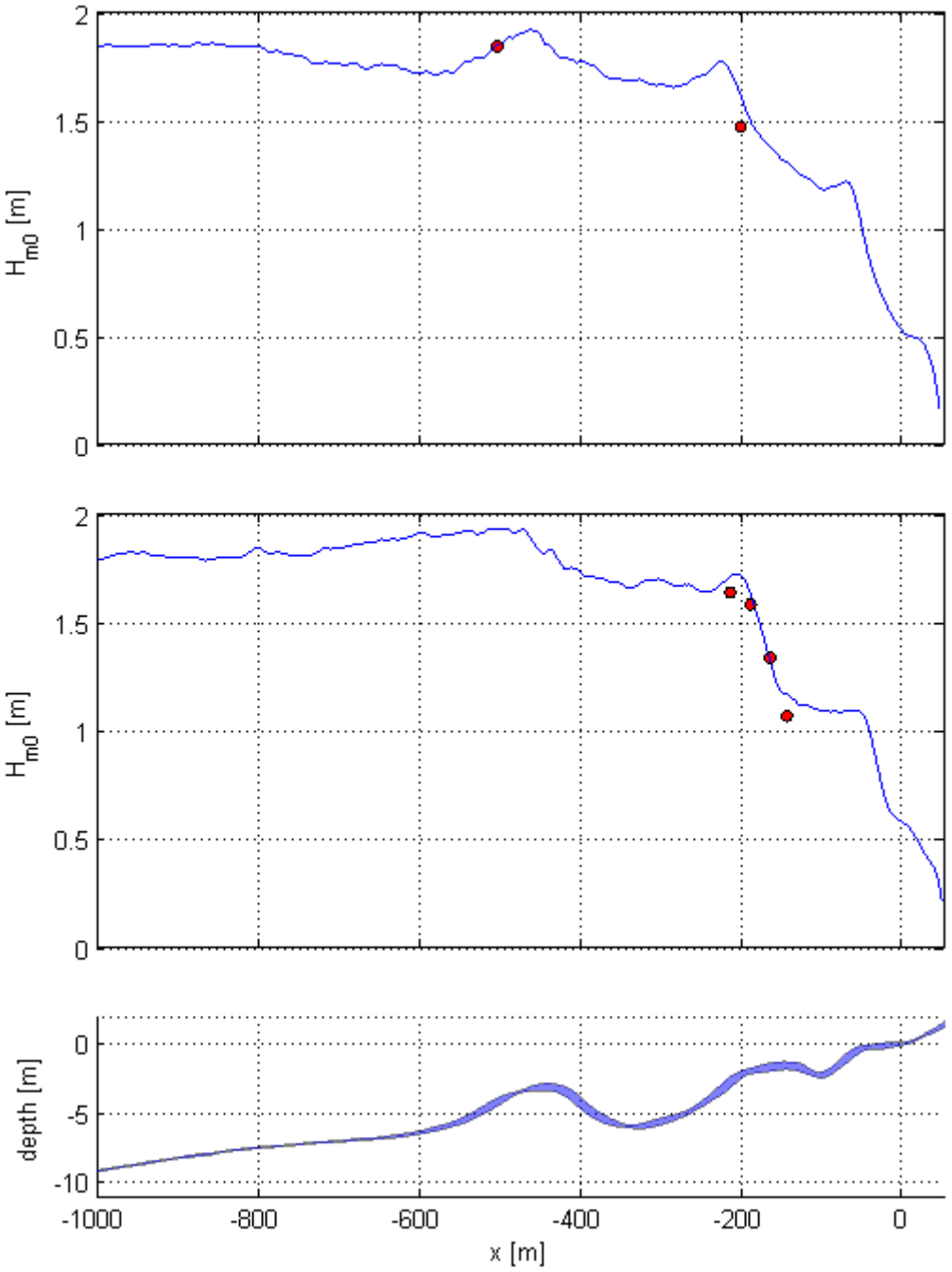

FIGURE K.5: Case V1; Wave transformation results for North transect and Main transect with corresponding depth

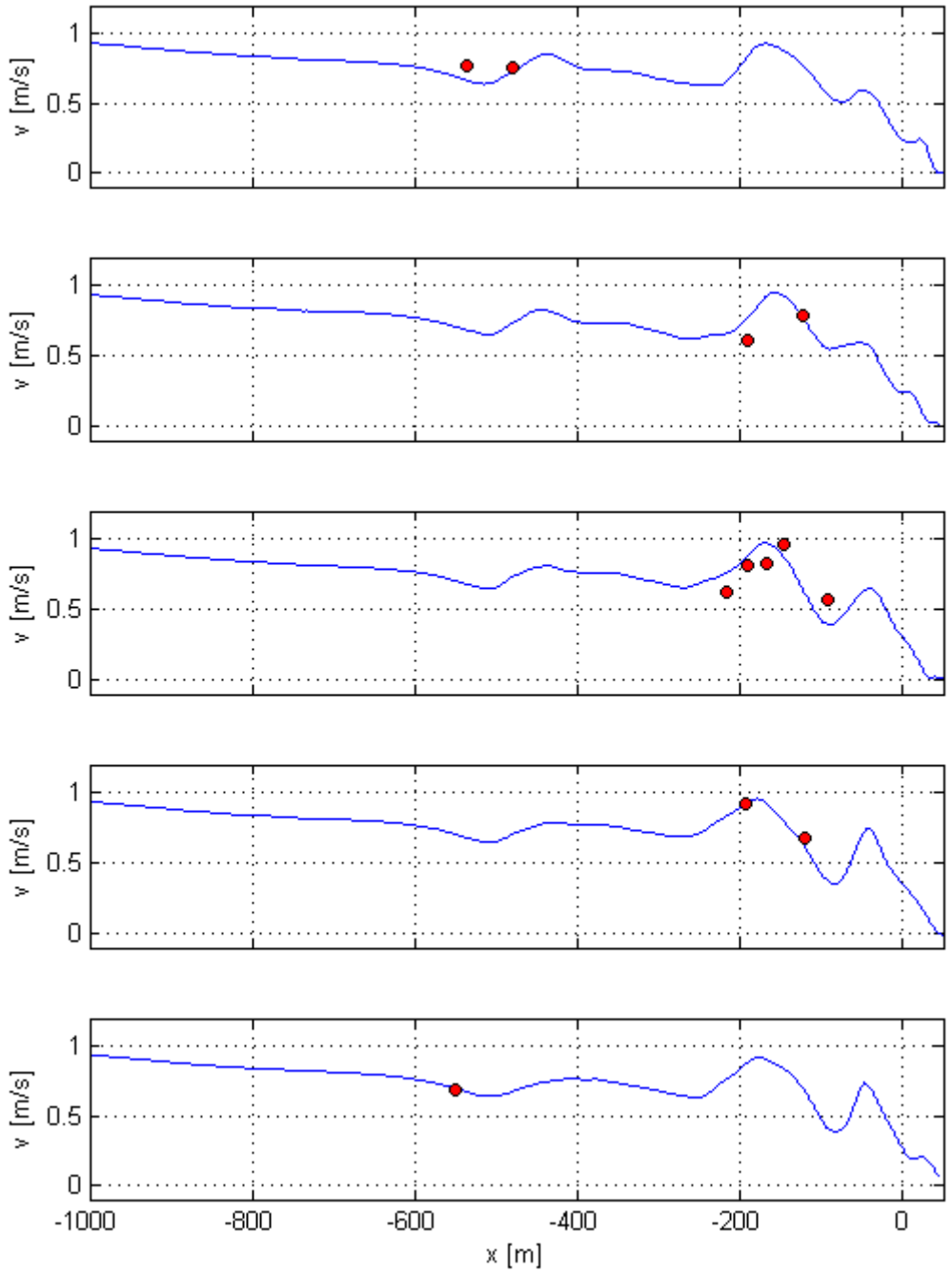

FIGURE K.6: Case V1; Velocity results for North-, Middle-North-, Main-, Middle-South and South transect

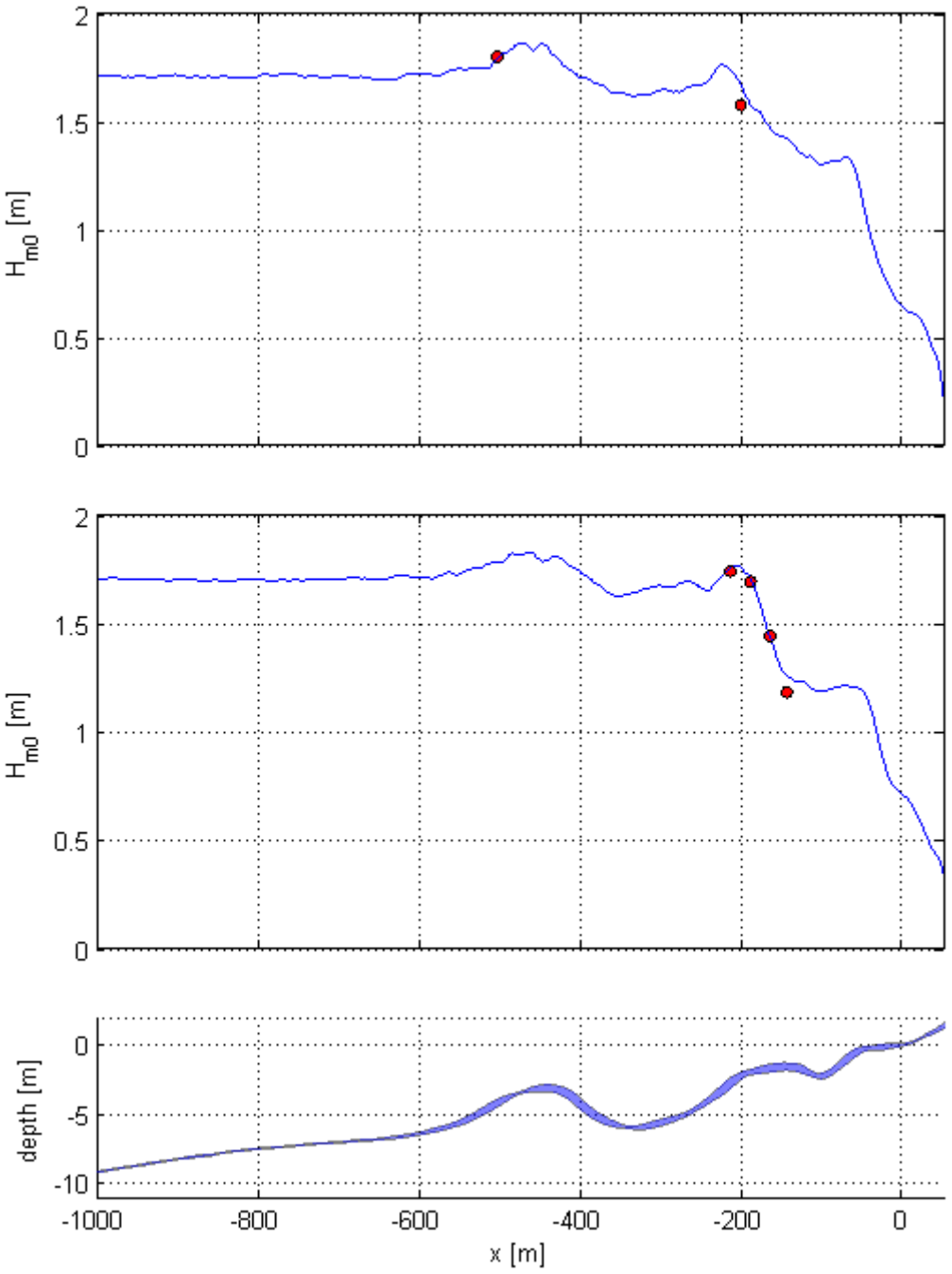

FIGURE K.7: Case V2; Wave transformation results for North transect and Main transect with corresponding depth

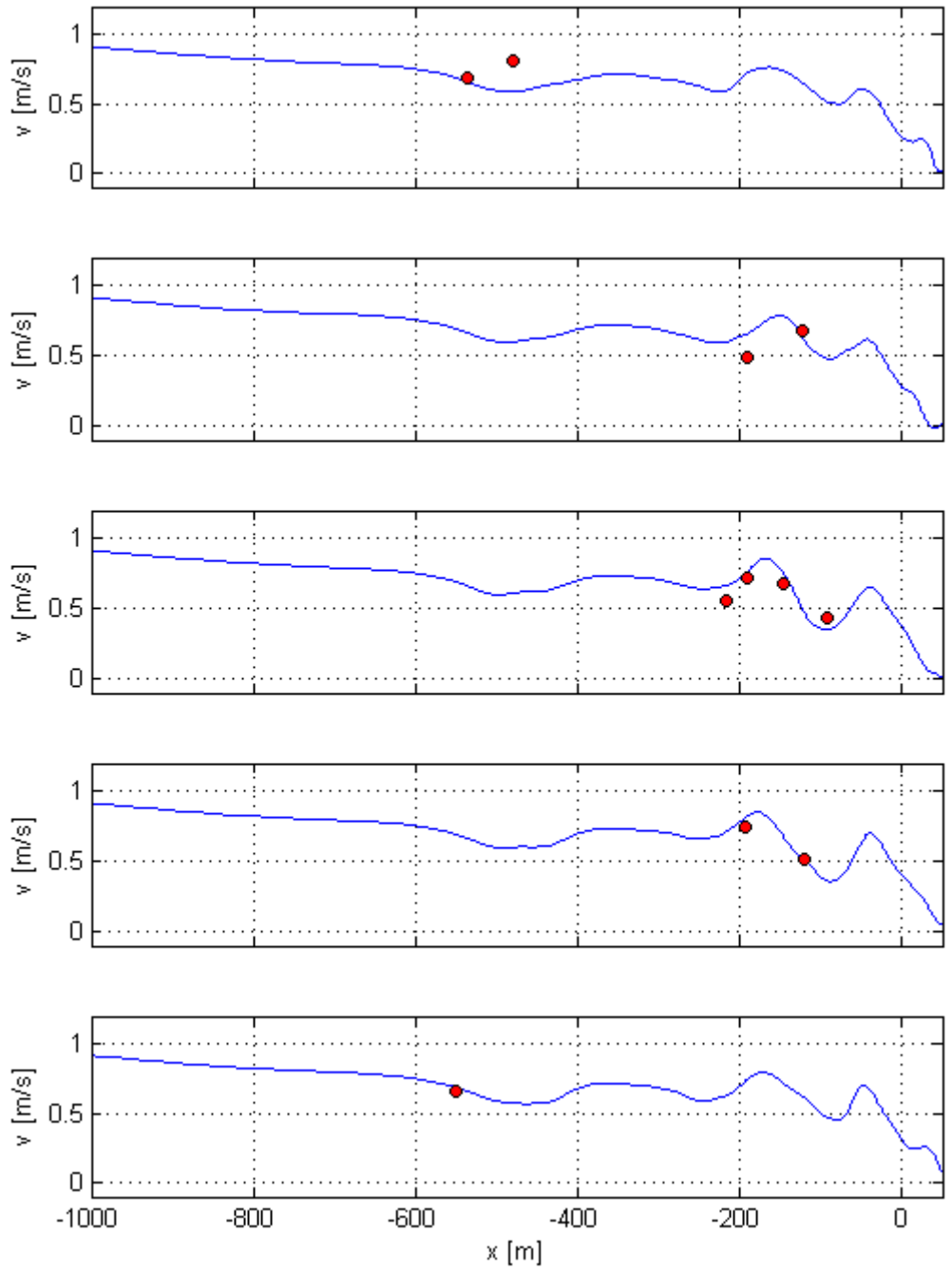

FIGURE K.8: Case V2; Velocity results for North-, Middle-North-, Main-, Middle-South and South transect

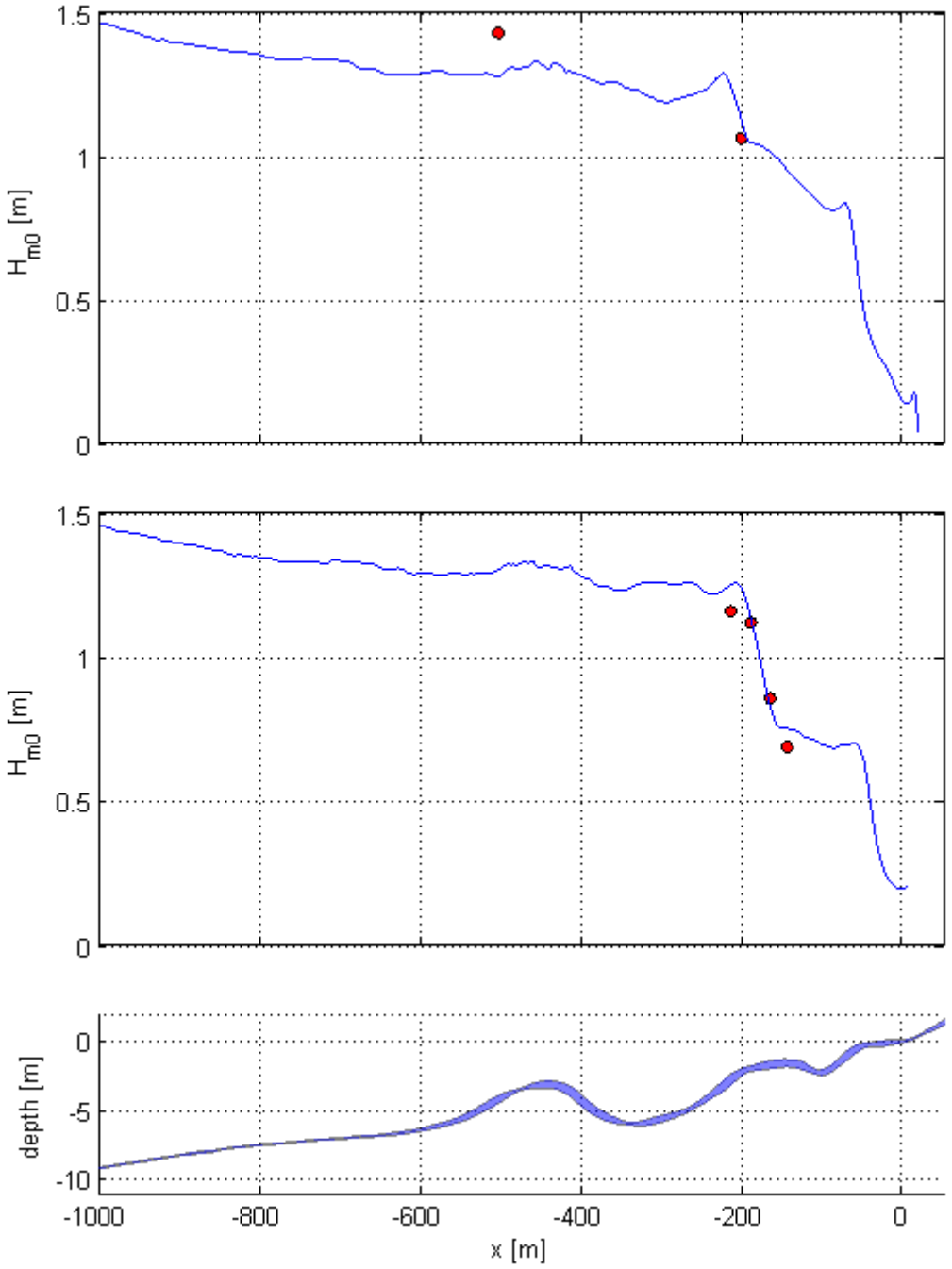

FIGURE K.9: Case V4; Wave transformation results for North transect and Main transect with corresponding depth

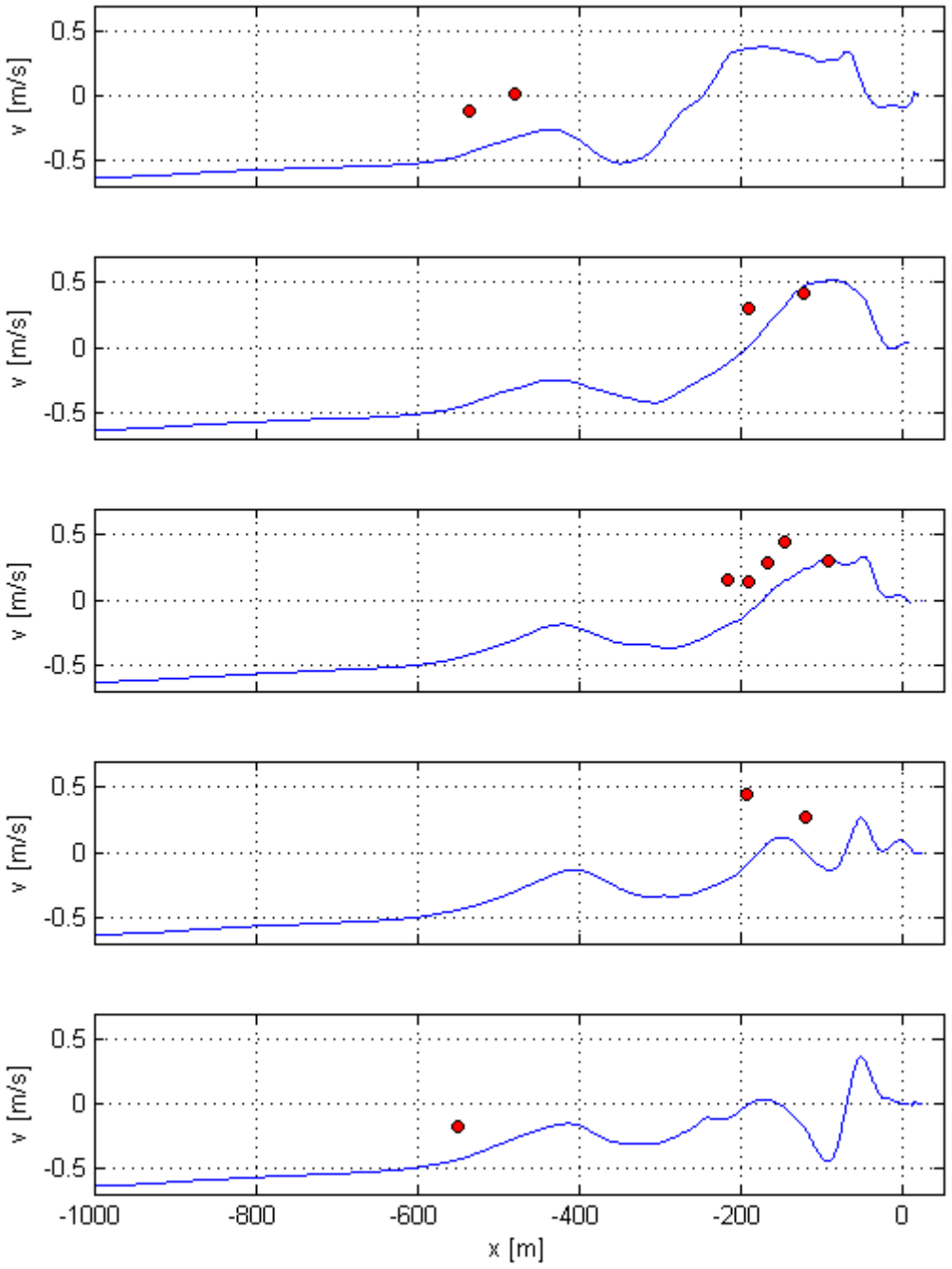

FIGURE K.10: Case V4; Velocity results for North-, Middle-North-, Main-, Middle-South and South transect

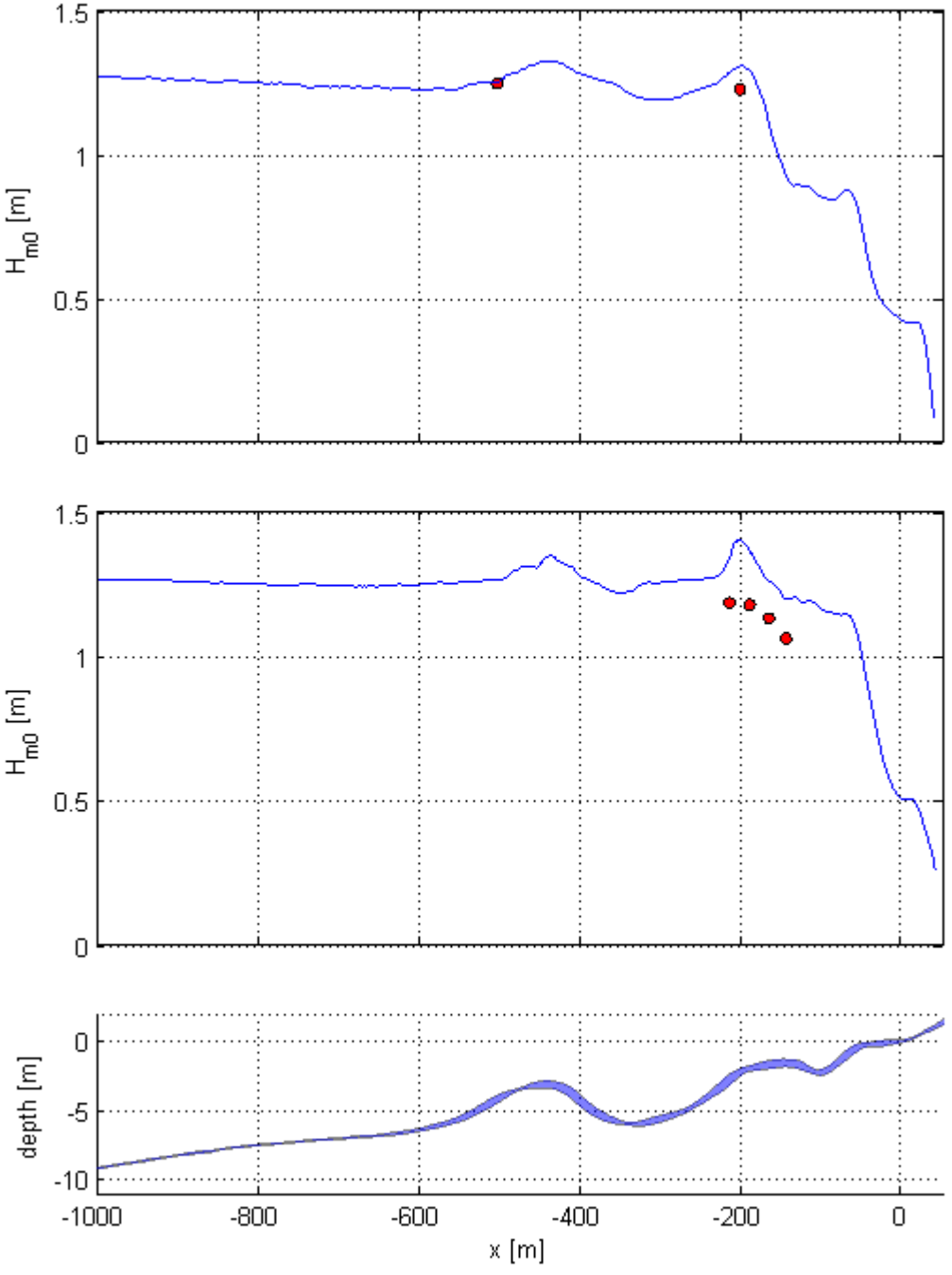

FIGURE K.11: Case V7; Wave transformation results for North transect and Main transect with corresponding depth

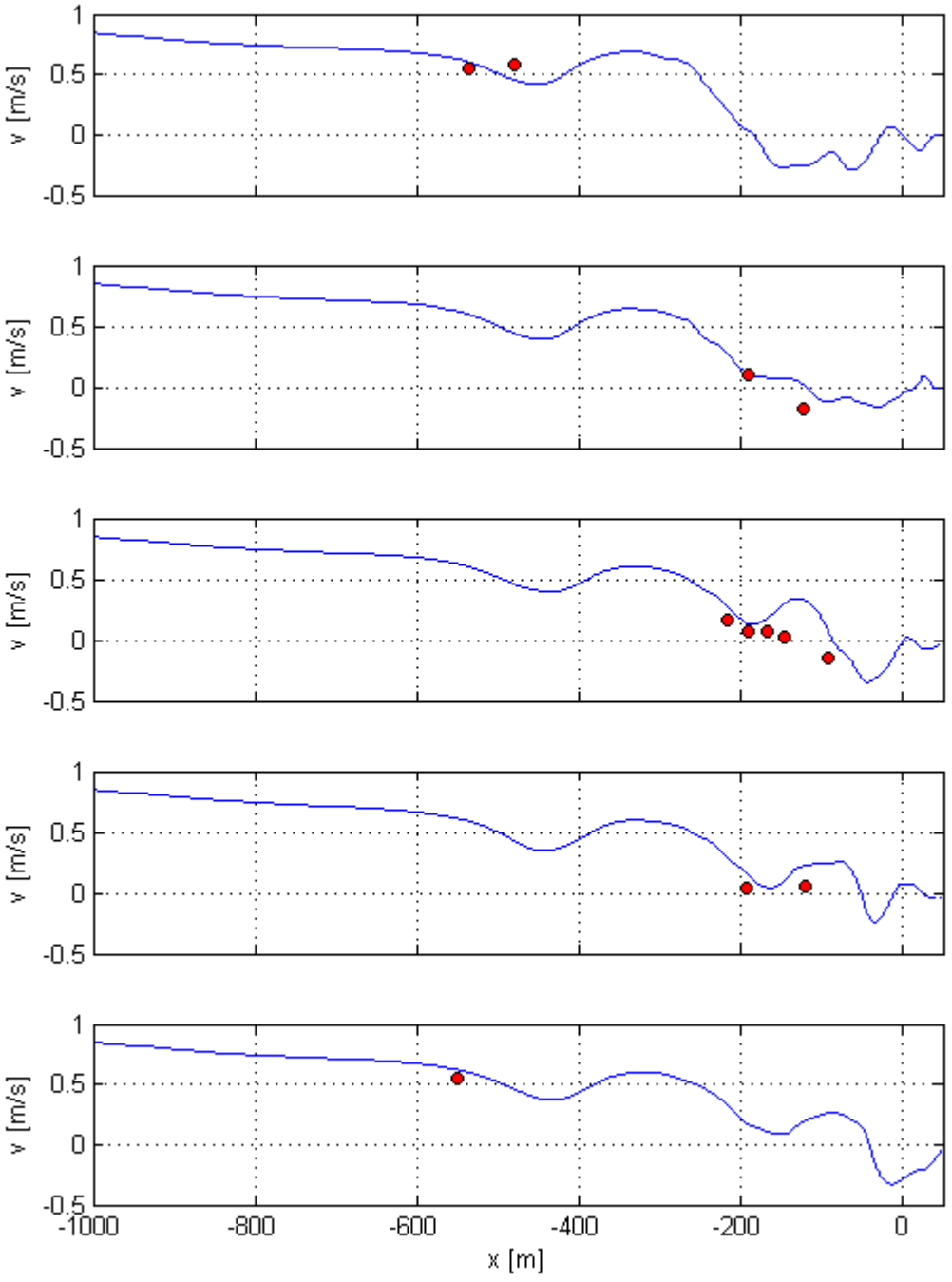

FIGURE K.12: Case V7; Velocity results for North-, Middle-North-, Main-, Middle-South and South transect

Appendix L

Instabilities in validation simulations

As was mentioned in Section 7.4, all five simulations with a forcing term in southern direction showed instabilities. It was discussed that for runs V3, V5 and V6, instabilities had grown so large that it had taken over the incoming wave field. On the other hand, for runs V4 and V7, instabilities could be observed in the form of small ripples, but dominant wave energy was still in the correct direction. To demonstrate this, Figures L.1 until L.7 show snapshots of the instantaneous surface elevation and alongshore current at the last time step of the simulation.

What can be observed, is that no signs of the instabilities can be found in cases V1 and V2. Furthermore, wave propagation looks quite good for cases V4 and V7. Nevertheless, clearly instable ripples can be observed in these simulations as well, but they are still rather small. For cases V3, V5 and V6 both the wave field as well as the alongshore velocity are completely taken over by the instabilities.

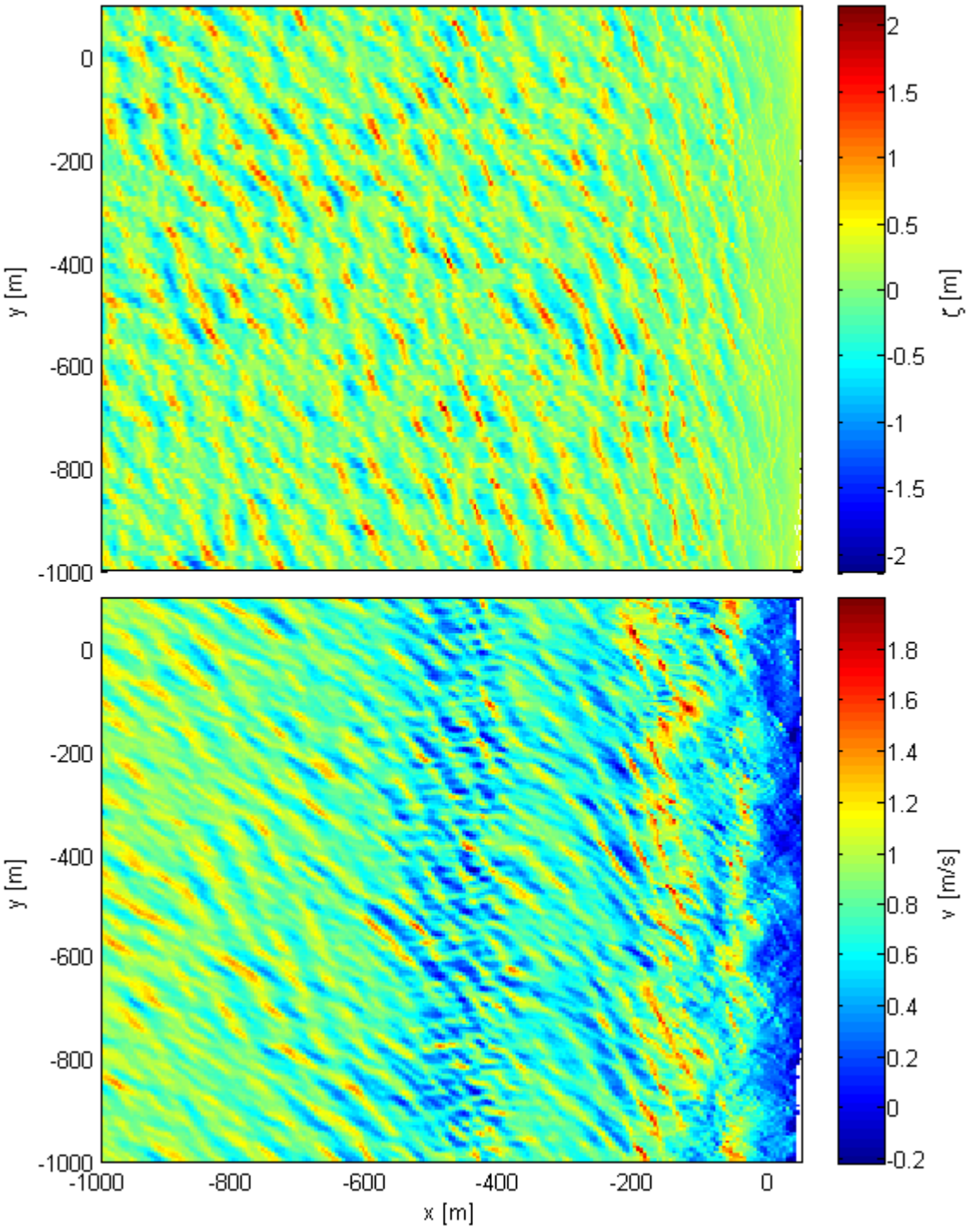

FIGURE L.1: Instantaneous surface elevation and alongshore current at end of the simulation for case V1

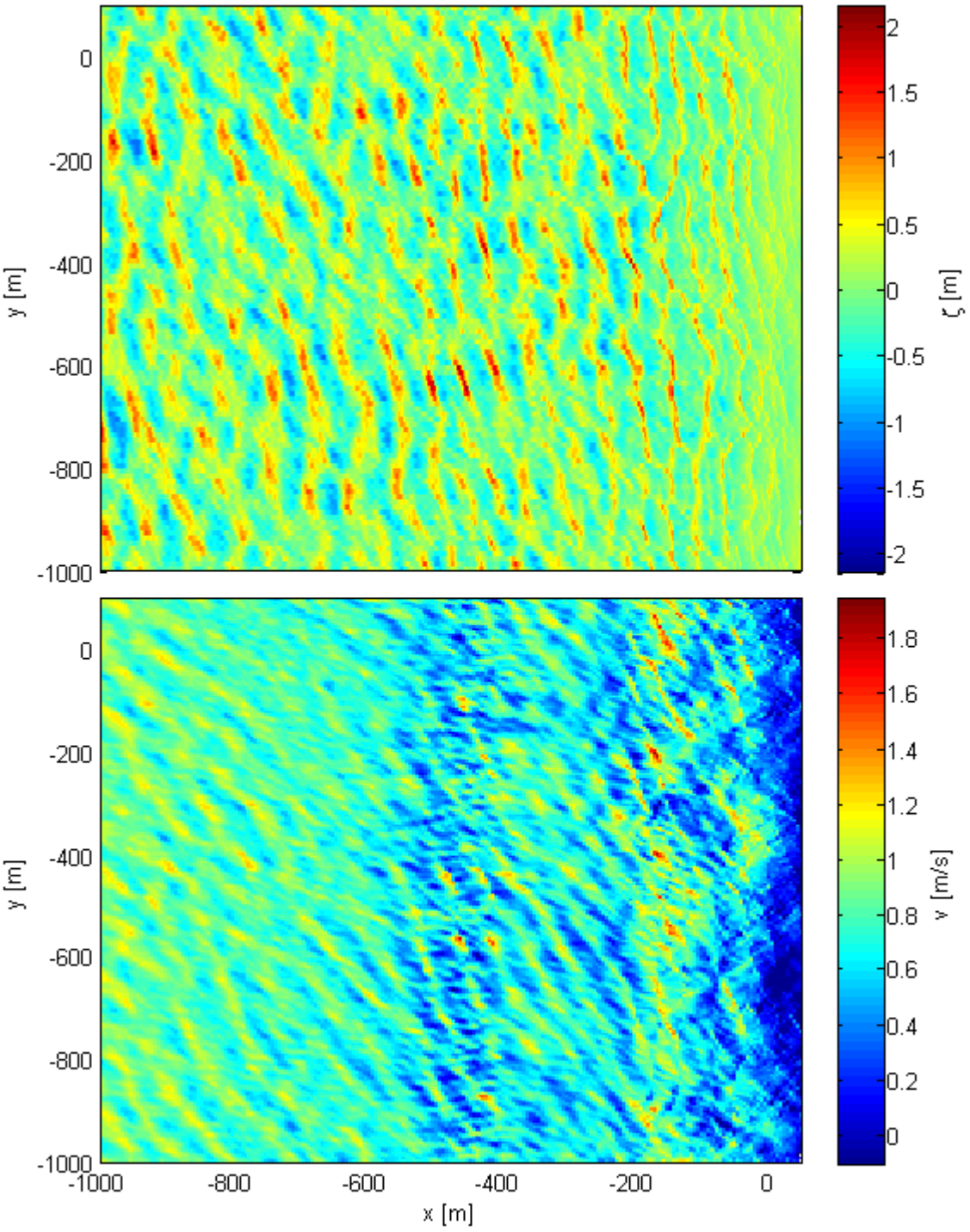

FIGURE L.2: Instantaneous surface elevation and alongshore current at end of the simulation for case V2

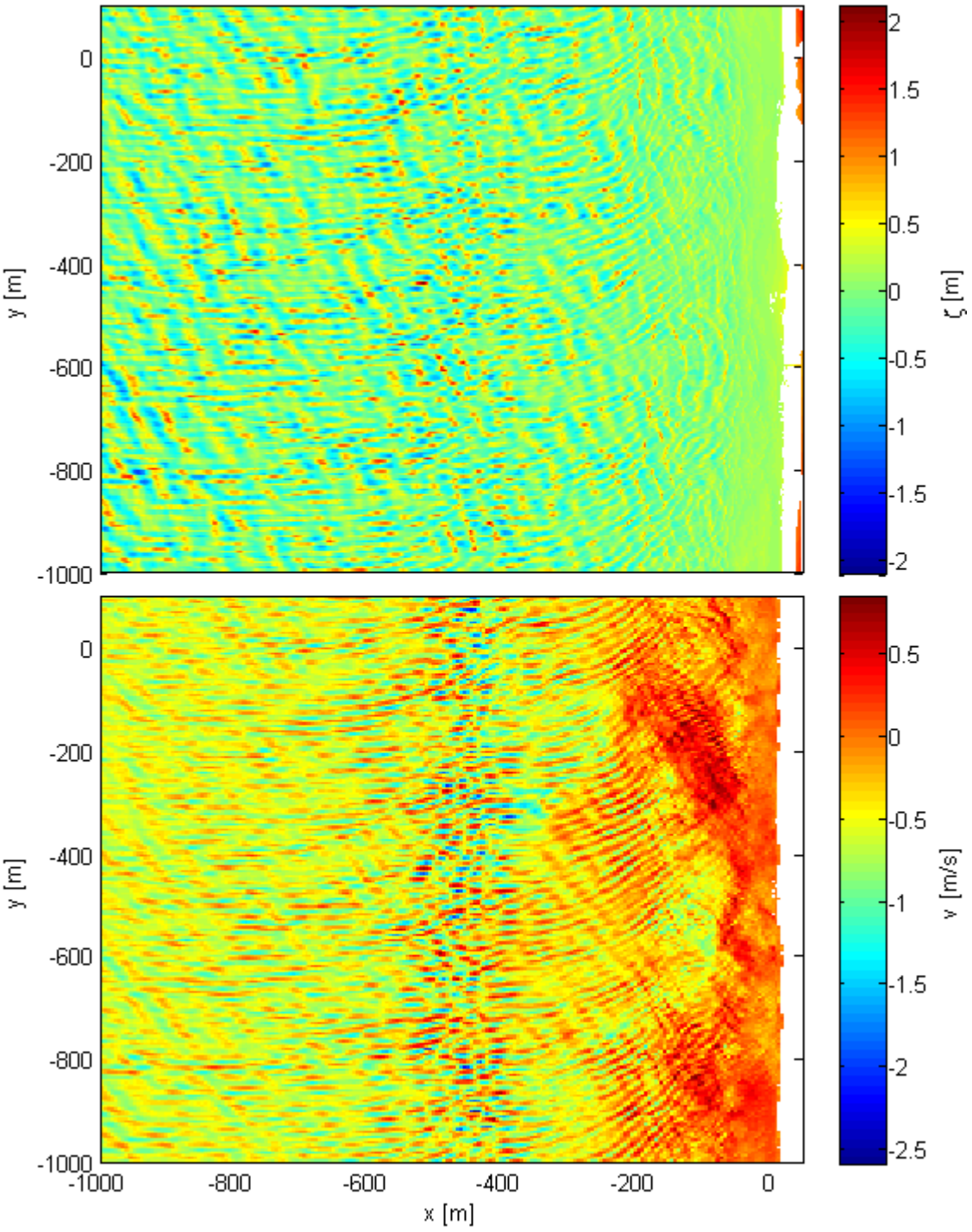

FIGURE L.3: Instantaneous surface elevation and alongshore current at end of the simulation for case V3

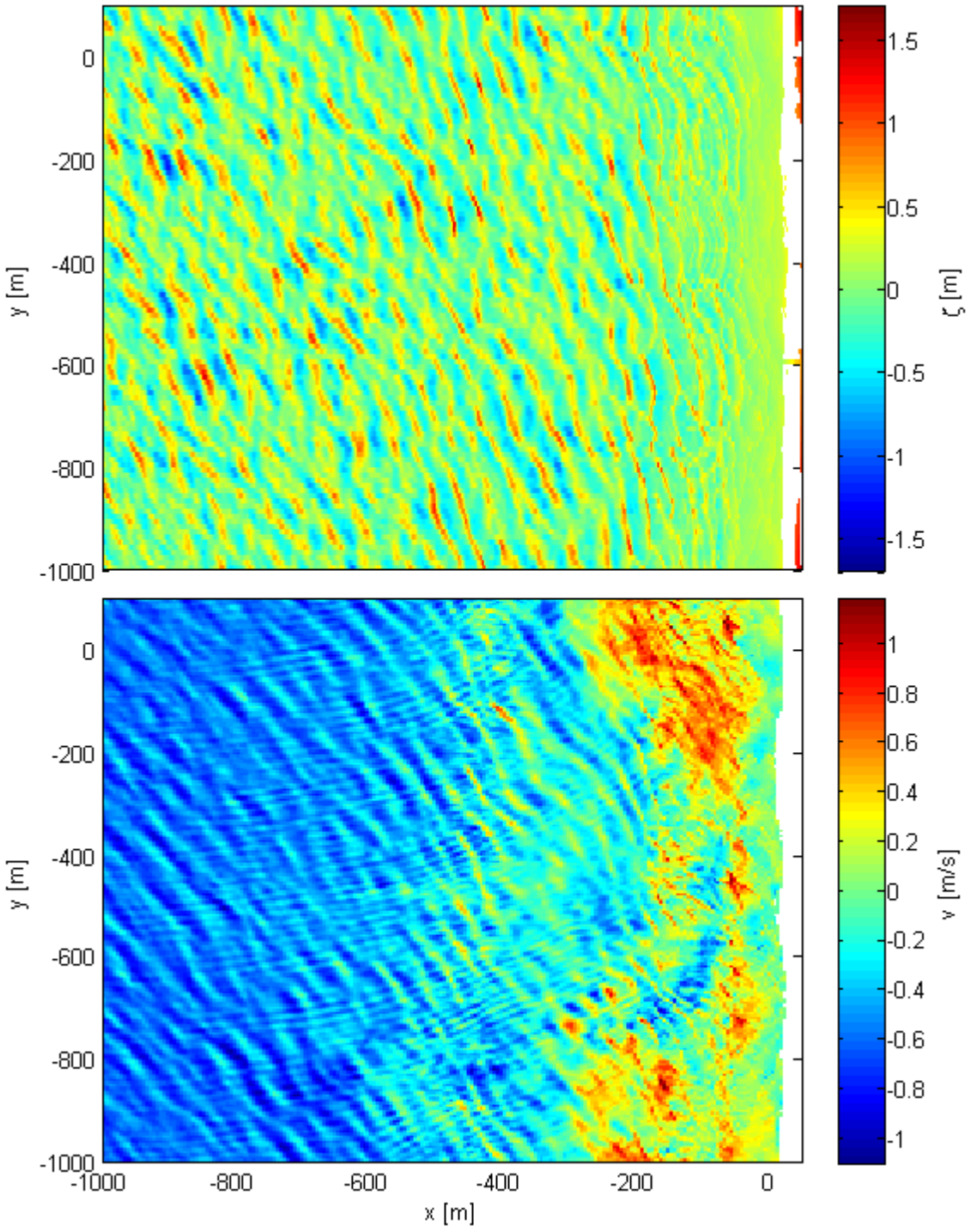

FIGURE L.4: Instantaneous surface elevation and alongshore current at end of the simulation for case V4

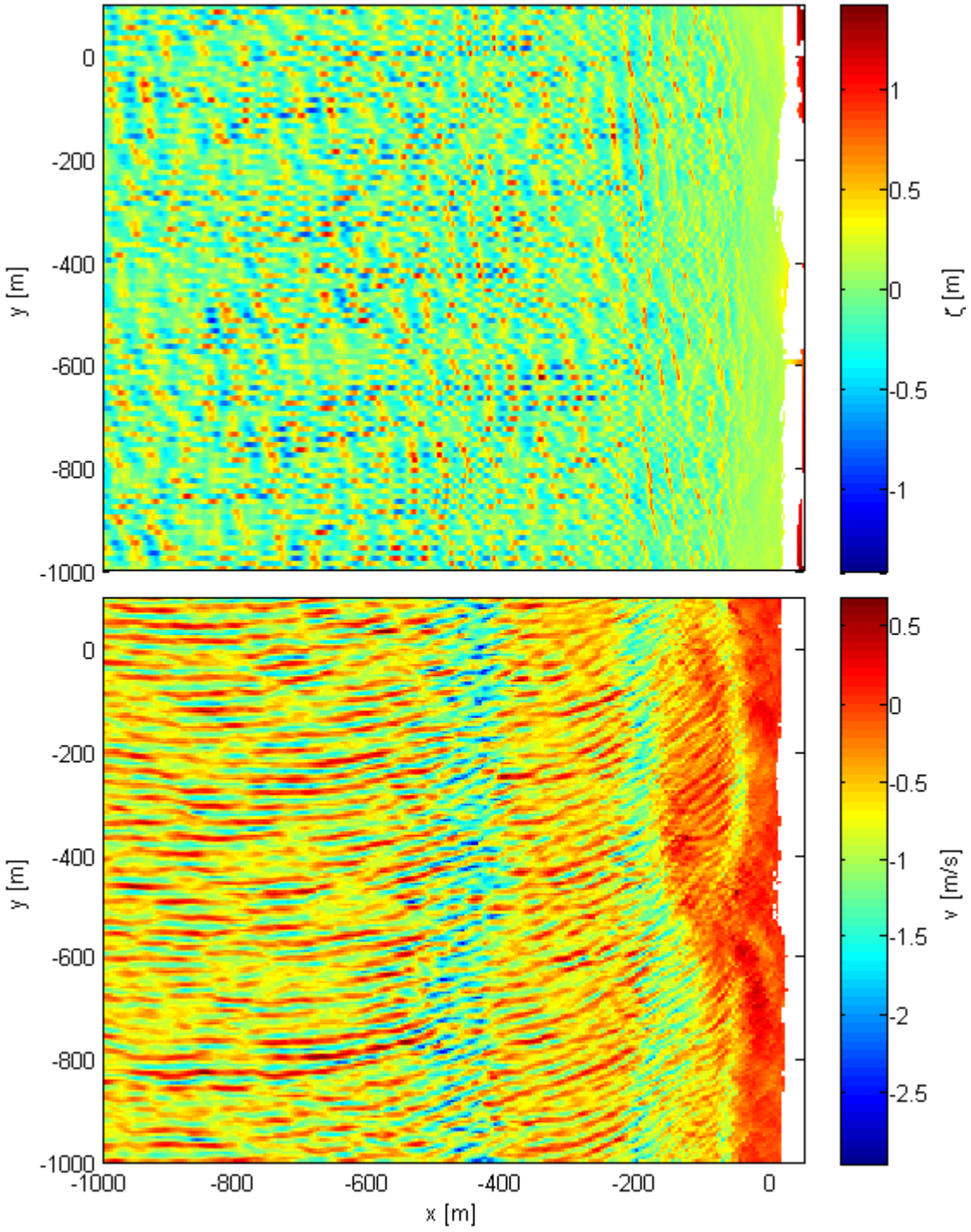

FIGURE L.5: Instantaneous surface elevation and alongshore current at end of the simulation for case V5

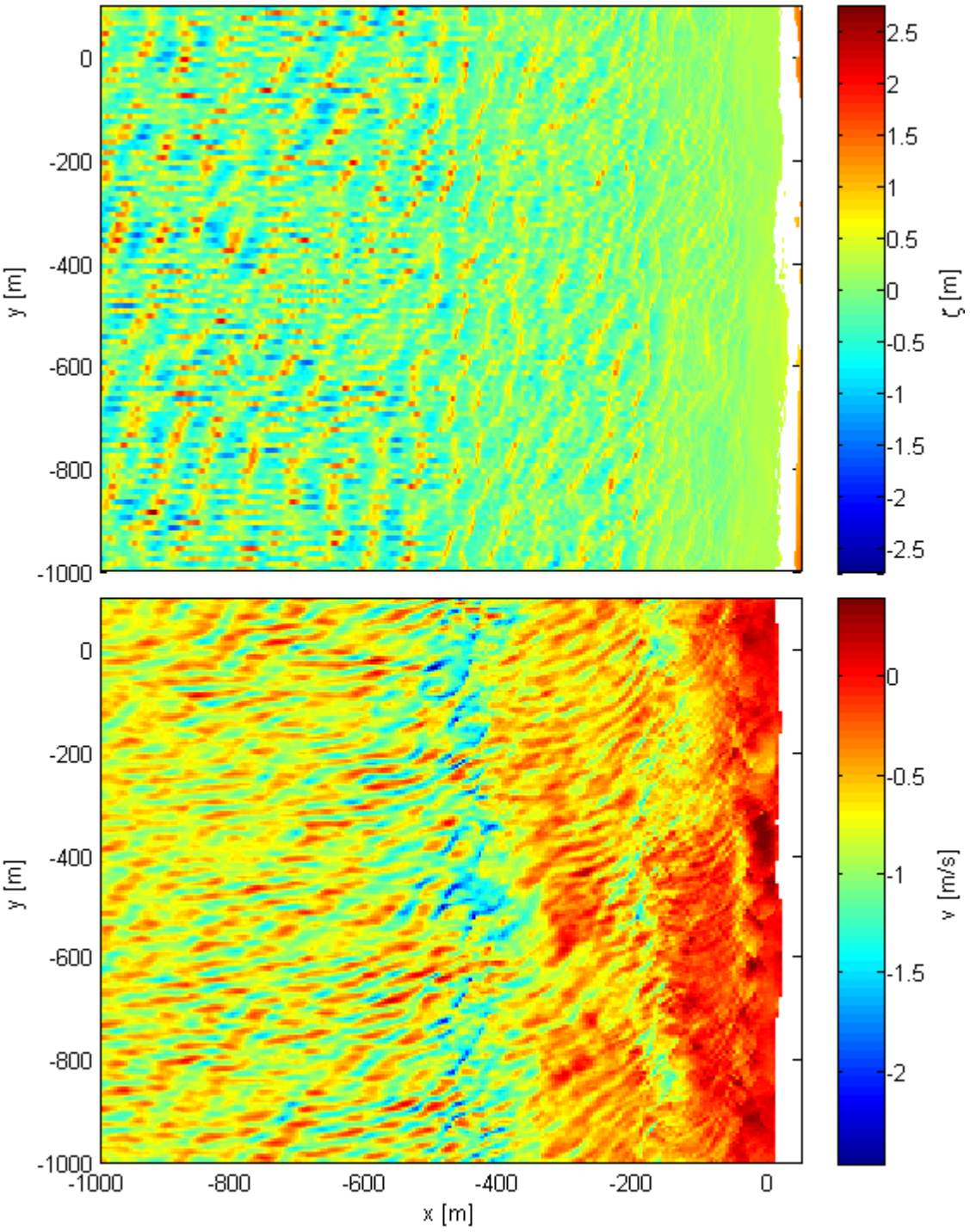

FIGURE L.6: Instantaneous surface elevation and alongshore current at end of the simulation for case V6

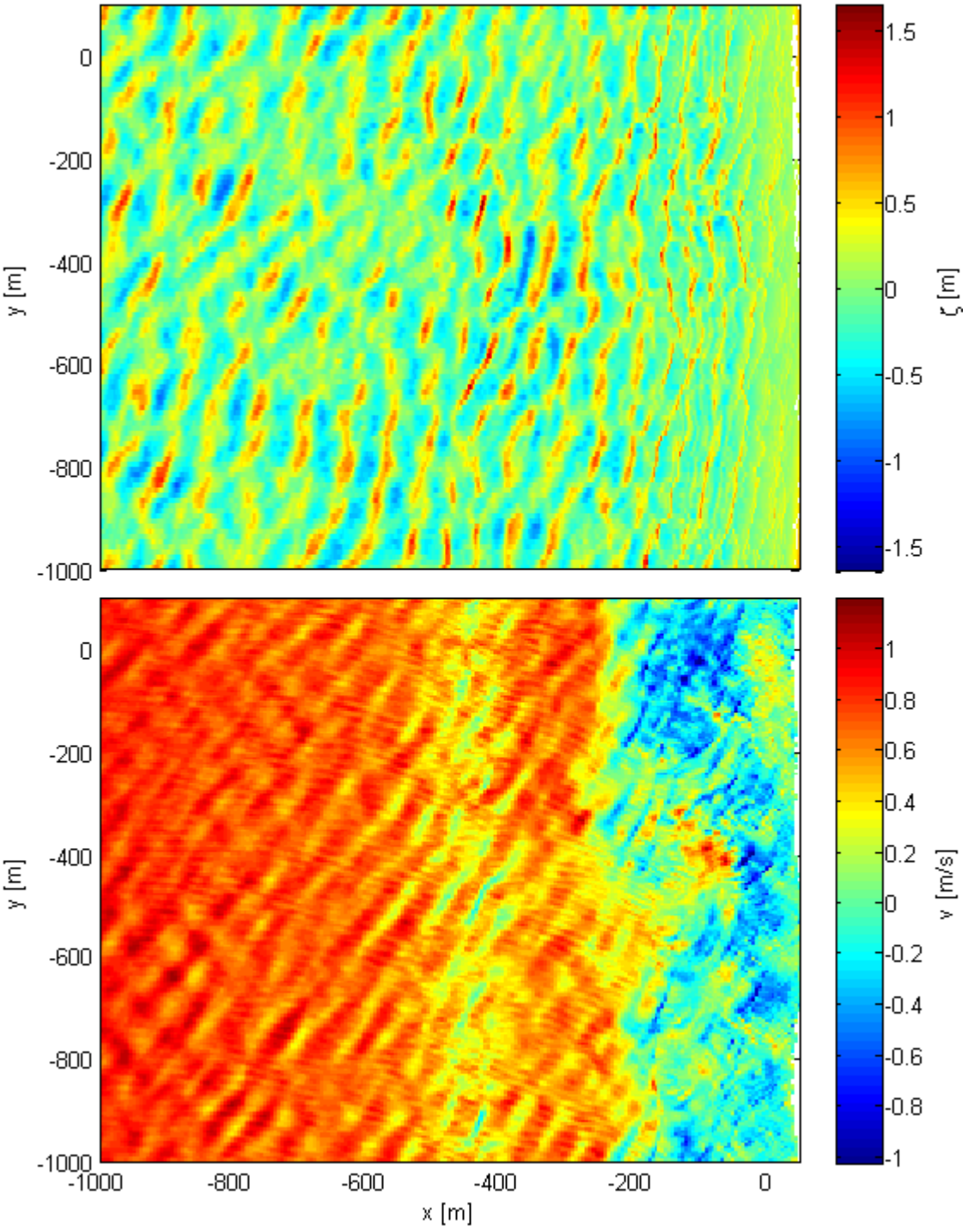

FIGURE L.7: Instantaneous surface elevation and alongshore current at end of the simulation for case V7

Appendix M

Relative influence of inertia

Within this appendix an estimation will be made of the influence of inertia. This will be done with a simple hand calculation under certain assumptions which will be explained here. The alongshore propagating tide can be represented by:

$$\underbrace{g\frac{\partial \zeta}{\partial y}}_{\substack{\text{alongshore water} \\ \text{level gradient}}} = \underbrace{-\frac{\partial v}{\partial t}}_{\text{inertia}} \quad \underbrace{-\frac{c_f v|v|}{h}}_{\text{friction}} \tag{M.1}$$

For water depths of 2, 5 and 10m the order of magnitude of the inertia and friction terms are calculated.

- The inertia term is estimated by dividing the tidal velocity range for a certain depth by 6 hours.
- The friction term is calculated with velocity obtained from a numerical solution of equation M.1 and shown in Table M.1, and friction coefficient c_f from Equation M.2

$$c_f = \frac{g}{C^2} = \frac{g}{(18\log(12h/k_r))^2} \tag{M.2}$$

With C is Chezy constant, h is water depth and k_r is roughness height.

Results are shown in Table M.2. What can be seen is that in 2m water depth friction clearly dominates inertia. However, it can not be neglected. For 10m of water depth

friction and inertia are equal of magnitude for ebb flow and inertia is halve the magnitude of friction for flood flow. So inertia is more present for larger water depths and for ebb flow as ebb velocities are lower due to the asymmetrical tide.

d [m]	v_{flood} [m/s]	v_{ebb} [m/s]	v_{range} [m/s]
2	0.35	-0.30	0.65
5	0.60	-0.50	1.10
10	0.80	-0.60	1.40

TABLE M.1: Velocity input per water depth to estimate magnitude inertia and friction terms

d [m]	Inertia [m/s^2]	Friction flood [m/s^2]	Friction ebb [m/s^2]
2	0.30	1.59	1.17
5	0.51	1.51	1.05
10	0.65	1.15	0.65

TABLE M.2: Magnitude of inertia versus friction terms for ebb and flood flow

To verify what the effect of inertia is on the tidal motion and how long it takes for the tide two change direction, two SWASH simulations are performed:

- The first simulation is performed with an equilibrium flood tidal velocity field as initial velocity (so velocity to the south). An oppositely directed ebb tidal forcing is applied.
- Vice versa, the second simulation has an ebb tidal initial velocity field a flood tidal forcing.

Both simulations are performed with a coarse grid size (because wave propagation does not have to be solved) for 10 hours. The Egmond bathymetry is used with cyclic boundary conditions. Both forcing and initial velocity fields are created with values for spring tide. Forcing is constant in time and a maximum forcing value is used for the entire simulation time of 10 hours. So forcing is overestimated. For both simulations it is observed after how many hours the equilibrium velocity has developed. Alongshore velocity for a location in the middle of the model domain can be seen in Figure M.1.

What can be seen in Figure M.1, is that it takes much longer for the ebb forcing to turn around the tidal direction and develop in a new equilibrium velocity. It takes two hours to change the direction and five hours to reach a new equilibrium. For flood

tidal forcing this is only one and three hours, respectively. One tidal cycle only takes slightly more than twelve hours. During this cycle, forcing is certainly not all the time maximum, but significantly lower. Therefore, it is doubtful whether the equilibrium velocity is reached within one tidal cycle. Certainly for ebb tidal forcing. To investigate this further, the pseudo alongshore water level gradient should be implemented time varying. Subsequently a simulation for an entire tidal cycle will provide more certainty on this topic.

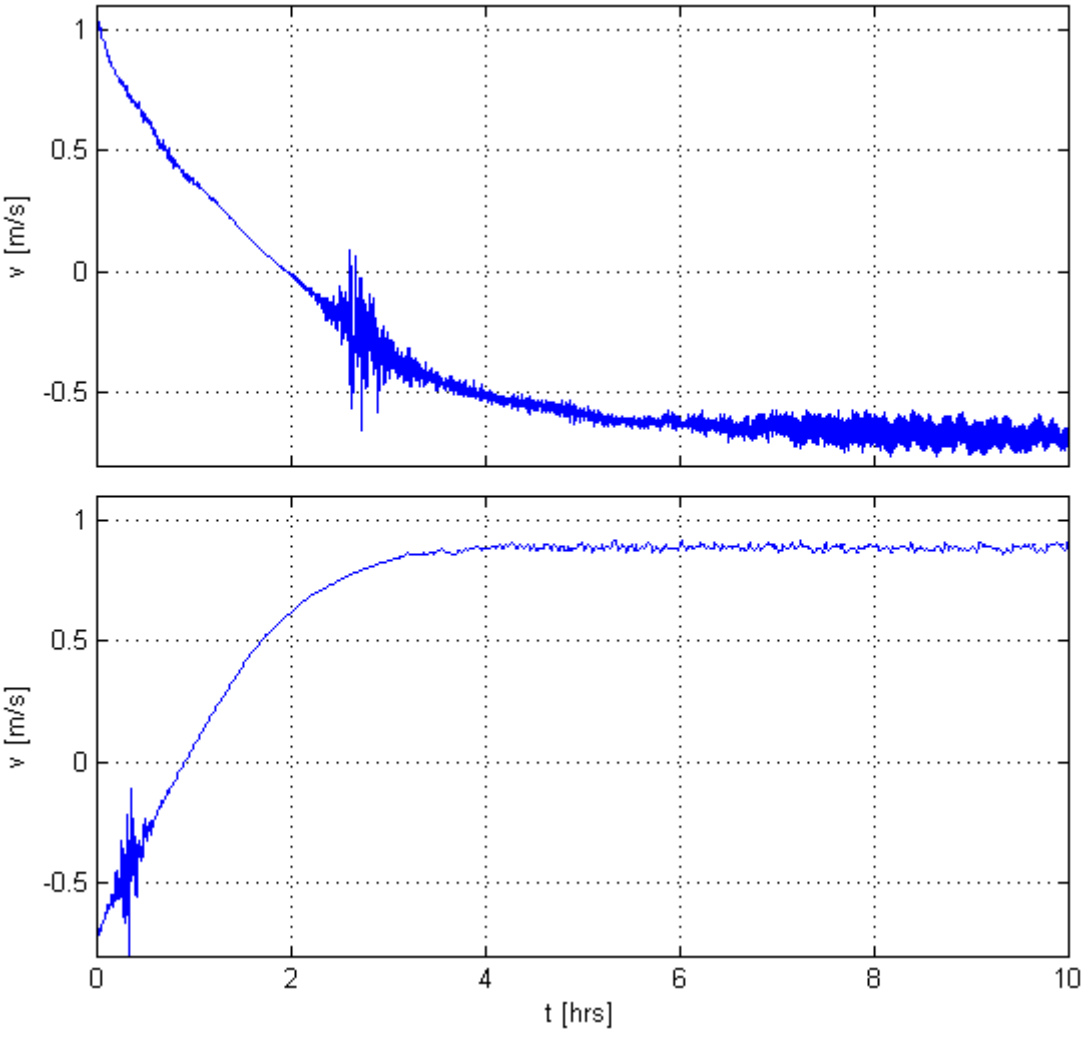

FIGURE M.1: Experiment simulations. Upper panel: initial flood current field and ebb tidal forcing. Lower panel: initial ebb tidal current field and flood tidal forcing.

Appendix N

Bug in the source code

From validation results it was noticed that simulations can be divided in two categories:

- Simulations without forcing and flow to the north. So cases with flood tide and waves from SW. For these simulations were good.
- All other simulations contain forcing and thus velocities to the south due to waves and or tide. Results were less good and for all runs disturbances were observed. The magnitude of these instabilities ranged from small ripples to big disturbances taking over the initially imposed wave field.

A test model was developed to investigate the cause of these disturbances. The domain spans 900m in cross-shore and 200m in alongshore direction with cyclic lateral boundary conditions. An alongshore uniform constant sloping beach with slope 0.01 is used as bathymetry. With numerical settings as described in Sections 3.2.1 and 4.2.1. Waves are imposed according to a Jonswap spectrum with $H_{m0} = 1m$ and $T_p = 7s$. All simulations are performed twice. Once with $\theta = 30°$ and once with $\theta = -30°$. In this way the influence of exactly opposite directed forcing can be seen.

Both simulations are identical with the exception of the mirrored wave angle of incidence. Therefore, the model should give similar results for wave energy transformation and exactly opposite signal for the alongshore velocity. Unfortunately, this was not the case. As can be seen in Figure N.1, both wave height and velocity signals disagree considerably.

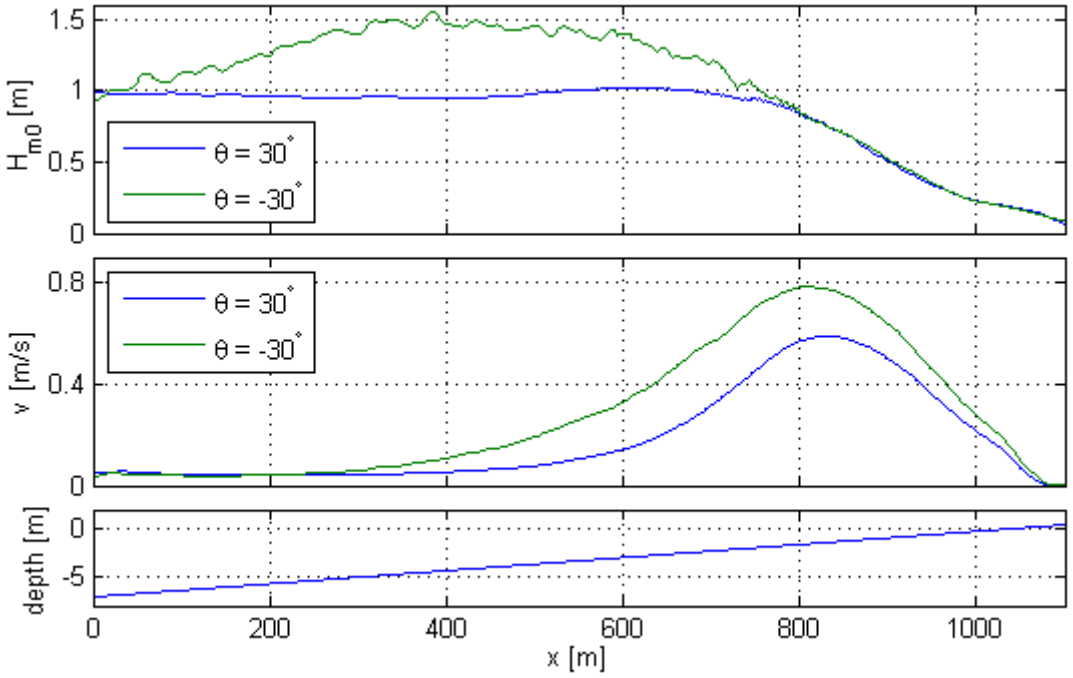

FIGURE N.1: Wave height and alongshore current results for $\theta = 30°$ (blue line) and $\theta = -30°$ (green line)

To identify the cause of this disagreement, numerous simulations were performed with different model settings. Eventually, a model configuration was found which gives identical results for waves with an angle of incidence of $+30°$ and $-30°$. Figure N.2 shows results for a run with the following numerical settings:

- JONSWAP spectrum with $H_{m0} = 1m$, $T_p = 7s$ and $\theta = +/-30°$
- No directional spreading
- LOGLAW friction with k-ϵ
- Smagorinski horizontal mixing model
- All advective terms are approximated with a first order upwind scheme

When directional spreading of $20°$ is added to both simulations, a small distinction occurs between results (see Figure N.3). Distinctions are already present at the wavemaker boundary. This indicates that there probably is a minor difference in the way the wave field is imposed. A considerable bigger disagreement occurs when the horizontal advective terms are approximated by a higher order numerical scheme instead of a first order upwind scheme. This is illustrated in Figure N.4. The horizontal advective terms,

present in the momentum balances, are: $u\frac{\partial u}{\partial x}$, $v\frac{\partial u}{\partial y}$, $u\frac{\partial v}{\partial x}$and $v\frac{\partial v}{\partial y}$. Other factors like the number of layers and other advective terms did not seem to have influence on the model results. So the higher order advective terms are the cause of disagreements in model results.

When it is chosen by the user to approximate the horizontal advective terms with a higher order scheme, firstly a first order upwind approximation is made by the SWASH model. Subsequently this is corrected with a higher order correction by the model. As differences are so considerable, as seen in Figure N.4, this indicates that there must be a bug in the source code where the second order correction is calculated and added. Shortly before handing in this thesis, bugs were found in both the higher order advective correction and directional spreading. As is shown in Figure N.5, no differences can be seen in predictions with the new source code for both simulations. This is what was expected for these two simulations. Therefore, these bug fixes seem to solve problems which occurred with negative velocities. Unfortunately, no time was left to run validation simulations again and include those in this report. Therefore, they will later be added by means of an addendum.

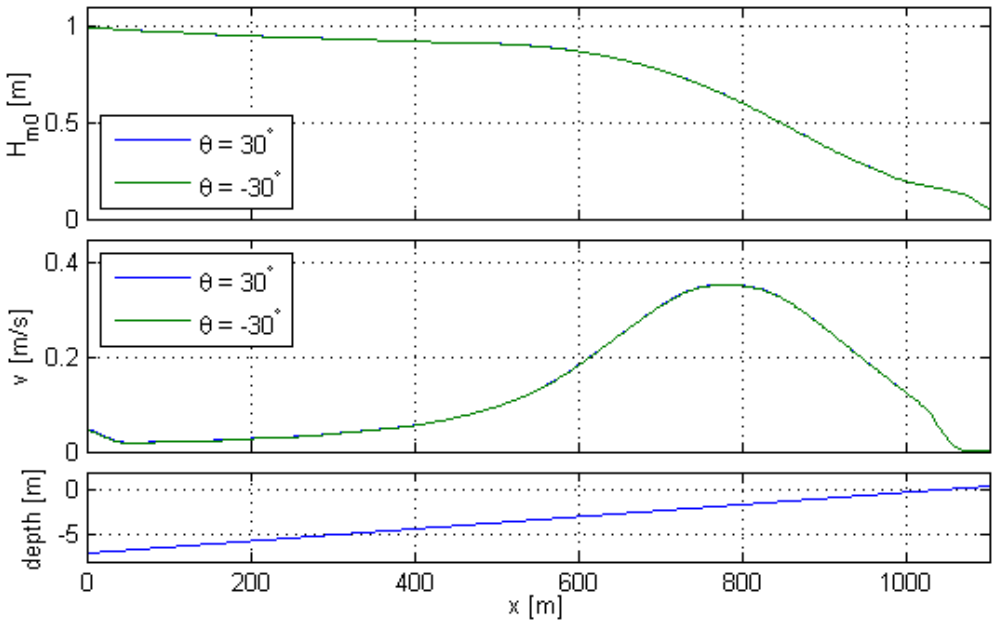

FIGURE N.2: Wave height and alongshore current results for $\theta = 30°$ (blue line) and $\theta = -30°$ (green line). In this case no directional spreading is applied and all advective terms are approximated with a first order upwind scheme.

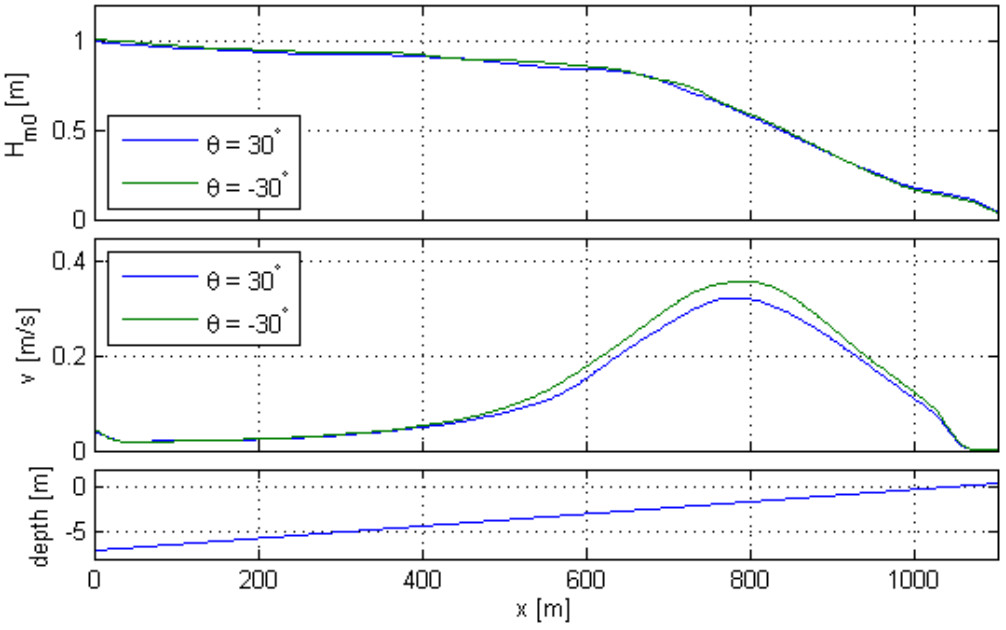

FIGURE N.3: Wave height and alongshore current results for $\theta = 30°$ (blue line) and $\theta = -30°$ (green line). In this case with directional spreading and all advective terms are approximated with a first order upwind scheme.

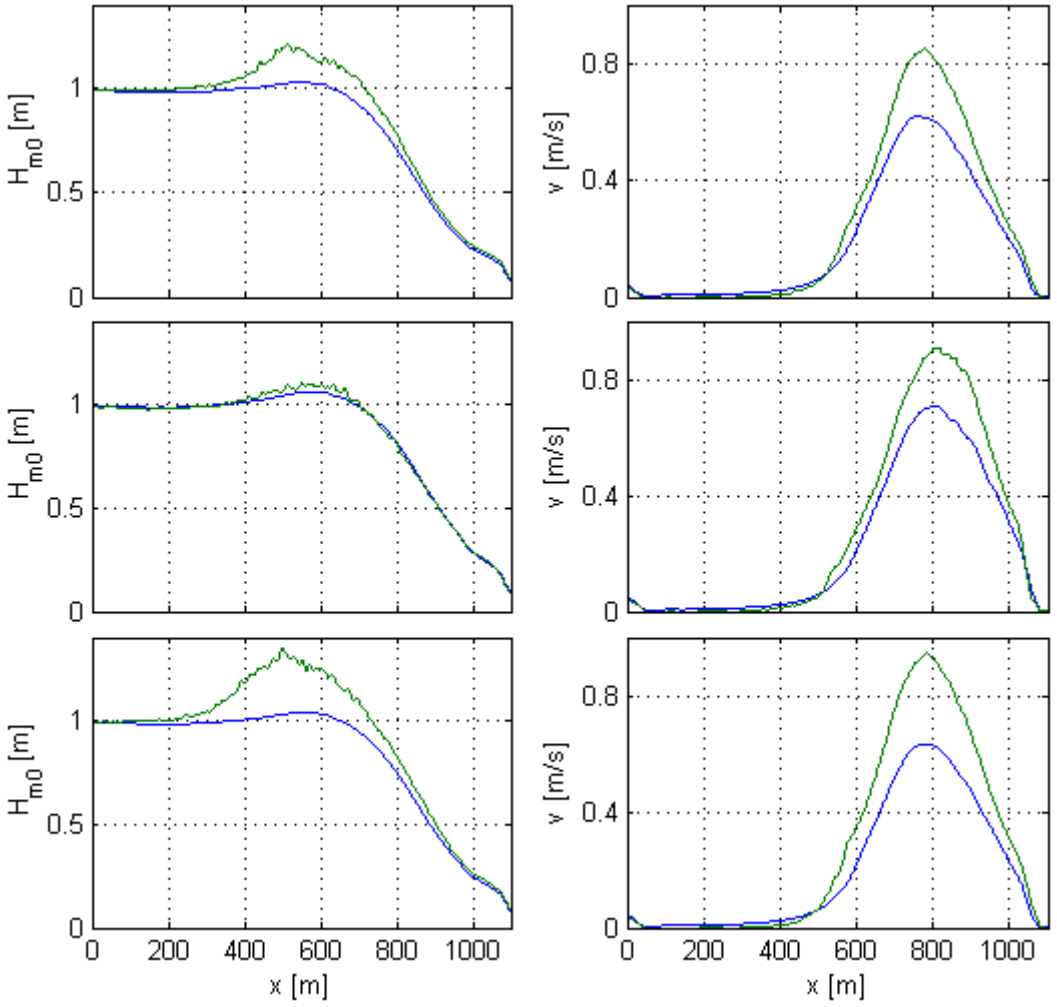

FIGURE N.4: Wave height and alongshore current results for $\theta = 30°$ (blue line) and $\theta = -30°$ (green line). In this case no directional spreading is applied and the horizontal advective terms are approximated with second order accurate schemes. From top to bottom, a Backward Differences, Central Differences and MUSCL scheme is used.

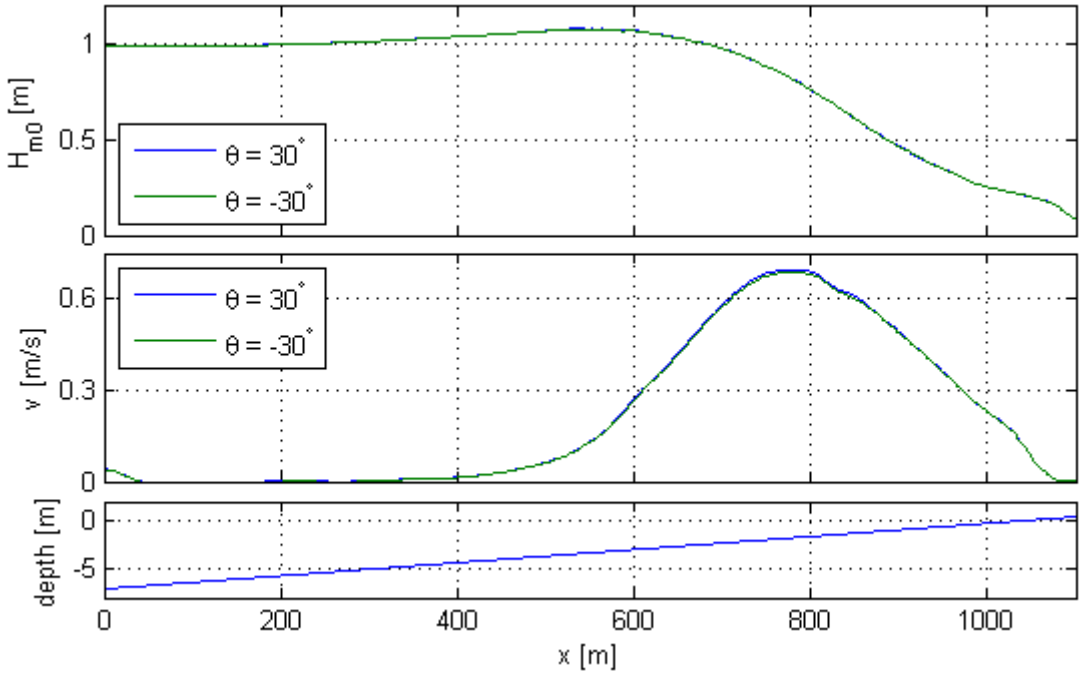

FIGURE N.5: Wave height and alongshore current results for $\theta = 30°$ (blue line) and $\theta = -30°$ (green line). In this case with directional spreading and horizontal advective terms are approximated with a MUSCL scheme.

Bibliography

Booij, N., Ris, R., and Holthuijsen, L. H. (1999). A third-generation wave model for coastal regions: 1. model description and validation. *Journal of Geophysical Research: Oceans (1978–2012)*, 104(C4):7649–7666.

Bosboom, J., Aarninkhof, S., Reniers, A., Roelvink, J., and Walstra, D. (2000). Unibest-tc 2.0, overview of model formulations. *WL Delft Hydraulics*.

Bosboom, J. and Stive, M. J. (2012). *Coastal Dynamics I: Lectures Notes CIE4305*. VSSD.

Bowen, A. and Holman, R. A. (1989). Shear instabilities of the mean longshore current: 1. theory. *Journal of Geophysical Research: Oceans (1978–2012)*, 94(C12):18023–18030.

Brinkkemper, J. (2013). Modeling the cross-shore evolution of asymmetry and skewness of surface gravity waves propagating over a natural intertidal sandbar. Master's thesis.

Bühler, O. and Jacobson, T. E. (2001). Wave-driven currents and vortex dynamics on barred beaches. *Journal of Fluid Mechanics*, 449:313–339.

Deigaard, R. (1993). A note on the three-dimensional shear stress distribution in a surf zone. *Coastal Engineering*, 20(1):157–171.

Dobrochinski, J. P. (2014). A combination of swash and harberth to compute wave forces on moored ships. Master's thesis, TU Delft, Delft University of Technology.

Elgar, S. (1987). Relationships involving third moments and bispectra of a harmonic process. *Acoustics, Speech and Signal Processing, IEEE Transactions on*, 35(12):1725–1726.

Elias, E., Walstra, D., Roelvink, J., Stive, M., and Klein, M. (2001). Hydrodynamic validation of delft3d with field measurements at egmond. In *COASTAL ENGINEERING CONFERENCE*, volume 3, pages 2714–2727. ASCE AMERICAN SOCIETY OF CIVIL ENGINEERS.

Herbers, T. and Burton, M. (1997). Nonlinear shoaling of directionally spread waves on a beach. *Journal of Geophysical Research: Oceans (1978–2012)*, 102(C9):21101–21114.

Hirsch, C. (1988). Fundamentals of numerical discretization.

Holthuijsen, L. H. (2007). *Waves in oceanic and coastal waters*. Cambridge University Press.

Kleinhout, K. (2000). *Hydrodynamics and morphodynamics in the Egmond field site: data analysis and UNIBEST-TC modelling*. PhD thesis, TU Delft, Delft University of Technology.

Long, J. W. and Özkan-Haller, H. (2009). Low-frequency characteristics of wave group–forced vortices. *Journal of Geophysical Research: Oceans (1978–2012)*, 114(C8).

Longuet-Higgins, M. S. and Stewart, R. (1964). Radiation stresses in water waves; a physical discussion, with applications. In *Deep Sea Research and Oceanographic Abstracts*, volume 11, pages 529–562. Elsevier.

Peregrine, D. (1998). Surf zone currents. *Theoretical and computational fluid dynamics*, 10(1-4):295–309.

Reniers, A. and Battjes, J. (1997). A laboratory study of longshore currents over barred and non-barred beaches. *Coastal Engineering*, 30(1):1–21.

Reniers, A. J., Roelvink, J., and Thornton, E. (2004). Morphodynamic modeling of an embayed beach under wave group forcing. *Journal of Geophysical Research: Oceans (1978–2012)*, 109(C1).

Rijnsdorp, D. P. (2015). Infragravity-wave dynamics in a barred coastal region, a numerical study. *Journal of Geophysical Research*.

Rijnsdorp, D. P., Smit, P. B., and Zijlema, M. (2014). Non-hydrostatic modelling of infragravity waves under laboratory conditions. *Coastal Engineering*, 85:30–42.

Ruessink, B., Miles, J., Feddersen, F., Guza, R., and Elgar, S. (2001). Modeling the alongshore current on barred beaches. *Journal of Geophysical Research: Oceans (1978–2012)*, 106(C10):22451–22463.

Smagorinsky, J. (1963). General circulation experiments with the primitive equations: I. the basic experiment*. *Monthly weather review*, 91(3):99–164.

Smit, P., Janssen, T., Holthuijsen, L., and Smith, J. (2014). Non-hydrostatic modeling of surf zone wave dynamics. *Coastal Engineering*, 83:36–48.

Smit, P., Stelling, G., Roelvink, D., de Vries, J. v. T., McCall, R., Zwinkels, A. v. D. C., and Jacobs, R. (2010). Xbeach: Non-hydrostatic model. *Report, Delft University of Technology and Deltares, Delft, The Netherlands*.

Smit, P., Zijlema, M., and Stelling, G. (2013). Depth-induced wave breaking in a non-hydrostatic, near-shore wave model. *Coastal Engineering*, 76:1–16.

Soulsby, R. (1998). Coastal sediment transport: the coast3d project. *Coastal Engineering Proceedings*, 1(26).

Spydell, M., Feddersen, F., Guza, R., and Schmidt, W. (2007). Observing surf-zone dispersion with drifters. *Journal of Physical Oceanography*, 37(12):2920–2939.

Stelling, G. and Zijlema, M. (2010). Numerical modeling of wave propagation, breaking and run-up on a beach. In *Advanced Computational Methods in Science and Engineering*, pages 373–401. Springer.

Svendsen, I. A. (1984). Mass flux and undertow in a surf zone. *Coastal Engineering*, 8(4):347–365.

Svendsen, I. A. et al. (2006). *Introduction to nearshore hydrodynamics*, volume 24.

SWASH-User-Manual (2015). Swash user manual version 3.14.

Tissier, M., Bonneton, P., Marche, F., Chazel, F., and Lannes, D. (2012). A new approach to handle wave breaking in fully non-linear boussinesq models. *Coastal Engineering*, 67:54–66.

Van Dongeren, A., Reniers, A., Battjes, J., and Svendsen, I. (2003). Numerical modeling of infragravity wave response during delilah. *Journal of Geophysical Research: Oceans (1978–2012)*, 108(C9).

Van Rijn, L., Grasmeijer, B., and Ruessink, B. (2002). Accuracy of measurement instruments. *Delft Hydraulics, University of Utrecht.*

van Rijn, L., Ruessink, B. G., and Mulder, J. (2002). *Coast3D-Egmond: The Behaviour of a Straight Sandy Coast on the Time Scale of Storms and Seasons: Process Knowledge and Guidelines for Coastal Management: End Document, March 2002.* Aqua Publications.

WAQUA/TRIWAQ (2012). Technical documentation waqua/triwaq.

Zijlema, M., Stelling, G., and Smit, P. (2011). Swash: An operational public domain code for simulating wave fields and rapidly varied flows in coastal waters. *Coastal Engineering*, 58(10):992–1012.